CZECH TECHNICAL UNIVERSITY IN PRAGUE

Faculty of Electrical Engineering
Department of Measurement

Magnetometer for Space Applications

Doctoral Thesis

Ing. David Novotný

Supervisor: d*oc. Ing. Antonín Platil, Ph.D.*
Supervisor-Specialist: *Ing. Vojtěch Petrucha, Ph.D.*

Ph.D. Programme: P2612, Electrical Engineering and Information Technology
Branch of study: 2601V006, ***Measurement and Instrumentation***

Prague, ***2024***

Declaration

I declare that this work is all my own work and I have cited all sources that I have used in bibliography.

In Prague, 11. 9. 2024

Prohlašuji, že jsem předloženou disertační práci vypracoval samostatně a že jsem uvedl veškerou použitou literaturu.

V Praze, 11. 9. 2024

…….
David Novotný

Acknowledgements

I would like to express my gratitude to my supervisor doc. Ing. Antonín Platil, Ph.D. and my supervisor-specialist Ing. Vojtěch Petrucha, Ph.D. and also to Ing. Michal Janošek, Ph.D. for their scientific guidance and patience during my studies. This thesis also would not be possible without the support and patience of my family, which I very appreciate.

Following research has been funded (or partially funded), by grants:

SGS18/081/OHK3/1T/13: *Development of a digitally compensated AMR magnetometer*

SGS19/177/OHK3/3T/13: *Design and evaluation of radiation tolerant magnetometer*

SGS22/170/OHK3/3T/13: *Research on reduction of power consumption in space grade magnetometers*

LVICE^2 ESA project - https://lvice2.cz

Abstract

This dissertation is devoted to the research and development of magnetometers suitable for use in the inhospitable environment of space. Due to the large body of published research in the field of fluxgate sensors, this work deals only marginally with them and focuses mainly on sensors with anisotropic magnetoresistors (AMRs). The main goal is to determine the applicability of commercially available off-the-shelf components (COTS) in a radiation-demanding and temperature-unstable environment. Compared to the more widespread fluxgate, AMR sensors show 1 or 2 orders of magnitude more noise (worse resolution/sensitivity), but in all other parameters (size, mass, power consumption, …) they are either comparable or better. Above all, for the segment of satellites (Cube-Sat/Small-Sat), which usually operate in low Earth orbits, where the measured magnetic field is relatively strong and there is no need for extreme sensitivity/low noise, AMR sensors are thus attractive.

In the first part of the thesis, the state-of-the-art in the field of magnetometers for space applications is described and the requirements that such a magnetometer should meet or should be aimed at are summarized (radiation resistance, temperature stability, noise properties, linearity). Furthermore, a search is made of the available information on the radiation resistance of the COTS components, which would be potentially suitable for the construction of the AMR magnetometer.

In the second part, author's own contribution to the issue is discussed. At first, the possibilities of moving the signal processing and feedback to the digital domain (as opposed to the more traditional analog processing) were investigated on the prototype of author's own construction of AMR and fluxgate magnetometer. Later, a comprehensive testing of the developed prototypes is described, both conventional (measurement of linearity, noise, temperature sensitivity), and then radiation testing using a Co^{60} gamma emitter. Based on both types of measurements, the prototype was iteratively modified to achieve better parameters and durability.

The next part is focused on reducing the power consumption of the magnetometer, as a key property, especially in space projects. The possibility of using pulsed power is shown, as well as algorithmic switching between operation with/without feedback, which accounts for a significant part of the total consumption and does not always need to be active.

The last part of the work deals with the potential use of the AMR magnetometer in a specific space mission ($LVICE^2$). Aspects that a magnetometer should satisfy, and which are the decisive ones are discussed.

Keywords: AMR, fluxgate, magnetometer, magnetic field, sensor, COTS, space, radiation resistant, low noise

Abstrakt

Tato disertační práce je věnována výzkumu a vývoji magnetometrů vhodných pro použití v nehostiném prostředí vesmíru. Vzhledem k velké probádanosti fluxgate senzorů se jim věnuje jen okrajově a zaměřuje se především na sensory s anizotropními magnetorezistory (AMR). Jedním z cílů je také ověřit použitelnost komerčně dostupných součástek (COTS) v radiačně náročném a teplotně nestabilním prostředí. AMR senzory oproti rozšířenějším fluxgate senzorům vykazují o 1 až 2 řády větší šum (horší rozlišení/citlivost), ve všech ostatních parametrech jsou buď srovnatelné nebo lepší (menší rozměry, hmotnost, spotřeba, …). Především pro segment malých satelitů (Cube-Sat/Small-Sat), které se obvykle pohybují na nízkých orbitách kolem Země, kde je měřené magnetické pole relativně velké, a tudíž není potřeba extrémní citlivost/nízký šum, jsou tak AMR sensory atraktivní.

V úvodní části práce je popisován současný stav v oblasti magnetometrů pro vesmírné aplikace a jsou sumarizovány požadavky, které by takový magnetometr měl splňovat nebo na jaké se zaměřovat (radiační odolnost, teplotní stabilita, šumové vlastnosti, linearita). Dále je provedena rešerše dostupných informací k radiační odolnosti COTS komponent, které by byly potencionálně vhodné v konstrukci vlastního AMR magnetometru.

V druhé části je rozebírán vlastní přínos k problematice. Zprvu jsou na vlastním prototypu AMR a fluxgate magnetometru zkoumány možnosti přesunu zpracování signálu a zpětné vazby do digitální domény (oproti tradičnějšímu analogovému uspořádání). Dále je popsáno komplexní testování vyvinutých prototypů, jednak obvykle měřených parametrů (měření linearity, šumu, teplotní citlivosti), poté i radiační testování na gama zářiči Co^{60}. Na základě výsledků obou oblastí měření byl prototyp iterativně upravován tak, aby dosáhl lepších parametrů a odolnosti.

Další část je zaměřena na snížení spotřeby magnetometru, jakožto naprosto klíčové vlastnosti zejména ve vesmírných projektech. Je ukázána možnost pulzního napájení a také algoritmické přepínání provozu s/bez zpětné vazby, která představuje značnou část spotřeby a není vždy potřeba, aby byla aktivní.

Poslední část práce se zabývá potencionálním využitím AMR magnetometru v konkrétní vesmírné misi ($LVICE^2$). Jsou rozebírány aspekty, které by měl magnetometr splňovat a které jsou rozhodující.

Klíčová slova: AMR, fluxgate, magnetometr, magnetické pole, sensor, COTS, vesmír, radiačně odolný, nízkošumový

Table of contents:

1. Introduction

Magnetometers are used in many different applications in space – both engineering and scientific. Navigation and orientation stabilization of a satellite using various actuators (e.g., magneto-torquers and reaction wheels) is a typical example, as is space weather monitoring to protect sensitive instruments - e.g. ESA's SOSMAG project [1], but they also have purely scientific applications like studying the magnetosphere of Earth and other planets and celestial bodies [2]. Precise magnetic sensors are usually based on the fluxgate principle [3,4] or anisotropic magnetoresistance (AMR) sensors [5,6]. When ultrahigh absolute accuracy and very low noise is necessary, optically pumped magnetometers (helium/potassium) are used [53]. Vector magnetometers are sometimes also combined with scalar types (optically pumped/Overhauser) for their high absolute precision. This precision can be in some situations transferred to vector magnetometer using calibration procedure as shown in [38] for Ørsted satellite and has been also utilized in Cassini mission (scalar helium + fluxgate).

While fluxgates achieve lower noise and better stability, AMRs are cheaper, lighter, and more widely available commercially; they can also potentially achieve stability like fluxgates, as will be presented in chapters below. These factors make AMRs attractive for low-cost, low power applications. Especially in SmallSat/CubeSat, where both power and cost budgets are limited and usually AMR's precision is sufficient (low Earth's orbit).

Space-grade magnetometers often use special parts—application-specific integrated circuits (ASICs) [8,9] or radiation hardened field programmable gate arrays (FPGA) — to achieve better radiation immunity and lower power consumption. But the use of ASICs or other special radiation-tolerant devices makes them costly and thus not easily obtainable for smaller projects with limited budgets.

Because of their interesting potential in these projects, this thesis is mainly focused on AMR sensors with digital signal processing realized with COTS components. It is also appropriate to use (carefully selected) ordinary parts instead of special radiation-hardened parts when the cost of instrument is important. As one of the criteria, signal processing must be designed in a way to ideally not be affected by parts degradation with increasing radiation dose. This makes the development complicated as ordinary electronic parts usually have no radiation specifications. Some radiation testing results of even ordinary components can be found [10], but they do not include many modern active components: microcontrollers, operational amplifiers, voltage stabilizers, references, analog-to-digital converters (ADCs), and so on. For this reason, multiple radiation testing campaigns have been performed with individual parts, to create our own specifications.

1.1. Applications of magnetometers in space missions

There are many reasons why it is important/useful to measure magnetic field in space missions. Magnetic field is one of the absolute measurements that can be done in space (together with acceleration and rotation), almost any other measurement is relative. One of the obvious applications is for navigation in known magnetic field (e.g. Earth's orbit). From there it is also useful to map magnetic field surrounding planets/bodies in solar system and in empty space in between to know what to expect and for further space missions to take advantage of it.

Another aspect is measurement of solar wind and activity. Our star has strong magnetic fields and occasionally throws charged particles towards Earth that interact with our magnetosphere. These phenomena can significantly affect sensitive electronics and electrical systems used by humans both in space (satellites) or on the ground (power distribution grid in northern regions). Monitoring of this activity can be crucial to facilitate an early warning. There are also other possible purposes, like magnetic prospections on objects like asteroids, etc.

There is also need to measure magnetic field to make proper maneuvers using magnetorquers. These devices use interaction of their own electrically generated magnetic field with surrounding natural magnetic field to create torque and thus rotate with the satellite. Magnetorquers are very useful devices as they don't saturate like reaction wheels that are used for the same purpose. For that reason, they are often used in missions where sufficient surrounding magnetic field is expected (e.g. Earth's orbits).

1.2. Required parameters for space missions

In contrast to magnetometers operating on Earth, space magnetometers have additional requirements because of harsh environment they operate in. There are at least 4 major causes of problems: wide temperature range, radiation dose, outgassing, vibrations/shocks.

With temperature there are even 2 sub-problems, one is big variation of temperature, and another is reduced ability to remove excess heat from electronics. When a satellite is in full sunshine, temperature can increase rapidly (how much depends on the surface of the satellite and its temperature shielding). Similar effects happen for solar eclipse when satellite is hidden in the shadow (of the Earth for example). Temperature then drops also steeply. This temperature swing can be from -50 °C to +100 °C when operating and even more in „survival state" [47]. The second issue with the temperature is that in space there is almost perfect vacuum, so the only way to cool down overheating electronics is through radiation. This means that the whole satellite can dispose of only limited amount of heat through its surface, so the lowest possible power dissipation is desired.

Radiation tolerance is probably the most problematic requirement during development as it is not possible to test in normal laboratory and there are only few specialized facilities, where it can be done. It is also not a specified parameter by manufacturers of COTS parts, so every part should be tested individually or at least in its normal operation (inside sub-circuit). Required radiation tolerance is usually specified in total ionizing dose (TID) during planned mission that instrument needs to survive (+ reserve). The TID obtained by onboard instruments depends strongly on distance of the device from the Sun as the main source of the radiation in our solar system (perhaps with the exception of probes operating in rather extreme radiation environment around Jupiter). When operating on Earth's orbit, typical TID is given by distance from the surface (low/high orbit) and also by trajectory [45-46].

As the satellite operates in high vacuum, some parts of it (typically plastic or glues) can dissipate gas that can then condensate on surface of instruments inside satellite and damage its

electronics/optics/mechanics. Therefore, every part of the satellite should be tested inside vacuum chamber and heated up to higher temperature (according to standard ASTM E-1559 125 °C) where outgassing reaches its maximum to check worst-case scenario [44] for 24 hours.

Vibrations are the mostly problematic during the launch of the rocket that brings the satellite with instrument into space. During that phase, vibrations are the strongest. But if vibration tolerance is considered already during design, it is usually not so problematic to meet. Vibration test can be performed in many scientific/commercial facilities that specializes on that kind of testing.

1.3. Sensors suitable for space applications

Magnetic field sensor types that are commonly used in space applications are mainly fluxgate (FG), anisotropic magnetoresistance (AMR), (giant/tunneling magnetoresistance) GMR/TMR, induction coil, resonant (proton/Overhauser) and optical magnetometers. In the following chapter, these magnetometers will be discussed with emphasis on AMR and FG magnetometers as they are the main focus of the current research.

2. State of the art

This chapter discusses magnetometers suitable for space applications. The state-of-the-art, low-noise vector magnetometers include fluxgate, AMR, GMR/TMR, induction coils, and resonant magnetometers. Each of these types has specific applications for which it is best suited.

2.1. Fluxgate sensors

Fluxgate sensors are based on modulation of permeability in a ferromagnetic core. Sensor is composed of a highly magnetically permeable alloy core that is periodically saturated (~1-100 kHz) by excitation winding. Another coil (pick-up) is used to sense saturation asymmetry of the core (or cores, depending on fluxgate type) that is caused by the external magnetic field to be measured. Voltage proportional to external magnetic field is induced on 2'nd harmonics of excitation signal (parallel fluxgate). Details about fluxgates can be found in many publications, such as [17, 18].

Typical signal processing circuit uses a phase sensitive detector for demodulation of pickup signal, feedback circuit compensating the external field to improve overall sensor parameters (gain stability, linearity) and excitation electronics. Signal acquisition and digitization (ADC) usually measures current through compensation winding (as voltage on sensing resistor). This means that all signal processing is typically done in analog domain. Some of space grade magnetometers employ digital signal processing using specialised ASIC [19] or FPGA with ADC + DAC [20]. Solution with an ASIC has many advantages over FPGA such as low power consumption, small dimensions, easier process of radiation hardening (as the device is not reprogrammable). But, on the other hand, it is also much more costly and not generally available. Using FPGA can also benefit from its better flexibility – front end electronics that is crucial for obtaining good parameters can be redesigned easily, so the newest state-of-the-art parts can be used.

Fluxgates are the most sensitive room-temperature vector magnetometers that are capable of sensing static magnetic field (higher sensitivity can be achieved with induction coil, but only for higher frequencies [21]). Their noise limit is approx. 10-50 pT/$\sqrt{Hz}$ at 1 Hz for a

commercially available types (for example Bartington MAG612 [22], Fig. 1. and Table 1), 3-5 pT/$\sqrt{Hz}$ at 1 Hz for high quality fluxgates and even about 1 pT/$\sqrt{Hz}$ at 1 Hz for special types [23].

In case of space applications, they have been used together with a scalar type of magnetometer [24] for possibility of on-the-fly calibration of fluxgate. This complementary design benefits from both inherent stability of scalar (proton/Overhauser) magnetometer and possibility of sensing vector components by set of fluxgates.

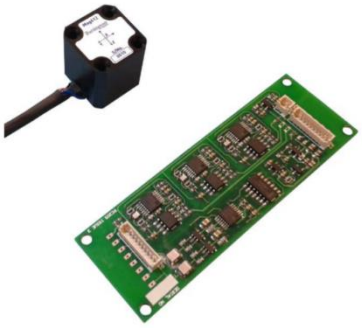

Fig. 1. Photo of Bartinghton MAG612 fluxgate sensor taken from [22]

Table 1 – parameters summary

PARAMETERS TAKEN FROM [22]

Parameter	Value
Range	± 90 μT
Noise density @ 1 Hz	<20 $pT_{RMS}/\sqrt{Hz}$
Bandwidth (-3 dB)	3000 Hz
Linearity error	15 ppm of FS
Offset TC	< 1 nT/K
Sensitivity TC	< 100 ppm/K
Power consumption	700 mW @ ±12V
Output sensitivity	89 kV/T
Dimensions - sensor	20x20x20 mm
Dimensions - electronics	30 x 90 x 3 mm

2.2. Anisotropic magnetoresistors

Anisotropic magnetoresistors (AMRs) are based on magnetoresistance effect in ferromagnetic film. Electrical resistance of AMR element depends on direction of its magnetization. For consistent measurement and removal of perming effects, it is advisable that the default magnetization of material is periodically recreated by strong impulse of artificial field along the material easy axis. Used ferromagnetic material has two stable states of magnetization that can be set by applying "flipping" or “set/reset” magnetic field that is generated through flipping coil (usually embedded in AMR sensor). Summary of magnetoresistive sensors and details of AMR can be found in [11, 12].

Available commercial sensors contain four AMR elements with barber-pole pattern of highly conductive aluminum deposited on resistive permalloy layer. This forces current path in permalloy to shift by 45° relative to easy axis and makes transfer function odd around zero measured magnetic field. Sensitive elements are usually connected into full Wheatstone bride configuration. This solution improves most of sensor parameters - sensitivity, linearity, and temperature stability. Some available sensors come with already integrated digital output (thus facilitating one chip solution: sensor + flipping + demodulation + A/D converter) such as HMC5883 [13]. But their parameters are not sufficient for precise measurement due to poor resolution (high noise) and bad temperature stability. For precise measurements, an analog sensor using flipping technique and feedback compensation should be used. When considering sensors available from worldwide distributors, the best candidate for that purpose seems to be Honeywell HMC1021/1001 [14]. Also, Sensitec AFF755 [15] seemed to be good choice, but during research it was found out that it has problems with flipping that caused excess noise (or offset instability).

The best reported parameters of an AMR magnetometer suitable for space applications can be found in magnetometer for SOSMAG project [1]. These parameters are summarized in Table 2. In this magnetometer HMC1021 is utilized and signal processing is done using ASIC + auxiliary FPGA (Fig. 2).

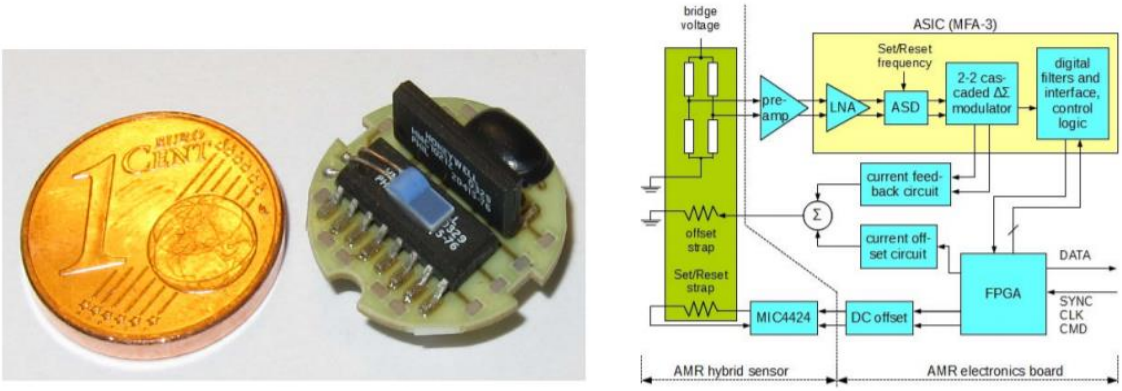

Fig. 2. SOSMAG sensor head and block diagram, taken from [1]

Table 2 – SOSMAG parameters

PARAMETERS TAKEN FROM [1]

Parameter	SOSMAG magnetometer
Range	± 70 μT
Noise density @ 1 Hz	100 $pT_{RMS}/\sqrt{Hz}$
Bandwidth (-3 dB)	30 Hz
Power consumption	1460 mW[a] @ 28V
Interface	RS422, UART
Dimensions	183 x 123 x 15 mm

[a] Two AMR magnetometers when both exposed to 60 μT magnetic field

An example of AMR magnetometer that is commercially available and suitable for CubeSat applications is NewSpaceSystems NMRM-001-485 [16]. Photo of magnetometer with case can be seen on Fig. 3. Summary of key parameters are in Table 3.

Fig. 3. Photo of NewSpace System's NMRM-001-485 taken from [16]

Table 3 – NMRM-001-485 parameters

PARAMETERS TAKEN FROM [16]

Parameter	Value
Range	± 60 μT
Noise density @ 1 Hz	<8000 $pT_{RMS}/\sqrt{Hz}$
Bandwidth (-3 dB)	< 9 Hz
Sample rate	< 18 Sa/s
Maximum TID	10 krad
Power consumption	550 mW @ 5V
Interface	RS485
Dimensions	45 x 69 x 20 mm

2.3. GMR/TMR sensors

Giant Magneto-Resistance and Tunneling Magneto-Resistance sensors are in some terms similar to AMR sensors, their electrical resistance changes with applied magnetic field. But they exploit differently the underlying physical (electron spin-related) mechanisms. They both promise lower power consumption, and higher sensitivity. For this reason, GMRs replaced AMRs in HDD reading heads and later TMRs replaced GMRs. But precise linear measurement of magnetic field is not practical with these sensors because of their high non-linearity, non-monotonicity and hysteresis [48]. From the point of view of noise, they are similar as AMR

[49]. Representative linear TMR sensor is TMR9082 with similar noise as AMR sensor HMC1021.

For the mentioned reasons, GMR/TMRs are not much used in space applications, although GMR based magnetometer can be found in nano-sat OPTOS, launched in 2013.

2.4. Induction coils

Induction coils are based on Faraday's induction law: temporal change of magnetic flux causes induced voltage in coil, proportional to rate of change times number of turns. This is important to understand – with induction coils we measure change of magnetic field, not field itself. This means that induction coils are capable only to measure AC magnetic field, not DC. In some applications, measurement of rather low frequencies is still feasible [52]. Induction coils can take advantage of very high sensitivity and low noise at higher frequencies (because their sensitivity naturally increases with frequency) if that high frequency band is interesting for given scientific goal. The high frequency operating range is usually limited by resonance caused by inter-turn parasitic capacitances. Sometimes, induction coils are used in symbiosis with other type of magnetometer (e.g. fluxgate), where DC to low frequency is covered by fluxgate while mid to high frequency by induction coil [34]. Induction coils have also advantage of being low power because from principle they are passive – the only power consumption is taken by preamplifier or some DAQ if they provide digital output. For a space application, there may be issues with their dimensions and weight, as they are usually bulky and heavy – because of long magnetic core (usually rod) and many turns of coil (a lot of copper) to obtain high sensitivity/low noise / see Fig. 4.

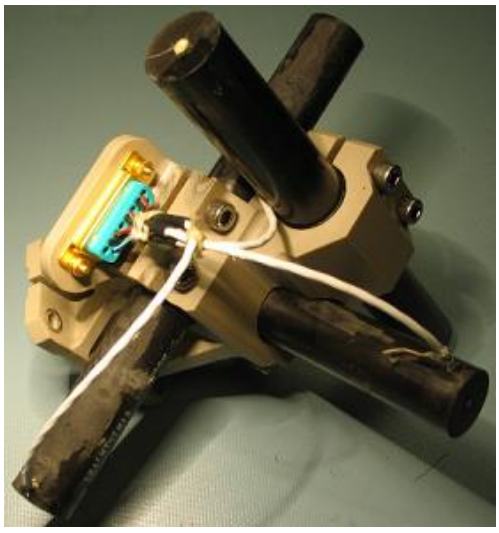

Fig. 4. Photo of 3-axis search coil magnetometer from THEMIS mission [NASA]

2.5. Resonant magnetometers

Resonant magnetometers, suitable for low magnetic field measurements, are proton precession magnetometers, Overhauser magnetometers (improved version of proton precession) and optically pumped magnetometers (using typically helium/cesium vapor). Their magnetic field resolution/noise is even better than most fluxgates [53]. But they are power hungry and bulky. They are from the principle scalar type and cannot measure magnetic field weaker than certain limit, because otherwise amplitude of signal is too low to detect reliably. There are also some tricks [35] to extract vector information (Fig. 5) and extend range below such a limit but they are dimensionally extensive and even more power hungry, while limiting bandwidth of measurement.

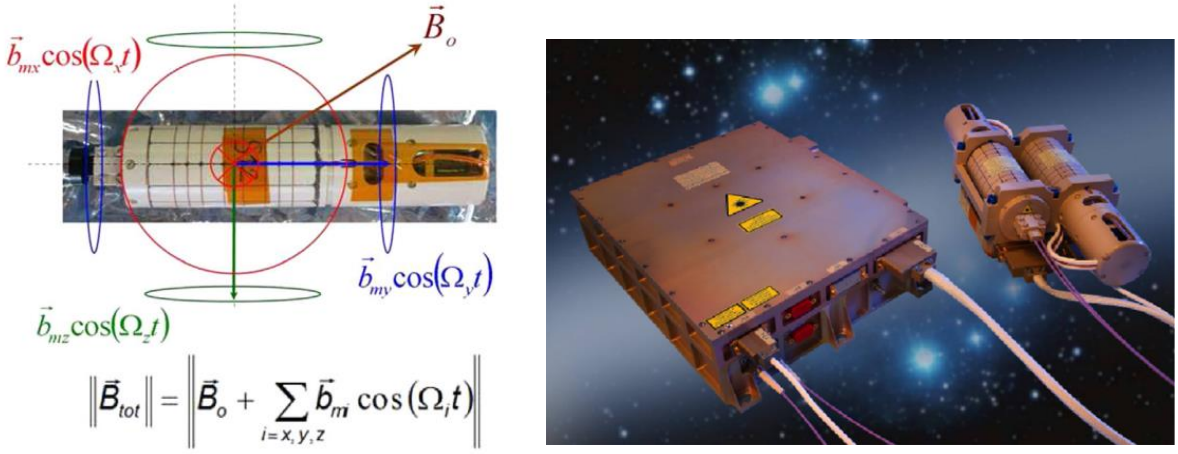

Fig. 5. Photo of Swarm Mission's Absolute Scalar Magnetometer (right) and extracting of vector information (left), both taken from [35]

2.6. Available COTS parts radiation testing reports

When designing with COTS parts for space mission, radiation tolerance is problematic as it is not tested and specified by manufacturers in contrast with conventional testing (operating temperature, shock/vibration test, …).

Some testing of electronics parts can be found substantiated in related publications, but most of them focus on parts that are already obsolete (examples in Table 4 below taken from [39-43]).

Table 4 – summary of the available COST part radiation testing

Type of device	Part number	Survival TID (krad)	Cited from
Level translator for GPIO	TXB0108	100	[43]
Level translator for I2C	TXS0108	80	[43]
Quad multiplexer	M74HC157RM13TR	70	[43]
MOSFET N-channel	2N7002	<10	[43]
Atmel microcontroller	ATMega1280	18.3	[43]
Microchip Microcontroller	PIC16F88	20	[43]
Signal Processor	OMAP3530	35	[43]
Atmel 1 Mbit Flash Memory	AT25FS010N	15	[43]
ARM Cortex-M7 microcontroller	SAMRH71E	100	[39]
RS232 interface IC	MAX3221-EP	8 - 24	[40]
TXCO Oscillator	FOX924B	8 - 24	[40]
PIC24F series microcontroller	PIC24FJ256	8 - 24	[40]
Over-current protected switch	FPF2700	> 24	[40]
2GB SD card Delkin	SE02SAMHL-C1000-D	> 24	[40]
2GB SD card Sandisk	SDSDB002G-AFFP	8 - 24	[40]
2GB SD card Transcend	TS2GUSD	< 8	[40]
Op. amp. with a FET input stage	OPA656	7.7	[42]
Low noise CMOS op. amp.	TLC2272	12	[42]
Micro-power, CMOS op. amp.	LMC6062	16	[42]
CMOS rail-to-rail op. amp.	LTC6081	5 - 7.5	[42]
A low voltage, low power CMOS op. amp.	LMV341	20	[42]
A high voltage, low offset CMOS op. amp.	AD8657	15	[42]
A low noise, precision, CMOS op. amp.	AD8662	10	[42]

More recent and concentrated database can be found in European Space Components Information Exchange System (ESCIES). But there cannot be found any tests of ADCs and microcontrollers, which are necessary for digital magnetometer's operation, thus own research and radiation testing was necessary.

3. Objectives of this thesis

Based on the previous chapter, the most suitable magnetometer for further research appears to be the AMR (with potential consideration of fluxgate) using COTS parts as suitable for low-budget, cubesats or small satellites. The AMR is expected to consume less power than the fluxgate, although it comes with the trade-off of higher noise. The issue with COTS parts is their low radiation tolerance and the lack of manufacturer testing for radiation. This thesis addresses these issues through the following four objectives.

I. Design AMR (and/or fluxgate) magnetometer with COTS components, that has the best possible parameters (at least comparable to state-of-the-art) and put emphasis to possible radiation tolerance (chapters 4.1. to 4.3. and 4.6).
II. Perform set of tests and measurements on key parameters and radiation tolerance and try to enhance these parameters by finding and replacing susceptible parts (chapters 4.4 and 4.5 and 4.10)
III. Reduce power consumption as much as possible to make that magnetometer most suitable for the space applications (chapters 4.7 and 4.8).
IV. If possible, prepare flight-ready magnetometer for real space mission (chapters 4.9 and 4.11).

4. Own work/results

My own results are presented below in the form of eight published conference/journal papers and one journal paper currently under peer-review process, that are listed in chapter 6.1 as [1] - [8] and accepted abstract [9]. Articles are commented and ordered in logical order (usually in chronological order, but not always). In the end of this chapter, unpublished part of research is shown (radiation testing on HIMAC in Japan and some notes on test-flight of designed AMR magnetometer on student's sounding rocket).

4.1. Digitally processed and compensated AMR magnetometer

To make own research on AMR magnetometers, firstly it was necessary to design own prototype. Because in terms of radiation tolerance and temperature stability digital electronics is generally more suitable, it was preferred choice to make as much signal processing in digital domain as possible.

In terms of signal processing and following the signal path, the first part is measurement of AMR bridge output and its demodulation (as flipping modulates sensitivity). Second part is feedback loop operation (i.e. applying compensating current to feedback coil holding sensor in zero magnetic field). Both parts can be done, more or less, digitally. First presented paper below shows progress on this initial development.

Before this first presented paper, I already had some experience with multiple commercially available AMR sensors. Using this knowledge, in all future work I decided to use Honeywell's HMC1021 as relatively cheap AMR sensor (in comparison with HMC1001), with very low noise (in comparison with AFF755) and with high current to magnetic field constant of internal compensation winding embedded within the sensor.

For even further reducing application of sensitive components, the current source was not made of discrete digital-to-analog converter (DAC) and voltage to current converter but rather using pulse-width-modulation (PWM) generated directly by main microcontroller unit, amplified by MOSFET transistor H-bridge. This AC voltage has been then fed through an RC network that has two purposes – to filter out AC components and to act as a simple, passive, voltage to current converter as its serial resistance is much higher than resistance of compensation winding.

Synchronous demodulation and feedback loop operation is also handled by software, signal is acquired by ADC on higher sample rate than is flipping (modulation) frequency. In this case, modulation frequency is approx. 400 Hz while sampling frequency is approx. 4 kHz (1:10 ratio). Digital feedback loop is realized as simple integral feedback, similar to analog solution where integrator is often used after demodulation as feedback controller. Integrator constant then defines the bandwidth of magnetometer (but also can cause oscillations when too fast/too high gain, due to other zeros/poles in transfer function of magnetometer).

In reference to IEEE copyrighted material which is used with permission in this thesis, the IEEE does not endorse any of CTU's products or services. Internal or personal use of this material is permitted. If interested in reprinting/republishing IEEE copyrighted material for advertising or promotional purposes or for creating new collective works for resale or redistribution, please go to http://www.ieee.org/publications_standards/publications/rights/rights_link.html to learn how to obtain a License from RightsLink. If applicable, University Microfilms and/or ProQuest Library, or the Archives of Canada may supply single copies of the dissertation. DOI: 10.1109/TMAG.2018.2873235

A Digitally Compensated AMR Magnetometer

David Novotný, Vojtěch Petrucha, and Michal Janošek

Department of Measurement, Faculty of Electrical Engineering, Czech Technical University in Prague, 16627 Prague, Czech Republic

This paper considers the possibilities of using digital feedback for precise anisotropic magneto-resistance (AMR) magnetometers using commercial off-the-shelf (COTS) components. Requiring only a few analog parts, most of the signal processing is done digitally within an STM32 microcontroller. Because most of the precision is made by the feedback circuit, the analog-to-digital converter (ADC) can be a low-cost type. The compensation source is made with a pulsewidth modulation-driven H-bridge sourced from a voltage reference, so the cost reduction when compared to a "full-analog" design is large. The demodulation of a flipped-AMR signal is done with software after the AD conversion because it improves the offset stability and brings the reduction of the preamp's and ADC's LF noise. This paper presents the full characterization of a real instrument, including its noise, linearity, stability, and power consumption.

***Index Terms*— Anisotropic magneto-resistance (AMR), commercial off-the-shelf (COTS), digital feedback, magnetic sensor, STM32.**

I. Introduction

ANISOTROPIC magneto-resistance (AMR)-based magnetometers are typically used for measuring weak magnetic fields (2 nT/1 mT). They generate a higher noise than traditional fluxgate sensors (approximately one order of magnitude or more) but can have a smaller sized sensor head (by mass and volume), lower power consumption, and their sensors are generally available on the commercial market [1], [2]. Typical applications include compassing, general navigation, current measurements, and recently even space research [3], [4]. AMRs can be used as the main sensor [5] or as an auxiliary sensor to clean out the measurements of a precise fluxgate sensor—to remove disturbances caused by the satellite itself [6].

Most magnetometers [1], [7], [8] use a "analog feedback" solution because a digital feedback design has been related to costly application-specified integrated circuit (ASIC) ICs [9], [10]. In this paper, we show a novel method of how a readily available commercial off-the-shelf (COTS) STM32 microcontroller (MCU) can replace an ASIC while preserving the precision of an analog or ASIC digital solution. Using digital feedback is also very advantageous for possible applications in space where it is generally easier to provide radiation tolerance for the digital parts [(with a single field-programmable gate array (FPGA)] rather than for a large amount of precise analog parts.

Feedback compensation of a sensor is an indirect measurement method that uses the sensor only as a "zero indicator." The measurement output is proportional to the compensation value, which is the current through the compensation coil. This improves the main measurement parameters, because a sensor operates only in a small range, with close to a zero value. Nonlinearity, hysteresis, and gain drift are minimized and are caused mostly by the compensation system itself. Offset drift and noise are still given by sensor parameters and can potentially be a bit worsened by feedback compensation.

The main part of a compensation concept is the controlled current source for the feedback coil. One possibility is to use a precise, COTS DAC, but the relatively high cost must be considered. On the other hand, almost all modern MCUs have many pulse-width modulation (PWM) channels; when an MCU is combined with an external H-bridge and a precise voltage reference, a precise, low-cost DAC is created. However, the disadvantage to this method is the low resolution of the PWM, since its output frequency is given by the main MCU peripheral frequency divided by the resolution. If the output frequency is high, a high main frequency is also needed. High resolution can be obtained, for example, by using an FPGA, for which multiple delay-locked loops, delay lines, or ring oscillators are available, or by using a special type of microcontroller. STM32F334 is designed particularly for use with dc/dc and motor drivers. It can generate a PWM signal with the equivalent of 4.6 GHz main frequency by calibrated delay taps, which interpolate 32 fractions of a single PWM cycle, running at ∼144 MHz.

The DAC's voltage to current conversion is accomplished according to Ohm's law and uses a stable serial resistor with a much larger value than the feedback coil's resistance. This simple, efficient method has some constraints. The added resistance value must be much larger than the coil's resistance; however, the maximum current is limited by the DAC's full-scale (FS) output divided by this resistance, which constrains the magnetometer's FS range.

A vector compensation of the measured magnetic field was used so that it should cause a better cross-field effect attenuation [11]. However, the comparison with an individual compensation which was also realized did not show any significant difference.

II. Magnetometer Design

A. Principle of Operation

Because the feedback-compensated sensor works only in a small range around zero, the preamplifier and analog-to-digital

Manuscript received July 15, 2018; revised September 6, 2018; accepted September 17, 2018. Date of publication October 24, 2018; date of current version December 18, 2018. Corresponding author: D. Novotný (e-mail: novotd12@fel.cvut.cz).

Color versions of one or more of the figures in this paper are available online at http://ieeexplore.ieee.org.

Digital Object Identifier 10.1109/TMAG.2018.2873235

0018-9464 © 2018 IEEE. Personal use is permitted, but republication/redistribution requires IEEE permission.
See http://www.ieee.org/publications_standards/publications/rights/index.html for more information.

Authorized licensed use limited to: CZECH TECHNICAL UNIVERSITY. Downloaded on April 25,2024 at 13:47:07 UTC from IEEE Xplore. Restrictions apply.

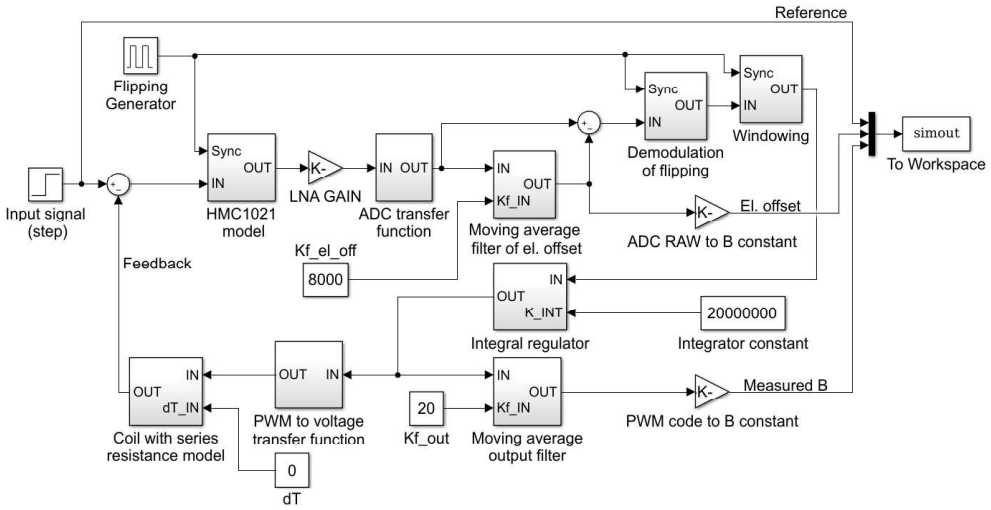

Fig. 1. Simulink model of magnetometer.

converter (ADC) gain can be set at a high value to achieve the noise floor below the sensor's noise. Only a large signal response can be affected by a large gain, since the feedback loop propagation delay causes the ADC to go over-range and thus causes a short-term nonlinear behavior in a feedback loop. This effect can, however, be reduced if the compensation is faster than the desired magnetometer output bandwidth by using output smoothing/filtering.

The measured magnetic field is completely compensated. Our approach uses a single range bipolar-PWM DAC (using an SMT32 high-resolution timer), which has a better linearity and a simpler design compared to a two-DAC solution [9]. The PWM duty cycle is also held in 5%–95% range to keep the nonlinearity low in the FS range (50% ≡ zero compensation field). The disturbing signal at the PWM frequency is suppressed through multiple means. First, a capacitor is connected parallel to the compensation coil, effectively short-circuiting the ac component of the PWM signal.

Care must be taken to avoid the resonance mode of the *RLC* circuit. In this manner, an attenuation of about 60 dB is achieved. Suppression is performed by the ADC input filter (about 20 dB). Last, the sigma-delta ADC's (MCP3912) over-sampling ensures a further attenuation of about 60 dB. A total attenuation of >140 dB is sufficient to prevent the PWM waveform from affecting the measurement.

To keep offsets and offset drifts low, the AMR sensors are periodically "flipped" with a frequency of ∼420 Hz, which also suppresses the LF noise of the preamplifier and ADC through modulation and demodulation [12].

A simulation circuit of the magnetometer can be seen in Fig. 1. This MATLAB-Simulink model has been used for the magnetometer's behavior verification.

B. Feedback Compensation

A current source for the compensation coils is created by a PWM-controlled voltage source with a large resistance in series with the coils as can be seen in Fig. 2.

For a coil with a resistance of R_C [Ω], a magnetic constant K [T/A], a voltage source with a maximum

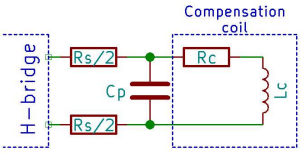

Fig. 2. Compensation coil connection.

voltage U_{ref} [V], a PWM codeword C [−], and a serial resistance R_S [Ω], we get (1) for the compensation field if an N [bit]-resolution PWM is used. The maximum compensated field can be then calculated by (2)

$$B = K \cdot \frac{2 \cdot U_{\text{ref}}}{(R_c + R_s)} \cdot \left(\frac{C}{2^N} - 0.5\right)[T] \tag{1}$$

$$B_{\text{MAX}} = \pm K \cdot \frac{U_{\text{ref}}}{(R_c + R_s)}. \tag{2}$$

Temperature drifts caused by this method can be derived by substituting both resistances in (3), and the resulting absolute drift rate is shown in (4)

$$R_x(\Delta T) = R_{0_x}(1 + \alpha_x \Delta T) \tag{3}$$

$$\frac{\partial B}{\partial \Delta T} = -K \cdot \frac{2 \cdot U_{\text{ref}} \cdot (R_c\alpha_c + R_s\alpha_s)}{(R_c + R_s + (R_c\alpha_c + R_s\alpha_s) \cdot \Delta T)^2} \cdot \left(\frac{C}{2^N} - 0.5\right)\left[\frac{T}{K}\right]. \tag{4}$$

The relative drift rate is then equal to (5) and neglecting the temperature-dependent term leads to (6) since it has a very small influence

$$\frac{\frac{\partial B}{\partial \Delta T}}{B} = -\frac{R_c\alpha_c + R_s\alpha_s}{R_c + R_s + (R_c\alpha_c + R_s\alpha_s) \cdot \Delta T}[\text{K}^{-1}] \tag{5}$$

$$\frac{\frac{\partial B}{\partial \Delta T}}{B} \cong -\frac{R_c\alpha_c + R_s\alpha_s}{R_c + R_s}[\text{K}^{-1}]. \tag{6}$$

It can be seen that for the lowest drift, R_s, should be kept as high and as stable as possible. Also, the coil's resistance and drift should be minimized if the design allows, also the geometric stability affects the coil's constant. In the developed prototype, the following values were used: $R_c = 100\ \Omega$,

Authorized licensed use limited to: CZECH TECHNICAL UNIVERSITY. Downloaded on April 25,2024 at 13:47:07 UTC from IEEE Xplore. Restrictions apply.

$\alpha_c = 3900$ ppm/K, $R_s = 2000\ \Omega$, and $\alpha_s = 20$ ppm/K. These inputs lead to the overall sensitivity drift of the magnetometer being equal to 205 ppm/K. For the best performance of the FS range-to-drift rate ratio, U_{ref} and the coil's constant K should be kept as high as possible.

In our case, the reference voltage was 10 V and the coil constant $K = 34\ \mu$T/mA. The magnetometer range calculated by (2) is $B_{\text{MAX}} = \pm 162\ \mu$T.

The parallel capacitor C_P used to attenuate the PWM's ac component had a value of 3.3 μF.

C. Theoretical Noise Limits of the AMR Sensor (HMC1021)

If the magnetic noise is neglected (since it cannot be removed by any signal processing method), the noise limits can be calculated only through the thermal noise of the equivalent bridge resistance. Using the AMR's sensitivity S [V/T] and its equivalent bridge resistance R [Ω], the theoretical limit of the noise density B_n can be calculated as follows:

$$B_n = \frac{\sqrt{4k_B T R}}{S} \cong \frac{1.3 \cdot 10^{-10} \cdot \sqrt{R}}{S} \left[\frac{T}{\sqrt{\text{Hz}}}\right] \tag{7}$$

where k_B is Boltzmann's constant $[J/K]$, T is the absolute temperature $[K]$.

For the Honeywell HMC1021 sensors used, which are powered by a voltage 10 V ($R = 1100\ \Omega$, $S = 100$ V/T), a value of $B_n \cong 43\ pT/\sqrt{\text{Hz}} \equiv U_n \cong 4,3\ \text{nV}/\sqrt{\text{Hz}}$ is obtained. A preamplifier with a white noise density of 1–3 nV/$\sqrt{\text{Hz}}$ does not add much noise to the measurement. With a bridge resistance of 1100 Ω, the current noise of the op-amp is non-negligible—an amplifier with a maximum current density of 1–2 pA/$\sqrt{\text{Hz}}$ should be used.

The total noise of the magnetometer is mostly given by the root of the sum of the squares of the sensor noise and preamplifier voltage and current noise (8)

$$B_{\text{TOT.}} = \sqrt{B_{n\_\text{SENSOR}^2} + \left(\frac{U_{n\text{PREAMP}}}{S}\right)^2 + \left(R_B \cdot \frac{\text{I}_{n\text{PREAMP}}}{S}\right)^2}. \tag{8}$$

The bridge amplifier developed for this purpose uses low-cost, low-noise ADA4004 op-amps with a total voltage and current noise of $U_{n\text{PREAMP}} = 2.5\ \text{nV}/\sqrt{\text{Hz}}$ and $I_{n\text{PREAMP}} = 1.7\ \text{pA}/\sqrt{\text{Hz}}$, and leads to 53 pT/$\sqrt{\text{Hz}}$ theoretical noise density of the magnetometer. Additional, amplification ($G = 32$) provides a gain stage built into the ADC converter.

D. Power Considerations

The setup requires minimal power, most of which is needed for the AMR bridges excitation with their low-noise preamps and feedback compensation. Because the AMR's noise level indirectly depends on the voltage/current supply value, it is best to keep the supply as high as possible, unless lowering power consumption is of higher priority. Attention must be given when increasing the AMR bridge supply current/voltage because power dissipation within the sensor is quadratically dependent on the current/voltage.

In a feedback circuit, the main cause of power dissipation is considered to be the current through the compensation coils times the H-bridge voltage, with the dropout voltage in a regulator (because the power of a bipolar PWM-waveform is constant over the full range).

A low-noise amplifier is another non-negligible source of power loss that should be considered. The amplifier with two ADA4004s per channel has a power consumption of 0.2 W for all three measurement axes together.

The contribution of these different parts to the total power consumption of the developed magnetometer is shown in Table I.

Other factors that increase power consumption include the microcontroller, ADC, H-bridge drivers, and flipping. Because one input voltage is desired, the power supply efficiency plays an important role.

TABLE I
CONTRIBUTIONS TO TOTAL POWER CONSUMPTION

Attribute	Value
Bridge power	3x 0.15 W (0.45 W)
Compensation	3x 0.08 W (0.24 W)
Preamplifier	3x 0.07 W (0.21 W)
Total	3x 0.3 W (0.9W)

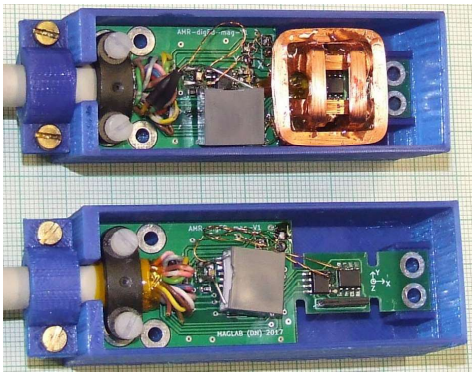

Fig. 3. Photograph of both individual and vector-compensated sensor heads.

III. PROTOTYPE OF THE MAGNETOMETER–PARAMETERS

In Fig. 3, a photograph of both the individual and the vector-compensated sensor heads can be seen.

As an important parameter of any measurement device, the linearity of the digitally compensated magnetometer has been tested. The sensor head has been placed in the Lee-Whiting coils [13] driven by a PC-controlled current source. The magnetic field has been swept and the output of the magnetometer is recorded. The FS linearity error of the vector-compensated sensor head can be seen in Fig. 4 (four independent measurements; the spikes at zero field are most likely caused by the current source used). It is clear that the linearity error is within about ± 60 ppm of FS for a ± 150-μT range; for a smaller range, e.g., $\pm 100\ \mu$T, a linearity error of ± 20 ppm can be achieved.

The noise floor—as it limits the dynamic range—has also been measured. Fig. 5 shows a comparison of the calculated and measured values of noise density versus the frequency using Welch's method. For further comparison, the noise density at 10 Hz can be used as it is above the $1/f$ corner

Authorized licensed use limited to: CZECH TECHNICAL UNIVERSITY. Downloaded on April 25,2024 at 13:47:07 UTC from IEEE Xplore. Restrictions apply.

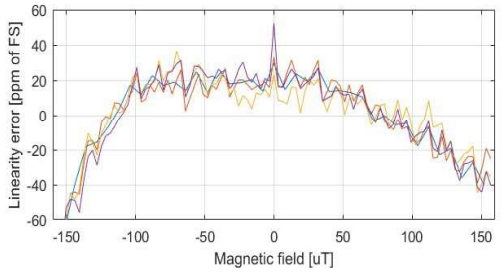

Fig. 4. Linearity error in magnetic field range ±150 μT.

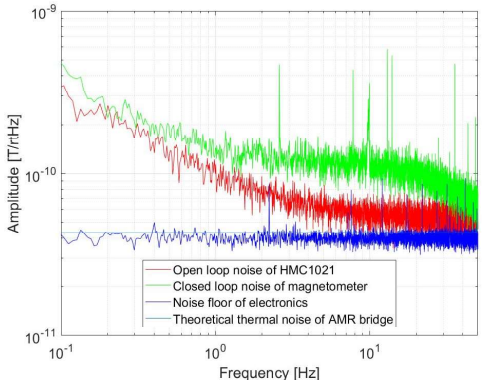

Fig. 5. Comparison of noise density spectra.

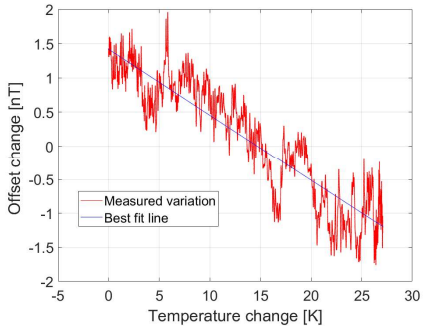

Fig. 6. Measured offset drift as temperature changes.

of the magnetic LF noise. The noise floor of the electronics, when measured with an equivalent bridge resistance, was found to be 38 pT/$\sqrt{\text{Hz}}$ and the overall magnetometer noise in an open loop was 55 pT/$\sqrt{\text{Hz}}$ with a limited ±15-μT range. It increased in a closed loop to 110 pT/$\sqrt{\text{Hz}}$. It can be seen that for very low frequencies (<1 Hz), the magnetic noise dominates as the noise in the open and closed loop slowly converges toward similar values greater than the electronics noise. All measurements have been made with flipping and were obtained inside a six-layer, permalloy magnetic shield.

In Fig. 6, the offset measurement can be seen. The sensor head has been placed inside a thermostatic, six-layered magnetic shield. The temperature slope has been created and the magnetometer output is recorded. The best-fit line has a slope of ~0.1 nT/K. Such a good value for an AMR magnetometer has been achieved through the software demodulation of flipping because the resulting drift is caused only by the magnetic drift of the sensor. The gain drift was found as approximately 200 ppm/K, which has been measured simultaneously with the offset drift by applying an ac magnetic field with a constant amplitude of about 10 μTpp created in the Lee-Whiting coils, in which the sensor was placed.

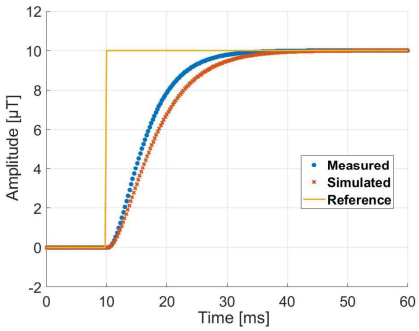

Fig. 7. Simulated and measured step response comparison.

TABLE II
PARAMETERS OF THE DEVELOPED TRI-AXIAL MAGNETOMETER

Attribute	Value
Full-scale range	± 150 µT
Nonlinearity	± 60 ppm
Noise density at 1 Hz	150 $pT/\sqrt{Hz}$
Integral noise (0.1-10 Hz)	440 pT_{RMS}
Offset drift	0.1 nT/K
Gain drift	200 ppm/K
Digital resolution	20 bit
Datarate (max/normal)	4000/250 Sa/s
Power consumption	2.2 W
Input voltage range	10-30 V

Fig. 7 shows the measured dynamic behavior (10-μT step response) which agrees with the waveform predicted by the Simulink model. The sensor head in this measurement has been placed into the Lee-Whiting coil, which has been connected to the square wave generator with a high output amplitude (20 V_{PP}) and a high series resistance because it lowers the L/R time constant while achieving the desired magnetic field step.

IV. CONCLUSION

This paper has presented a complete design and operating model for a digitally compensated magnetometer using COTS components, together with the measured parameters of a real prototype (Table II). The measured noise, linearity, and stability proved the usability of the concept because the parameters were comparable to a state-of-the-art magnetometer [9].

A second prototype is currently in development, with the aim of decreasing the power consumption by improving the power supplies as well as lowering the gain drift using feedback coils with a higher field constant and a lower resistance.

ACKNOWLEDGMENT

This work was supported by the Czech Technical University, Student Grant Competition Award No SGS18/081/OHK3/1T/13.

REFERENCES

[1] P. Ripka, *Magnetic Sensors and Magnetometers*. Norwood, MA, USA: Artech House, 2001.
[2] M. J. Caruso, T. Bratland, C. H. Smith, and R. Schneider, "A new perspective on magnetic field sensing," *Sensors Mag.*, vol. 15, no. 12, pp. 34–46, Dec. 1998.

Authorized licensed use limited to: CZECH TECHNICAL UNIVERSITY. Downloaded on April 25,2024 at 13:47:07 UTC from IEEE Xplore. Restrictions apply.

[3] M. Díaz-Michelena, "Small magnetic sensors for space applications," *Sensors*, vol. 9, no. 4, pp. 2271–2288, 2009.
[4] W. Magnes and M. Díaz-Michelena, "Future directions for magnetic sensors for space applications," *IEEE Trans. Magn.*, vol. 45, no. 10, pp. 4493–4498, Oct. 2009.
[5] P. Bown *et al.*, "Corrigendum: Magnetoresistive magnetometer for space science applications," *Meas. Sci. Technol.*, vol. 23, no. 5, p. 025902, 2012.
[6] U. Auster *et al.*, "Space weather magnetometer set with automated AC spacecraft field correction for GEO-KOMPSAT-2A," in *Proc. ESA Workshop Aerosp. (EMC)*, 2016, pp. 1–6, doi: 10.1109/AeroEMC.2016.7504585.
[7] J. M. G. Merayo, P. Brauer, F. Primdahl, J. R. Petersen, and O. V. Nielsen, "Scalar calibration of vector magnetometers," *Meas. Sci. Technol.*, vol. 11, no. 2, pp. 120–132, 2000.
[8] V. Fúra *et al.*, "Construction of an AMR magnetometer for car detection experiments," *IOP Conf. Mater. Sci. Eng.*, vol. 108, no. 1, p. 012028, 2016.
[9] S. Leitner *et al.*, "Design of the magnetoresistive magnetometer for ESA's SOSMAG project," *IEEE Trans. Magn.*, vol. 51, no. 1, Jan. 2015, Art. no. 4001404.
[10] W. Magnes *et al.*, "Highly integrated front-end electronics for space-borne fluxgate sensors," *Meas. Sci. Technol.*, vol. 19, no. 11, p. 115801, 2008.
[11] V. Petrucha, V. Fúra, and A. Platil, "Cross-field effect in a triaxial AMR magnetometer with vector and individual compensation of a measured magnetic field," *IEEE Trans. Magn.*, vol. 53, no. 4, Apr. 2017, Art. no. 4000305.
[12] J. Včelák, P. Ripka, A. Platil, J. Kubík, and P. Kašpar, "Errors of AMR compass and methods of their compensation," *Sens. Actuators A, Phys.*, vol. 129, nos. 1–2, pp. 53–57, 2006.
[13] J. L. Kirschvink, "Uniform magnetic fields and double-wrapped coil systems: Improved techniques for the design of bioelectromagnetic experiments," *Bioelectromagnetics*, vol. 13, no. 5, pp. 401–411, 1992.

Authorized licensed use limited to: CZECH TECHNICAL UNIVERSITY. Downloaded on April 25,2024 at 13:47:07 UTC from IEEE Xplore. Restrictions apply.

4.2. Analog processed, digitally compensated fluxgate magnetometer

Fluxgate technology is also interesting due to its very low noise and long tradition in space applications. Proposed solution with dual feedback (analog + digital) originates from my bachelor thesis [54], but it has been further developed, tested and published later, as can be seen in conference proceedings article below.

This magnetometer has been mainly targeting geomagnetic applications as it measures only small portion of total magnetic field (it works as a variometer) while biggest part is statically compensated. This allows to obtain very high dynamic range as long as the static field removal method itself is stable enough. But this feature can be beneficial also in space applications where there are small variations of magnetic field being measured in relatively high common mode. Moreover, in the presented prototype, Actel's FPGA is used as this FPGA is made also in radiation tolerant variant (anti-fuse), suitable for space environment.

High dynamic range fluxgate magnetometer

David Novotný, Vojtěch Petrucha
Department of Measurement, Faculty of Electrical Engineering,
Czech Technical University in Prague

***Abstract*—In this paper, possibilities of achieving high dynamic range for fluxgate magnetometer are discussed. For a fluxgate sensor with its own noise in orders of few pT, operating in 60 uT Earth's magnetic field, dynamic range of >150 dB is necessary to exploit full potential of such a sensor. Even the most precise AD converters have usually maximum dynamic range of about 140 dB (given by its noise floor and full-scale range), so only digitization of the full sensor's output range isn't sufficient. In order to measure small variations in a large bias, a variometric arrangement can be used instead. ADC then digitizes only small range of the magnetometer as most of measured magnetic field is removed by a precise compensation system. This system must be very stable and low-noise as it has major impact on resulting noise and stability of the measurement. Low noise design based on precise analog components (AD, DA, voltage reference) controlled by FPGA with a soft-core processor is presented in this paper with a full characterization of the developed prototype.**

Keywords—fluxgate, FPGA, magnetometer, variometer

I. Introduction

Measurement of disturbances in Earth's magnetic field is important for many scientific and practical application such an earthquake detection and localization, Sun's activity measurement, geological prospecting, etc. [1,2]. These variations are very small, with magnitude in orders from tens of pT to few tens of nT in a frequency range approx. 1mHz-1Hz [2]. As a total value of Earth's magnetic field is around 50 µT (depending on location, 20-60 µT), high dynamic range of measurement is necessary. For this purpose, fluxgate sensors are preferred as they has lowest noise compared to other vector (room temperature operated) magnetometers [3]. Fluxgates are sometimes used in a combination with scalar type magnetometer [4] as this combination can benefit from their high long-term stability (and potentially can correct fluxgate drifts).

As one can found pretty hard to digitize signal with >150 dB dynamic range, another way is to remove "stable" part of measured signal instead and measure only small variations. Such concept is called variometer and requires very stable current source for driving compensation coils. Whole stability and noise of variometer is given by such a current source, and off course, by sensor itself.

One way is to use a constant current source for a stationary magnetometer, where bias field will be also static [5]. A prior knowledge is necessary to determine required current and coil constant leading to usability only in a small area of applications. Another option is to have controlled current source with at least few steps (only to get with measured value in ADC's range).

For this purpose, low noise, precise DAC AD5791B has been used. Its 20-bit resolution is unnecessary, but it has very good long term and temperature stability with a superior noise performance. With 167 nV_{RMS} noise in 0.1-10 Hz bandwidth and output span of 20 V, leads to noise floor of ~160 dB.

As DAC is in fact only a controllable voltage divider, stable and low noise voltage reference is a main part of the current source. It's parameters in a combination with DAC's parameters are determining resulting parameters of the whole circuit. State of the art bandgap reference LTC6655 has been used. It has 0.25 ppm_{p-p} noise in the 0.1 to 10 Hz range [6], to get even lower with the noise, four LTCs has been placed in parallel to get half of a single reference's noise (which brings theoretically 155 dB limit).

For controlling whole variometer, FPGA has been used as it can implement all necessary logic, timing and even a soft-core microcontroller (Cortex M1).

II. Magnetometer Design

A. Principle of operation

A magnetometer in a variometric arrangement usually incorporates a traditional analog fluxgate sensor that works only in a small range (e.g. ±3 µT) and output is held in approximately mid range (zero value) by variometric compensation system that has steps equal or smaller than half of fluxgate's range.

This compensation system can be done as dynamic (fluxgate is all the time controlled to not over-range) or "one-shot" when magnetometer's compensation is fixed (during installation at operation location) and after that doesn't change (potentially can get over-range, but high linearity and low signal distortion in that sub range is achieved).

Simplified diagram of the variometer operation can be seen in Fig. 1. Blue lines illustrates decreasing magnetic field, while red lines increasing. Hysteresis within half of ADC's range and equal to DAC step size can be seen.

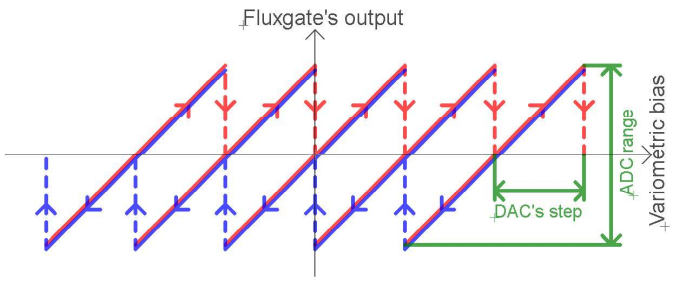

Fig. 1. Illustration of operation - dynamic ranging

B. Compensation system

As compensation current is always derived from the main voltage reference, it must be selected with high attention on noise and stability. Even state-of-the-art references aren't low-noise enough not to affect the measurement and the only way to lower their noise is using statistics (as their noise can be considered as uncorrelated, averaging output of N references lowers the noise by $\sqrt{N}$ factor).

Current through the compensation coils is controlled by a voltage to current converter (operational amplifier with a stable current sense resistor). Noise of such an amplifier and even the thermal noise of a sense resistor must be also taken into account.

Compensation coils are often tri-axial, compensating individual components of a magnetic field vector (in fluxgate's sensitivity directions).

C. *Fluxgate subsystem*

A traditional fluxgate circuit is used (processing of a second harmonic signal with an integrator feedback loop).

Sensor is kept in a precise zero magnetic field by feedback to maintain high linearity and stability, while variometric DAC keeps sensor only in approximately zero. Residuum compensated by fluxgate's feedback is digitized by ADC as measurement output (when summed with added variometric bias). Simple equation to combine DAC and fluxgate output is in (1).

$$B_{meas.} = C_{FG} \cdot U_{OUT\,FG} + C_{VAR} \cdot U_{OUT_{DAC}} \qquad (1)$$

Where $B_{meas.}$ is measurement output [T], C_{FG} is fluxgate constant [V/T], $U_{OUT\,FG}$ is fluxgate's output voltage, C_{VAR} variometric compensation's contant [T/V] and $U_{OUT_{DAC}}$ is output voltage of DA converter [V].

D. *FPGA controller*

For fluxgate excitation and synchronous demodulator control, FPGA can be used with the advantage of logic reprogramability. It is typically necessary to tune phase shift between excitation and demodulator signals which is easy to implement in the FPGA. Some of them also allows to use IP-core microprocessors such as Cortex-M1, designed for FPGAs or 8051-like cores [7].

III. PRACTICAL REALIZATION

A simplified block diagram of designed magnetometer can be seen in Fig 3. Fig 2 is a photograph of a complete magnetometer setup with all necessary supporting electronics.

Fig. 2. Photograph of complete magnetometer with sensor head in right corner

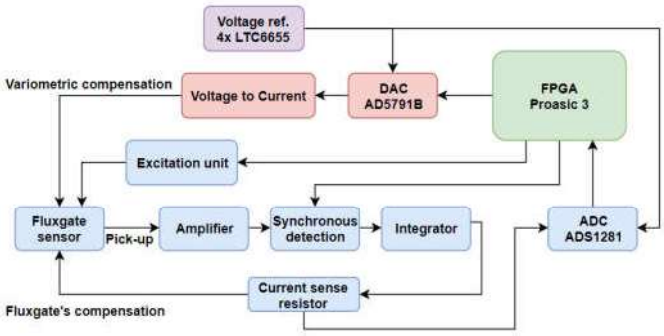

Fig. 3. Simplified block diagram of the instrument

A. *Voltage reference circuit*

To lower the drift of voltage references (LTC6655), four of them have been connected to average their outputs. Measured noise can be compared to theoretical $\sqrt{N}$ decay in Fig. 4.

With 5 V nominal voltage, specified 0.25 $ppm_{p\text{-}p}$ noise in 0.1 to 10 Hz band should equal to 1.25 $\mu_{p\text{-}p}$ and approx. 190 nV_{RMS}. It can be seen that such a value hasn't been achieved even through careful low-noise design (measured with a spectrum analyzer and very-low-noise preamp based on LT1028).

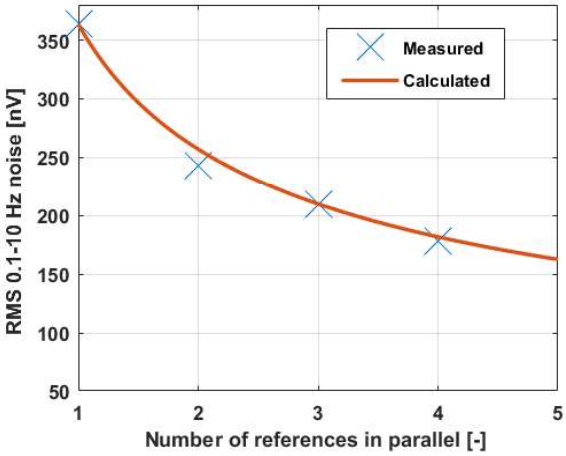

Fig. 4. Measured and calculated noise of multiple LTC6655

B. ***Digital to Analog converter***

AD5791B has been used as a currently available lowest noise and most stable DA converter. Noise measurement has been done with using only one and then with all four references. Initial noise of DAC, rising proportionally to output voltage can be seen in Fig. 5.

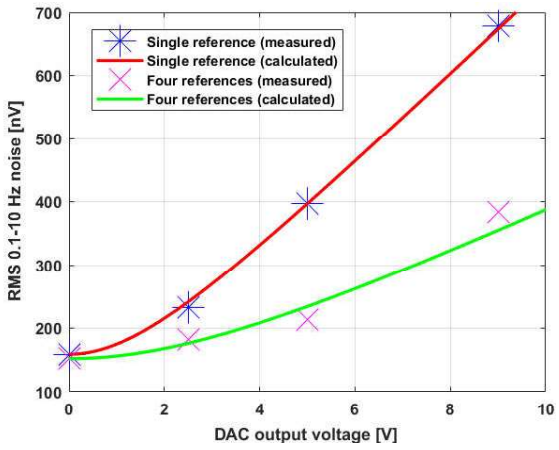

Fig. 5. Measured and modeled noise of DAC vs. output voltage

Dependence of noise on output voltage can be modeled as in (2), when noise is considered as uncorrelated.

$$U_{n_{TOTAL}} = \sqrt{U_{n_{DAC}}^2 + \left(U_{n_{REF}} \cdot \frac{U_{OUT}}{U_{REF_{NOM}}}\right)^2} \qquad (2)$$

With $U_{n_{DAC}}$ [VRMS] intrinsic noise of DAC, nominal reference voltage $U_{REF_{NOM}}$[V], noise of references $U_{n_{REF}}$ [VRMS] and output voltage of DAC U_{OUT} [V].

With measurement in Fig. 5. DAC's intrinsic noise of 160 nV_{RMS} can be found. This value can be compared to 1.1 $\mu V_{p\text{-}p}$ catalogue value [9] which is approx. equal to 167 nV_{RMS}. This measurement also leads to noise description of the whole magnetometer in dependence on measured field as in Fig. 6.

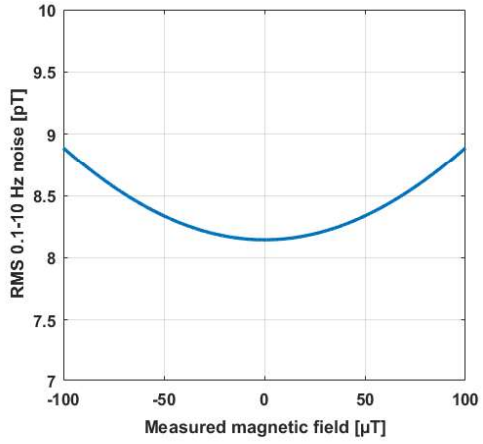

Fig. 6. Simulated noise dependence on measured magnetic field

C. Summing of compensation's

While most of measured magnetic field is compensated by variometric compensation, small residuum is still compensated by analog fluxgate's compensation. Summing of this two compensations can be done with two individual coils with separate voltage to current converters or with one converter and summing resistors node. Two coils design has been used and tested. Desired compensation constant's ratio is tuned with turn counts of used Merritt coils [8] and by current sense resistors.

D. Magnetometer model

For stability and step response verification, a Matlab Simulink model has been created. Small signal (without DAC bias change) and large signal step response (dynamic variometer mode) can be seen in Fig. 7 and Fig. 8. Fluxgate with its feedback (small-signal response) can be modeled as a LTI system with transfer function given by (3).

$$H(s) = \frac{U_{out}}{B_{meas.}} = \frac{\frac{R_S}{K_C}}{\frac{\tau \cdot (R_C + R_S)}{K_C \cdot G_d \cdot C_S} \cdot s + 1} \qquad (3)$$

Where U_{out} is output voltage [V], $B_{meas.}$ is measured magnetic field [T], R_s is resistance of current sense resistor [Ω], R_c resistance of feedback coil [Ω], τ time constant of an integrator [s], K_c coil constant [T/A], G_d gain of preamplifier [V/V], C_s open-loop sensitivity of fluxgate [V/T].

Time constant τ_s of a feedback compensation is given by (4) with real parameters of magnetometer and resulting low-pass cut-off frequency f_C by (5).

$$\tau_s = \frac{\tau \cdot (R_c + R_s)}{K_c \cdot G_d \cdot C_s} \cong \frac{1}{115{,}2} \cong 8.7\ ms \qquad (4)$$

$$f_C = \frac{1}{2 \cdot \pi \cdot \tau_s} \cong 18.3\ Hz \qquad (5)$$

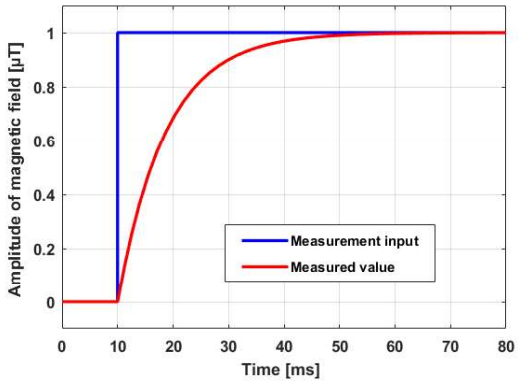

Fig. 7. Small signal step response of variometer

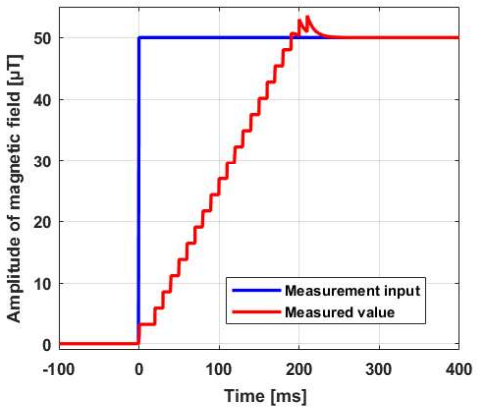

Fig. 8. Large signal step response of variometer (dynamic mode)

IV. Measured Parameters of the Magnetometer

A. Noise characterization

Firstly, sensor's intrinsic noise has been measured. Sensor head with a ring-core fluxgate has been placed into 6-layer Permalloy shielding, operated in open-loop, processed with

SR830 lock-in amplifier. In Fig. 9, measured noise spectral density can be seen with a typical 1/f character and marker placed at 1 Hz, showing amplitude of 2.08 $pT/\sqrt{Hz}$ and integral noise has been 8 pT_{RMS} (0.1-10 Hz).

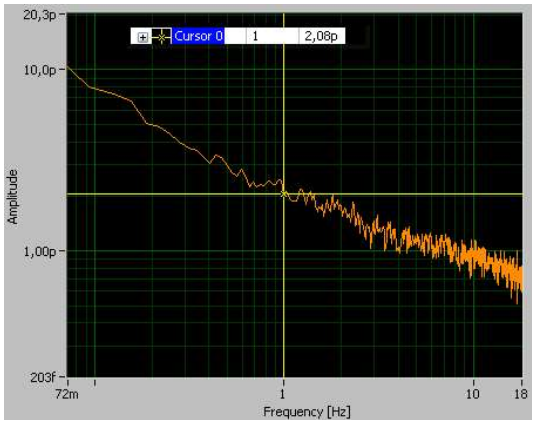

Fig. 9. Noise density spectrum of open loop fluxgate sensor

For a complete magnetometer working in a closed loop, total noise has been measured and can be found as approx. 18 pT_{RMS} and with noise density of 4.5 $pT/\sqrt{Hz}$ at 1 Hz (Fig. 10). A bit worse result in a comparison to open-loop measurement with lock-in amplifier is given by fluxgate's demodulator noise as disconnection of variometric feedback haven't noticeable effect on noise.

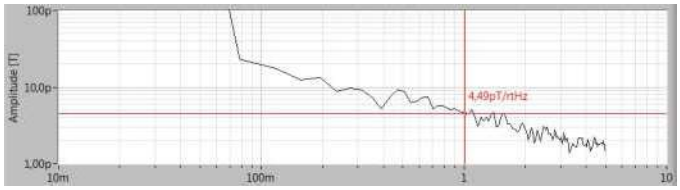

Fig. 10. Noise density spectrum of designed magnetometer

B. *Variometer's linearity in full range*

With correctly calibrated ratio between fluxgate's and variometric compensations, linearity error as small as in Fig. 11 has been measured (two separate measurements, red and blue line). Linearity error can be found as small as ±10 ppm in ±100 µT range.

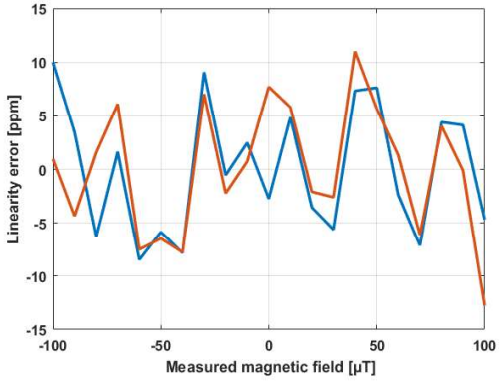

Fig. 11. Linearity error measurement

V. CONCLUSIONS

With the presented variometric method, desired dynamic range has been almost reached, with approx. 18 pT_{RMS} noise within ±100 µT range of measurement, noise floor is -141 dB. Reduction of fluxgate's electronics noise is still under progress, targeting to reach open-loop noise measured with a lock-in amplifier. Theoretically maximum limit given only by used fluxgate sensor is 8 pT_{RMS} (-148 dB), when measured and modeled noise of variometric compensation is taken into account, 9 pT_{RMS} (-147 dB) noise floor should be achieved.

When power consumption, price and dimensions of magnetometer's electronics aren't much important, LTZ1000A can be considered as LTC6655 replacement, as it has even lower noise (but requires moderate amount of supporting electronics and has not negligible power consumption as it is thermo-stated buried Zener diode).

Linearity of a presented variometer is reaching values typical for single-range "full-field" magnetometers and makes it very precise and versatile.

ACKNOWLEDGMENT

This work was supported by the Student Grant Competition (SGS) at CTU in Prague, No. SGS18/081/OHK3/1T/13.

REFERENCES

[1] J. Valenta, "Introduction to Geophysics: Lecture Notes", available at: http://www.geology.cz/ (7/2018).

[2] S. M. Potirakis, A. Schekotov, T. Asano, and M. Hayakawa, "Natural time analysis on the ultra-low frequency magnetic field variations prior to the 2016 Kumamoto (Japan) earthquakes", *Journal of Asian Earth Sciences*, vol. 154, pp. 419-427, 2018.

[3] P. Ripka, "Magnetic Sensors and Magnetometers," Artech House, 2001

[4] L. Tøffner-Clausen, V. Lesur, N. Olsen, and C. C. Finlay, "In-flight scalar calibration and characterisation of the Swarm magnetometry package", *Earth, Planets and Space*, vol. 68, no. 1, p. -, 2016.

[5] M. Janošek, V. Lesur, M. Vlk, and C. C. Finlay, "Low-noise magnetic observatory variometer with race-track sensors", *IOP Conference Series: Materials Science and Engineering*, vol. 108, no. 1, p. 012026-, Mar. 2016.

[6] Linear Technology (Analog Devices), "LTC6655 datasheet", available at: https://www.analog.com/ (7/2018)

[7] Microsemi, "FPGA IP Cores", available at: https://www.microsemi.com/ (7/2018)

[8] J. L. Kirschvink, "Uniform magnetic fields and double-wrapped coil systems: Improved techniques for the design of bioelectromagnetic experiments, " Bioelectromagnetics, vol. 13.5, pp. 401-411, 1992.

[9] Analog Devices, "AD5791 datasheet", available at: https://www.analog.com/ (7/2018)

4.3. Digitally processed and compensated fluxgate magnetometer

The goal of this phase of the development was to put also the rest of signal processing to digital domain, i.e. not only compensation feedback loop but also demodulation. This was done using FPGA development board. Principle is similar to the first shown paper with digital AMR prototype.

Typical parallel fluxgate excitation frequency is usually in 10-20 kHz range, pick-up signal that carry information is on second harmonic, i.e. 20-40 kHz. To meet Nyquist criteria, sampling frequency has been chosen to ten times of this frequency (fexcit = 20 kHz, fs = 200 kHz).

Sampled signal was then processed in FPGA – demodulated using simple synchronous demodulation (±1x multiplication) then filtered and decimated. From the point of view of noise, a little improvement can be obtained here when multiplying by pure sinewave, instead of ±1 rectangle, to obtain sensitivity only on second harmonics. But even with this simple implementation, the obtained noise spectra were promising.

A lot of attention was dedicated to linearity as an important, yet often omitted parameter of precise instrument. Excellent ±5 ppm linearity has been achieved using differential PWM based DAC.

In reference to IEEE copyrighted material which is used with permission in this thesis, the IEEE does not endorse any of CTU's products or services. Internal or personal use of this material is permitted. If interested in reprinting/republishing IEEE copyrighted material for advertising or promotional purposes or for creating new collective works for resale or redistribution, please go to http://www.ieee.org/publications_standards/publications/rights/rights_link.html to learn how to obtain a License from RightsLink. If applicable, University Microfilms and/or ProQuest Library, or the Archives of Canada may supply single copies of the dissertation. DOI: 10.1109/SENSORS47125.2020.9278852

High Dynamic Range Digital Fluxgate Magnetometer

David Novotný, Vojtěch Petrucha
Dept. of Measurement, Faculty of Electrical Engineering, Czech Technical University in Prague, Czech Republic
novotd12@fel.cvut.cz

***Abstract*— In this paper, we present an advanced fully digital solution of a fluxgate magnetometer with both demodulation and compensation carried out by a low-cost field programmable gate array (FPGA). For feedback operation, we avoid using a costly precise digital-to-analog converter, instead employing an FPGA to generate a hybrid pulse width modulation sigma-delta signal. Even with only a few additional components to process such signals, we were able to achieve excellent linearity, noise, and stability, as supported by measurements. On the front-end side only one pick-up signal preamplifier is necessary, greatly reducing the number of analog circuits needed. This can be an advantage in radiation-hazard sites like space missions, as there are fewer radiation-susceptible parts that can degrade. We provide a short description of the entire setup—electronics, fluxgate sensor construction, and final power budget—and a parameter summary in the conclusion.**

Keywords—fluxgate magnetometer, digital processing, FPGA, PWM DAC, feedback, radiation, tolerant, space, CubeSat

I. INTRODUCTION

Fluxgate sensors and magnetometers are applied in many areas where precise measurement of weak magnetic fields is desired, such as geological surveys [1], navigation [2], and scientific experiments [3]. Traditionally, in parallel fluxgates the second harmonic output signal from pickup winding is processed using amplifiers, band-pass filters, synchronous demodulation, and integration and often fed back to the sensor to compensate the measured magnetic field. This feedback operation then significantly improves parameters like linearity and stability [4]. The analog signal processing chain requires precise analog components that are expensive and sensitive to environmental conditions. Once digital electronic circuits became suitable for this task, efforts have been made to carry out ideally all or at least some of the signal processing using exclusively digital circuits. This should lead to magnetometers that are less susceptible to temperature changes and radiation, simpler, and, thus, less expensive. Analog signal processing with subsequent high-resolution digitalization is typically still used for applications demanding a very high dynamic range (>140 dB) but, as digital circuits become more powerful, the digital approach is quickly catching up.

In 1993 Primdahl et al. [5] digitized the broadband fluxgate output signal using an analog-to-digital converter (ADC) with just an 8-bit resolution to obtain a noise level of 1 nT for a 100 Sa/s data rate. Since then, many other researchers have implemented various topologies and techniques to obtain better parameters.

Auster [6] presented synchronous sampling at twice the signal frequency using ADC, field programmable gate array (FPGA) and digital-to-analog (DAC) topology for space research and geomagnetic applications, the principle was later used in the ROMAP instrument [7] and THEMIS fluxgate magnetometer [8]. A different approach is found in [9], which uses relaxation time measurement via digital counters. Feintuch et al. [10] patented a digital fluxgate magnetometer with multiplication of digitized reference and pick-up signals and further processing (infinite impulse response [IIR] filter and decimation). Korepanov and Berkman [11] analyzed the structure of analog and digital magnetometers and summarized the theoretical limits of their operation. Pedersen [12] presented a concept of a digital fluxgate magnetometer for the Astrid-2 space mission based on DSP and 18-bit DAC for feedback, which limited performance. Later, an application-specific integrated circuit (ASIC) was designed, implementing a similar principle with an analog front-end and digital parts [13,14]. O'Brien [15] designed a radiation-tolerant digital fluxgate magnetometer with second order $\Delta\sum$ modulator implemented in FPGA with good noise properties (10 pT/√Hz) but with an extremely limited measurement range of ±327 nT. Another approach by Zhi et al. [16] involves using two 16-bit DACs to supply the V/I feedback driver. Although the presented noise is low (7 pT/√Hz) with ±65 μT range, there is no detailed information concerning the linearity that might be affected by the dual DAC summing circuit.

In this paper, we present the development of a fluxgate magnetometer with digital signal processing with high dynamic range and excellent linearity and noise. As noted above, the properties are influenced by the DAC used for the compensation feedback. Based on previous good experience with pulse width modulation (PWM)-based DAC [17], we decided to use this technique together with precise 16-bit ADC at the input and state-of-the-art, low-power FPGA, because the data processing would not work at the desired rate (200–400 kHz) within a microcontroller, as was possible for the anisotropic magneto-resistance version flipped at 216 Hz.

II. DESCRIPTION OF OPERATION

The fluxgate magnetic core is excited by MOSFET bridge with resonant capacitor in series connection to an excitation coil for better power efficiency. The induced voltage from the pickup coil (second harmonic of excitation signal) is amplified by an AC-coupled differential amplifier that also acts as a low-pass filter and ADC driver. The signal is then converted to digital domain using a fast successive-approximation ADC (AD4005). Conversions are triggered by FPGA synchronously with an excitation unit (200 kSa/s). The digitized signal is then demodulated by a synchronous demodulator (±1 multiplication). After demodulation, the unwanted part of the frequency spectrum is removed by a

978-1-7281-6801-2/20/$31.00 ©2020 IEEE
Authorized licensed use limited to: CZECH TECHNICAL UNIVERSITY. Downloaded on April 25,2024 at 13:48:02 UTC from IEEE Xplore. Restrictions apply.

synchronous moving average (MA) filter. In the case of open-loop operation, this signal is decimated to a lower sample rate and streamed via a universal asynchronous receiver-transmitter (UART) link. For closed-loop operation, the demodulated and filtered signal is fed to a digital integrator. The output of the integrator is multiplied by a constant to obtain proper response and fed to the PWM module as a duty-cycle value. The PWM value is filtered by another moving average filter and sent through a serial link in closed-loop mode as an output variable (because it is proportional to the compensation magnetic field, which is the measured quantity). A simplified diagram is presented in Fig. 1, and photograph of the electronics is presented in Fig. 2.

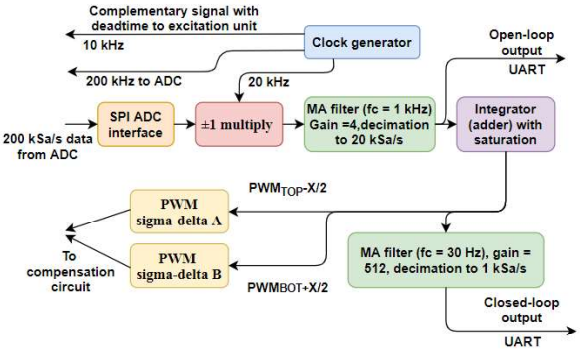

Fig. 1. Block diagram of digital signal processing on FPGA.

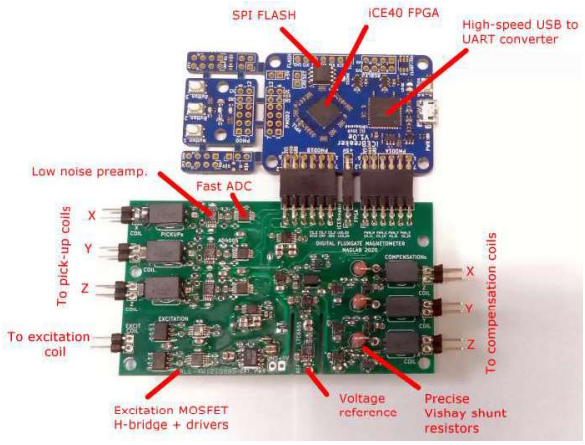

Fig. 2. Photo of three-axis fluxgate magnetometer's electronics (blue board is the iCEBreaker kit; green board is the electronics of the developed magnetometer on which this paper reports).

A. Hybrid PWM delta-sigma DAC

To achieve higher resolution at the same carrier frequency, PWM is improved by the delta-sigma principle. The least significant bit of PWM is modulated to fine trim its duty-cycle mean value. The base frequency of FPGA is 96 MHz; for a 15-bit PWM, this means a maximum frequency of ~3 kHz, while for a 20-bit PWM it is only ~93 Hz. With this hybrid scheme, it is possible to obtain 20-bit resolution at 3 kHz carrier frequency. The attenuation factor at 93 Hz (the worst-case delta-sigma cycle frequency) can then be 2^{15} = 32768 times lower than using 20-bit PWM without delta-sigma.

The DAC hardware is described in the schematic in Fig. 3. Two PWM signals from the FPGA drive analog multiplexers that create precise-amplitude PWM out of voltage reference (LTC6655-4.096V). The signals are then filtered with second order RC low pass filters and fed to voltage to a current converter.

The main challenge was that the analog multiplexer could not be heavily loaded because of its nonlinear R_{ON} resistance versus input voltage behavior that otherwise causes nonlinearity of the entire DAC. On the other hand, high resistance would lead to high Johnson-Nyquist noise. From measurement (Fig. 4), a compromise was found to be 100 kΩ of minimum load resistance.

Rail-to-rail operational amplifiers are another practical design problem, as low-noise versions often have nonlinear behavior of offset voltage/bias current with common-mode voltage that worsens the resulting linearity. To ensure the best performance, it was necessary to keep common mode voltage as close to half the supply voltage as possible, which was obtained by a differential DAC design (using two channels [A, B] of the PWM with an opposite duty cycle to create the resulting signal). This design also suppresses phase-jitter in the main clock by affecting both channels' duty cycles simultaneously. This is subtracted by this design; the residual nonlinear behavior of the loaded multiplexer DAC is also decreased (Fig. 5).

The noise of the current source was measured with an Agilent 35670A dynamic signal analyzer and found to be approx. 400 $pA_{RMS}/\sqrt{Hz}$ at 1 Hz, within ±7.5 mA full-scale range. In relative terms, this is noise of 0.03 $ppm_{RMS}/\sqrt{Hz}$ at 1 Hz. In a magnetometer with a range of ±75 μT, this relative noise will cause additional noise of 4 $pT_{RMS}/\sqrt{Hz}$ at 1 Hz.

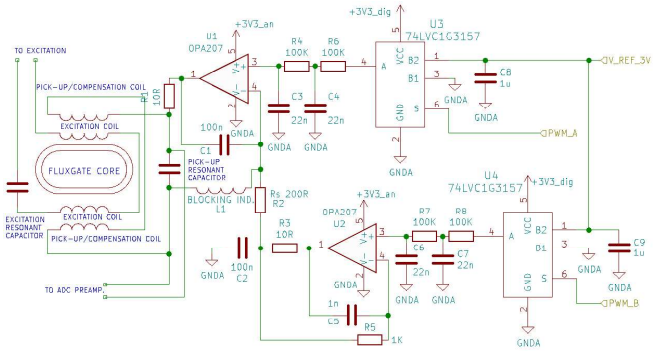

Fig. 3. Scheme of current source based on differential PWM design.

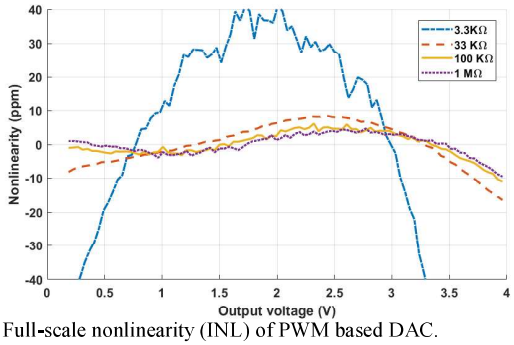

Fig. 4. Full-scale nonlinearity (INL) of PWM based DAC.

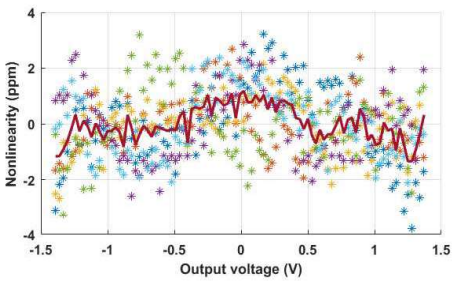

Fig. 5. Full-scale nonlinearity of differential PWM based DAC.

Authorized licensed use limited to: CZECH TECHNICAL UNIVERSITY. Downloaded on April 25,2024 at 13:48:02 UTC from IEEE Xplore. Restrictions apply.

B. Digital demodulation

For simplicity in initial testing, demodulation was performed by ±1 multiplication of acquired signal at twice the excitation frequency. This synchronization signal can be phase-shifted against excitation signal. For best performance, the phase should be adjusted for the highest mean value of demodulated signal when fluxgate is measuring a non-zero magnetic field.

C. Power consumption

Power consumption of each electronic section was measured separately (measurements include losses on low dropout regulators, common 5V input voltage for the entire magnetometer). The compensation circuit has 32 mW consumption (single channel, no compensation current, 68 mW when compensating for full 75 µT). Power consumption of sensor excitation is 320 mW. Input circuit (ADC + amplifier/driver) requires 200 mW/channel. FPGA + UART interface takes 250 mW. Total power drawing is 800 mW for one axis; it should thus be 1.2 W for the tri-axial version.

D. Sensor head

Fluxgate sensor (Figs. 6,7) has a race-track core (17.4 mm long) laser-cut from highly permeable soft magnetic material Vitrovac 6025. The magnetic core was field annealed to decrease sensor noise [18]. Support for compensation winding and the core is CNC milled out of FR4 material (glass-reinforced epoxy laminate). For the tri-axial magnetometer, sensors are mounted on a low thermal expansion composite plastic cube, which is CNC milled with very high precision so that the combination of four mounting holes for each sensor leads to a precise level of orthogonality. The excitation current was measured to be 800 mA_{p-p}. We also tested higher excitation current but obtained no additional improvements in noise.

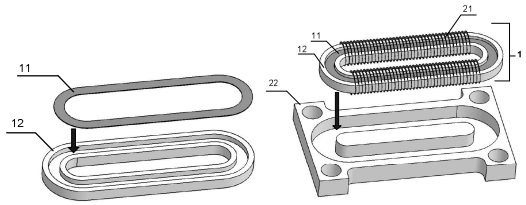

Fig. 6. Drawings of fluxgate sensor construction (11-magnetic core, 12-protection case for core, 22-support for compensation coil, 21-excitation winding; pick-up winding not shown).

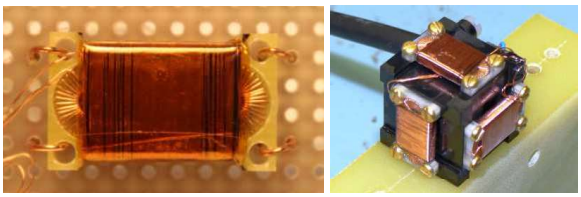

Fig. 7. Photos of fluxgate sensor heads (left-single axis; right-triaxial).

III. MEASURED PARAMETERS

A. Linearity measurement

Measurement of transfer function linearity was performed by sweeping the PWM value throughout its range while sending the actual value by serial link to a PC. The current output of DAC was connected to a precise and stable 120 Ω shunt resistor while an HP34401A multi-meter measured the voltage drop. The HP34401A was also connected to the PC via serial link; LabView-based software saved incoming values (actual PWM and measured voltage) to file for post-processing in MATLAB, where linear fit was subtracted from transfer function and a nonlinearity curve was obtained (Fig. 8). The same technique has also been used in previous linearity measurements (Figs. 4,5) but directly measured voltage without a shunt resistor.

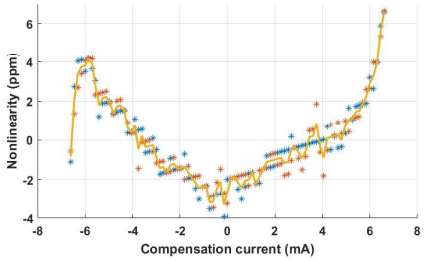

Fig. 8. Full-scale nonlinearity of current source based on differential PWM.

B. Noise measurement

In the first step of noise measurement, a lock-in amplifier SR830 was used instead of ADC and demodulation on FPGA. The sensor was excited by an excitation unit controlled by FPGA which also generated a synchronization signal. With the same excitation waveform and pickup resonant capacitor, the signal was then demodulated by FPGA (in open-loop operation with ±5 µT range). A comparison of the noise spectrum densities appears in Fig. 9. The slightly higher noise of the FPGA demodulated signal is caused by the noise floor of input differential amplifier (based on LTC6362).

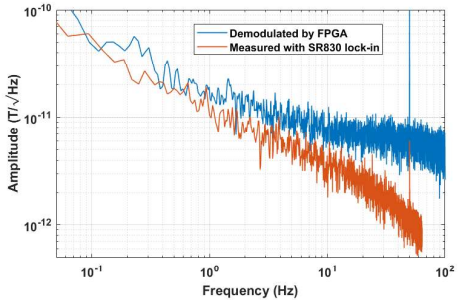

Fig. 9. Spectrum noise density of demodulated fluxgate comparison.

IV. CONCLUSION

The results presented in this paper suggest that even a simple PWM DAC approach can lead to a very precise current source. The presented prototype achieved key parameters of 20-bit resolution, ±5 ppm linearity, and 0.03 ppm/√Hz @ 1 Hz noise; it also has good preconditions for high time and temperature stability (as no voltage dividers or summing nodes can drift with temperature, only with the voltage reference and current sense resistor).

When combined with digital demodulation of the pickup signal, we obtain a fully digital solution of a fluxgate magnetometer at a very low cost in electronics for such a precise instrument. As a next step, the tri-axial version will be tested and optimized for low power consumption. We are also planning to perform measurement of temperature drifts and testing radiation effects by Co^{60} gamma-source.

ACKNOWLEDGMENT

This work was supported by a Student Grant Competition (SGS) at CTU in Prague (No. SGS19/177/OHK3/3T13).

Authorized licensed use limited to: CZECH TECHNICAL UNIVERSITY. Downloaded on April 25,2024 at 13:48:02 UTC from IEEE Xplore. Restrictions apply.

REFERENCES

[1] B. Gavazzi, P. Le Maire, J. Mercier de Lépinay, P. Calou, and M. Munschy, "Fluxgate three-component magnetometers for cost-effective ground, UAV and airborne magnetic surveys for industrial and academic geoscience applications and comparison with current industrial standards through case studies," Geomech. Energy. Envir., vol. 20, Article 100117, December 2019, https://doi.org/10.1016/j.gete.2019.03.002.

[2] J. Včelák, P. Ripka, and A. Zikmund, "Precise magnetic sensors for navigation and prospection," J. Supercon. Nov. Magn., vol. 28, no. 3, pp. 1077–1080, 2015.

[3] C. T. Russell, B. J. Anderson, W. Baumjohann, K. R. Bromund, D. Dearborn, D. Fischer et al., "The magnetospheric multiscale magnetometers," Space Sci. Rev., vol. 199, nos. 1–4, pp. 189–256, March 2016.

[4] P. Ripka, Magnetic Sensors and Magnetometers, Boston: Artech House Remote Sensing Library, 2001.

[5] F. Primdahl, B. Hernando, J. R. Petersen, and O. V. Nielsen, "Digital detection of the flux-gate sensor output signal," Meas. Sci. Technol., vol. 5, no. 4, pp. 359–362, April 1994.

[6] H. U. Auster, A. Lichopoj, J. Rustenbach, H. Bitterlich, K. H. Fornacon, O. Hillenmaier et al., "Concept and first results of a digital fluxgate magnetometer," Meas. Sci. Technol., vol. 6, no. 5, pp. 477–481, May 1995.

[7] H.U. Auster, I. Apathy, G. Berghofer, A. Remizov, R. Roll, K. H. Fornacon et al., "ROMAP: Rosetta Magnetometer and Plasma Monitor," Space Sci. Rev., vol. 128, pp. 221–240, 2007.

[8] H.U. Auster et al, "The THEMIS Fluxgate Magnetometer," Space Sci. Rev., vol. 141, pp. 235–264, 2008.

[9] J. Blazek, J. Hudak, and D. Praslicka, "A relax type magnetic fluxgate sensor," Sens. Actuators A Phys., vol. 59, pp. 287–291, 1997.

[10] Feintuch et al., US Patent 5652512, July 29, 1997.

[11] V. Korepanov and R. Berkman, "Digital flux-gate magnetometer structural analysis," Meas. Sci. Technol., vol. 10, no. 8, 734–737, August 1999.

[12] E. B. Pedersen, F. Primdahl, J. R. Petersen, J. M. G. Merayo, P. Brauer, and O. V. Nielsen, "Digital fluxgate magnetometer for the Astrid-2 satellite," Meas. Sci. Technol., vol. 10, no. 11, pp. N124–N129, November 1999.

[13] W. Magnes, D. Pierce, A. Valavanoglou, J. Means, W. Baumjohann, C. T. Russell, K. Schwingenschuh, and G. Graber, "A sigma–delta fluxgate magnetometer for space applications," Meas. Sci. Technol. vol. 14, no. 11, pp. 1003–1012, July 2003.

[14] W. Magnes, M. Oberst, A. Valavanoglou, H. Hauer, C. Hagen, I. Jernej et al., "Highly integrated front-end electronics for spaceborne fluxgate sensors," Meas. Sci. Technol., vol. 19, no. 11, Article 115801, November 2008, https://doi.org/10.1088/0957-0233/19/11/115801.

[15] H O'Brien, P. Brown, T. Beek, C. Carr, E. Cupido, and T. Oddy, "A radiation tolerant digital fluxgate magnetometer," Meas. Sci. Technol., vol. 18, no. 11, pp. 3645–3650, November 2007.

[16] M. Zhi, L. Tang, X. Cao, and D. Quao, "Digital fluxgate magnetometer for detection of microvibration," J. Sens., vol. 2017, Article 6453243, 2017, https://doi.org/10.1155/2017/6453243.

[17] D. Novotný, V. Petrucha, and M. Janosek, "A digitally compensated AMR magnetometer," IEEE T. Mag., vol. 55, no. 1, pp. 1–5, January 2018.

[18] Petrucha, V. "Low-cost dual-axes fluxgate sensor with a flat field-annealed magnetic core." In 2016 IEEE Sensors Applications Symposium (SAS), pp. 1-4, IEEE, 2016, https://doi.org/10.1109/TMAG.2018.2873235.

Authorized licensed use limited to: CZECH TECHNICAL UNIVERSITY. Downloaded on April 25,2024 at 13:48:02 UTC from IEEE Xplore. Restrictions apply.

4.4. Radiation testing of developed AMR magnetometer

As radiation tolerance is crucial parameter in space-grade electronics, its extensive testing was performed on developed AMR magnetometers (multiple prototypes). Most radiation testing has been done using radioactive isotope of cobalt - ^{60}Co in ÚJV Řež facility near Prague. Radiation from this source is highly penetrative gamma ray beam with mostly two energy levels 1.17 and 1.33 MeV. In chapter 4.10 there are also shown unpublished results from heavy ion testing in HIMAC facility in Japan.

From survival point of view, total-ionising-dose (TID) is often used parameter of space-grade electronics specification. It is the accumulated dose over time (usually survival dose). There is also standard (MIL-STD-883) used for this kind of tests. TID should be recalculated to absorbed dose by most affected part of electronics – silicon (while dosimetry almost always uses equivalent dose absorbed by water). The MIL-STD-883 also specifies whether ionising rate is fast or slow because of different effects on tested electronics.

To measure the most of possible parameters during one irradiation session, complex PXI frame-based measurement system has been developed utilizing 32ch 24bit simultaneous sampling sigma-delta NI-4302 data acquisition card, and an auxiliary NI-6251 multifunction data acquisition card. Total 2x 13 channels from 2 prototypes have been measured together with serial data output stream from both magnetometers.

In reference to IEEE copyrighted material which is used with permission in this thesis, the IEEE does not endorse any of CTU's products or services. Internal or personal use of this material is permitted. If interested in reprinting/republishing IEEE copyrighted material for advertising or promotional purposes or for creating new collective works for resale or redistribution, please go to http://www.ieee.org/publications_standards/publications/rights/rights_link.html to learn how to obtain a License from RightsLink. If applicable, University Microfilms and/or ProQuest Library, or the Archives of Canada may supply single copies of the dissertation. DOI: 10.1109/I2MTC43012.2020.9129039

This full text paper was peer-reviewed at the direction of IEEE Instrumentation and Measurement Society prior to the acceptance and publication

AMR Magnetometer With Digital Feedback for Space Applications

David Novotný
Faculty of Electrical Engineering
Czech Technical University in Prague
Prague, Czech Republic
novotd12@fel.cvut.cz

Vojtěch Petrucha
Faculty of Electrical Engineering
Czech Technical University in Prague
Prague, Czech Republic
petruvoj@fel.cvut.cz

Michal Dressler
Faculty of Electrical Engineering
Czech Technical University in Prague
Prague, Czech Republic
dressmic@fel.cvut.cz

Antonín Platil
Faculty of Electrical Engineering
Czech Technical University in Prague
Prague, Czech Republic
platil@fel.cvut.cz

***Abstract*—In this paper, we present research and development regarding a novel concept of a digitally compensated, low-noise magnetometer based on anisotropic magnetoresistance sensors that is suitable for space applications. The central idea of the design is to reduce the number of precise analog components while using the digital signal processing power available in a modern microcontroller. Our most recent effort targeted lowering power consumption and overall improvement of the parameters. Only commercial off-the-shelf components are used in the concept reported here, keeping costs manageable even for low-budget CubeSat missions. The principle of operation is presented in detail, along with a full characterization of a real instrument, including its noise, linearity, and temperature stability. The results of Total Ionizing Dose testing at a gamma-ray irradiation facility are discussed at the complete magnetometer and part levels; they suggest the instrument's good potential.**

Keywords—anisotropic magnetoresistance (AMR), magnetometer, commercial off-the-shelf (COTS), digital compensation, feedback, microcontroller, CubeSat, radiation, tolerant

I. Introduction

Magnetometers are used in many different applications in space. Navigation and orientation stabilization of a satellite using different actuators (e.g., magneto-torquers) is a typical example, as is space weather monitoring to protect sensitive instruments, but they also have purely scientific applications like studying the magnetosphere of planets and other celestial bodies. Precise magnetic sensors are usually based on the fluxgate principle [1] or anisotropic magnetoresistance (AMR) sensors [2]. While fluxgates achieve lower noise and better stability [3], AMRs are cheaper, lighter, and more widely available commercially; they can also potentially achieve stability similar to fluxgates, as presented in our previous research [4]. These factors make AMRs attractive for low-cost applications.

Most space-grade magnetometers use special circuits—application-specific integrated circuit (ASICs) [2,5]—to achieve better radiation immunity and lower power consumption. But the use of ASICs or other special radiation-tolerant devices makes them costly and thus not easily obtainable for smaller projects with limited budgets. To address this issue, we propose a concept that uses only commercial off-the-shelf (COTS) components. As a main controller STM32F334 [6] is employed for its high resolution PWM (pulse-width-modulation) capability used for a digital compensation. All signal processing after analog-to-digital conversion is software based. The magnetic field is sensed by HMC1021 [7] and the AMR sensor operated as a closed-loop compensation system using the built-in offset coil. With feedback compensation, the sensor is used only as a zero indicator, and measurement output is the amplitude of compensation current that is fed to the offset coils. Traditionally, this indirect method of measurement enables higher performance in linearity, stability, and hysteresis [8].

AMR sensors often implement flipping coils that can be used to change (or "flip") the polarity of sensor sensitivity. This process is usually done periodically with frequencies in the Hz to kHz range and offers many advantages like electrical offset elimination; therefore, we used it, as described in section II.

In the magnetometer described in this paper, we used only COTS parts, without previous knowledge of those components' radiation tolerance. It is an enhanced version of our previous design, with power supply subsystem redesign, improved compensation current generation, and part selection being the main changes. While lists of COTS-tested parts exist [9], they do not include many modern active components: microcontrollers, operational amplifiers, voltage stabilizers, references, analog-to-digital converters (ADCs), and so on. Some parts, including AMR magnetic sensors, have been tested in different published projects [10-13], but those data are typically restricted to only one test—a Total Ionizing Dose (TID) using ^{60}Co gamma ray, neutrons, and heavy ions—and do not provide complete information concerning their behavior in space conditions.

We present the results of a TID test done at a ^{60}Co irradiation facility. As access to the facility is extremely limited, we designed the test setup to collect the maximum amount of information. A custom measurement system based on a PXIe frame, two data acquisition cards, and the LabVIEW control software was employed to acquire a variety of analog and digital signals during a 72-hour irradiation session that involved a total of 105 krad. We acquired 18 channels to determine the degradation of different components, such as the effects of drifting voltage reference, any op-amp offset shift in the current source generator, or problems in the AMR sensor itself.

II. Principle of Operation

As noted above, magnetic domain magnetization flipping and feedback compensation are used to achieve

978-1-7281-4469-3/20/$31.00 ©2020 IEEE
Authorized licensed use limited to: CZECH TECHNICAL UNIVERSITY. Downloaded on April 23,2024 at 13:57:12 UTC from IEEE Xplore. Restrictions apply.

highly precise measurements. The static transfer function (TF) of the magnetometer in the SET/RESET state of the flipping mode is described in eqs. (1) and (2) below. Equation (3) is the result of a synchronous demodulation applied to the measurement data modulated by the flipping process.

$$V_{set} = K_{ADC} \cdot \left(AD_{off} + K_{LNA} \cdot \left(LNA_{off} + HMC_{off_{EL}} + K_{HMC} \cdot \left(B_{meas} + B_{off}\right)\right)\right) \quad (1)$$

$$V_{res} = K_{ADC} \cdot \left(AD_{off} + K_{LNA} \cdot \left(LNA_{off} + HMC_{off_{EL}} - K_{HMC} \cdot \left(B_{meas} + B_{off}\right)\right)\right) \quad (2)$$

$$V_{out} = V_{set} - V_{res} = 2 \cdot K_{ADC} \cdot K_{LNA} \cdot K_{HMC} \cdot \left(B_{meas} + B_{off}\right) \quad (3),$$

where V_{set}, V_{res} is the voltage output of the bridge in the SET/RESET state (V), V_{out} is the output voltage after demodulation (V), K_{ADC} is the internal gain of ADC (-), AD_{off} is the offset of ADC (V), K_{LNA} is the gain of LNA (-), LNA_{off} is the offset of LNA (V), $HMC_{off_{EL}}$ is the electrical offset of HMC bridge (V), K_{HMC} is the sensitivity of the HMC bridge (V/T), B_{meas} is the measured magnetic field (T), and B_{off} is the magnetic offset of sensor (T).

Equation (3) shows that, after demodulation carried out in the firmware, the offset of the magnetic measurement is given only by the magnetic offset of the sensor itself. There is no contribution of the signal conditioning chain, making it unnecessary to use precise analog parts like operation amplifiers or ADC converters. Another important advantage is implied; there are no low-frequency noise requirements on the signal chain. The flipping frequency is set to approximately 216 Hz as a compromise between the useful bandwidth of the magnetometer and the digital signal processing speed. This frequency was also selected to ensure minimal interference with the local 50 Hz disturbing signal and its harmonic frequency. For sensor preamplifier design, only noise at this frequency and the bandwidth of the magnetometer are relevant. Most op-amps have 1/f corner on lower frequencies, so only the white noise is important.

In the feedback topology, the gain stability is given only by the compensation circuit (Fig. 1). Only the dynamic performance is affected by the gain change of the sensor itself and its conditioning circuit. This can be obtained from the frequency TF at a zero frequency. Equations (4), (5), and (6) describe the simplified TF of this magnetometer in a Laplace image domain.

$$V_{out} = K_{HMC} \cdot \left(B_{meas} - DAC_{COMP} \cdot K_{coil} \cdot \frac{V_{DAC\_ref}}{R_{sens}}\right) \quad (4)$$

$$DAC_{comp} = \frac{K_i}{s} \cdot K_{LNA} \cdot \frac{V_{ADC\_ref}}{ADC_{range}} \cdot V_{out} \quad (5)$$

$$H(s) = \frac{DAC_{comp}}{B_{MEAS}} = \frac{1}{\frac{ADC_{range}}{K_i \cdot K_{LNA} \cdot V_{ADC\_ref} \cdot K_{HMC}} \cdot s + K_{coil} \cdot \frac{V_{DAC\_ref}}{R_{sens}}} \quad (6),$$

where DAC_{comp} is the value set on compensation-DAC (-), V_{ADC_ref} is the reference voltage of ADC (V), ADC_{range} is the top value of ADC (-), K_i is the integrator constant (-), K_{coil} is the embedded coil constant (T/A), R_{sens} is the sense resistor of the voltage-to-current converter (Ω), and V_{DAC_ref} is the reference voltage of DAC (V).

Equation (7) shows that, for a zero frequency (DC gain), the TF is given only by

$$H(s) = \frac{R_{sens}}{K_{coil} \cdot V_{DAC\_ref}} \quad (7).$$

This means that the only contribution to gain drift is given by the constant of the compensation coil, the sensing resistor, and the reference voltage. The stability of the compensation system should be inherent (single pole TF), but this description is only approximate and do not handle delays of preamplifier or ADC's sampling that can cause oscillations. Stability must be ensured by the proper setting of the integral constant.

In a practical implementation, this means that there are only a very few requirements of the design of the electronics:
1) stability and noise of the main voltage reference
2) stability of the sensing resistor
3) white noise (at 180–250 Hz) of the bridge amplifier
4) stability and low-frequency (LF) noise of op-amps in the voltage-to-current converter and in the voltage reference buffer.

A band-gap voltage reference was selected because it should be less susceptible to irradiation than Zener diode based reference [14]. Our previous design used REF102 (10V required), while REF3430 (3V required) is used in the present design. As a low-noise preamp, OPA2210 was chosen for its low voltage and current noise at a flipping frequency and its low-voltage, rail-to-rail operation. For all other op-amps, where low LF noise was necessary, a low-voltage, rail-to-rail ADA4805 was used.

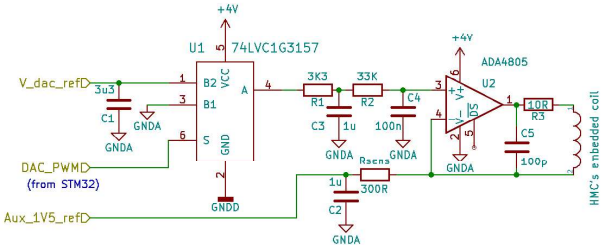

Fig. 1. Circuit diagram of PWM based compensation circuit

III. Radiation Testing

Because electronics operating in space must survive all types of radiation present in free space—gamma rays, neutron radiation, heavy ions, and electron beam radiation—it would be optimal to test for all types. However, different radiation sources are not easily accessible even for academic and research purposes, so we used ^{60}Co based gamma-ray irradiation that we could access through the ÚJV Řež facility near Prague. We consider this a first step in the instrument's qualification process. The test was planned in accordance with MIL-STD-883. The TID, based on the alanine-EPR dosimetry method, was 1.05 ± 0.03 kGy (105 ± 3 krad). This dose is related to the energy absorbed by water; for silicon (the main element in the tested electronics), it can be recalculated by eq. 8 [15].

$$D_{Si} = D_{H_2O} \cdot \frac{\mu_{Si}/\rho_{Si}}{\mu_{H_2O}/\rho_{H_2O}} = 0{,}898 \cdot D_{H_2O} \quad (8).$$

The corrected value for the TID absorbed by silicon is thus 943 ± 30 $Gy_{(Si)}$ (94.3 ± 3 $krad_{(Si)}$). Irradiation by this dose was performed in 72 hours. The results place the test in the low irradiation-rate category (0.36 rad/sec).

Authorized licensed use limited to: CZECH TECHNICAL UNIVERSITY. Downloaded on April 23,2024 at 13:57:12 UTC from IEEE Xplore. Restrictions apply.

Monitoring of internal signals of the magnetometer and logging serial data and the generation of the testing signal to the external coil were utilized with a PXIe frame with an embedded controller, an NI-4302 data acquisition card, and an auxiliary NI-6251 card as a software watchdog for the magnetometer (performing reset in case the magnetometer would stop sending serial data) and the generation of the sinusoidal signal to the testing coil (Fig. 2). Measurement setup was controlled through LabVIEW-based software with a remote access possibility.

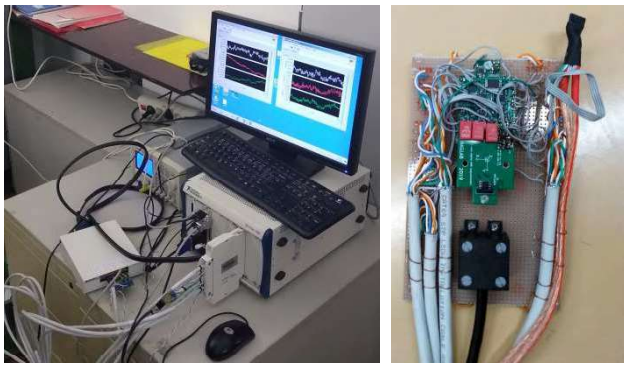

Fig. 2. Photo of a PXIe measurement setup (left) and D.U.T. (right)

Selected signals measured in the magnetometer are marked by letters A–N in Fig. 3. All channels had 60 Sa/s and measured voltage. Except for J, L, M, and N, signals were acquired at 5 kSa/s to be fast enough to measure the square (flipped) signal at 216 Hz. Channel A was the current measurement through a 0.25 Ω shunt resistor. Signal G was measured on a 300 Ω sense resistor of a voltage-to-current converter. Channels X and Z (the axes) were operated in open loop mode, while the Y axis was in a closed loop. The X axis had completely disconnected feedback (see the strikethrough of the signal in the diagram), while the Z axis had a constant value set on digital compensation to measure the drift of compensation current.

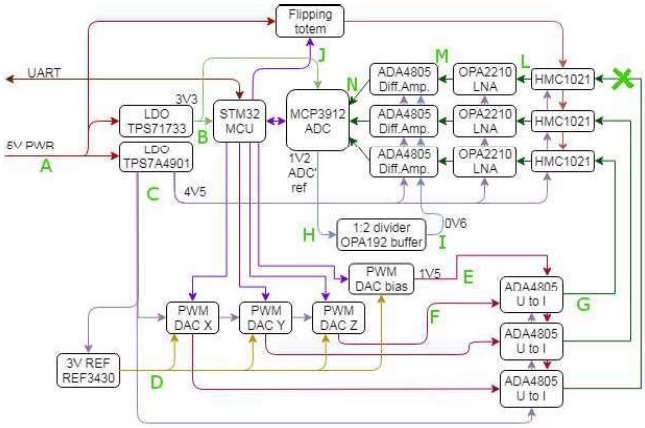

Fig. 3. Block diagram of magnetometer and test points

Fig. 4 shows the drift of low-dropout (LDO) regulators with rising TID. For reference, there was also a 5 V power supply measurement. TPS7A4901 showed almost no change (less than 1 mV deviation over a full 105 krad dose). On the other hand, TPS71733 degraded rapidly at 50 krad; its regulation feedback stopped working, the voltage dropped to about 1 V, and the magnetometer stopped working.

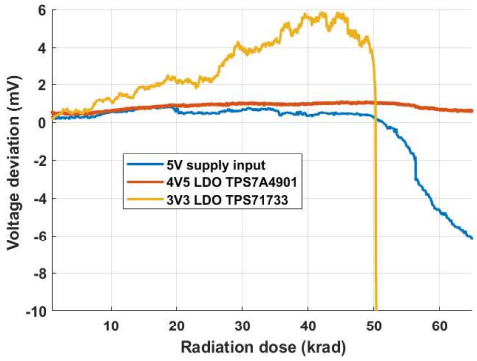

Fig. 4. Voltage regulators drift with irradiation

The voltage references drift is shown in Fig. 5. While the internal reference of ADC MCP3912 drifted only 1 mV/60 krad, the precision REF3430 reference showed a higher drift.

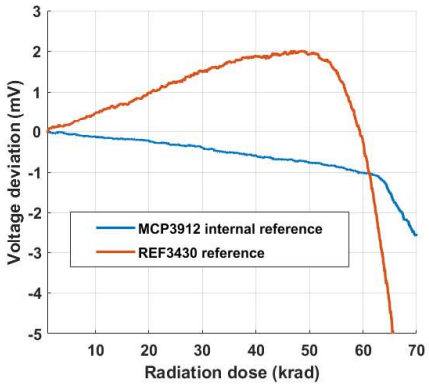

Fig. 5. Voltage reference drift with irradiation

Two different operation amplifiers populated on the magnetometer were tested for their offset drift as can be seen in Fig. 6. OPA197 had lower drift as the TID increased, but it stopped working because of a 3V3 voltage drop when the TPS71733 (discussed above) stopped working.

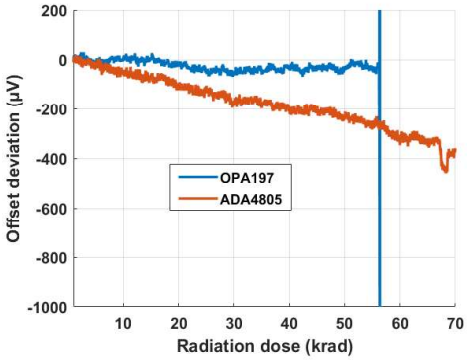

Fig. 6. Operation amplifiers offset drift with irradiation

As the offset and gain of the magnetometer are also directly given by the drift of the PWM digital-to-analog converter (DAC) feedback compensation, Fig. 7 shows the measurement of its drift when feedback was disabled and compensation was set to a constant drive of 800 µA. In Fig.

Authorized licensed use limited to: CZECH TECHNICAL UNIVERSITY. Downloaded on April 23,2024 at 13:57:12 UTC from IEEE Xplore. Restrictions apply.

7, the drift of reference (shown in Fig. 5) is compensated for to see only the PWM DAC drift. Current change was measured to be about 0.15 % after 60 krad.

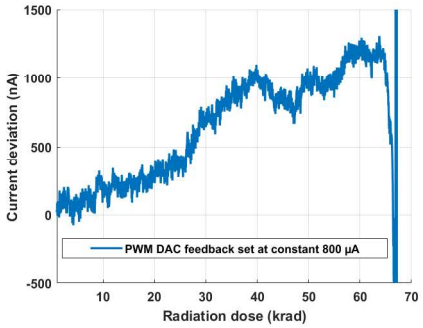

Fig. 7. PWM DAC amplitude drift with irradiation

At the same time as the PXI frame measured analog signals, serial data from the magnetometer were recorded to see what happened to output data from the magnetometer (with its output). Fig. 8 displays low-pass filtered (0.01 Hz) data from all three axes, showing the offset drift of the magnetometer. Unfortunately, there was a lot of surrounding magnetic noise (we had no magnetic shielding in the testing facility). However, noticeable drift could be extracted at approx. -0.27, -0.7, and +0.8 nT/krad for the x, y, and z axes, respectively.

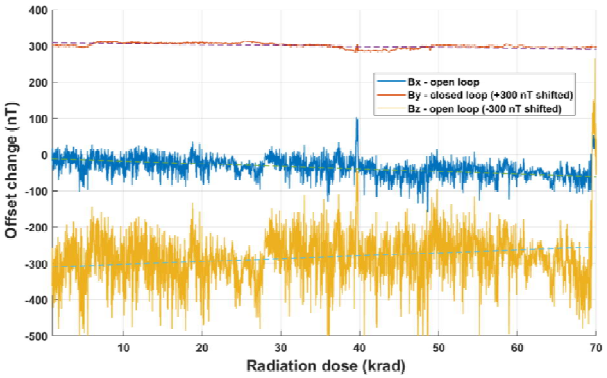

Fig. 8. Offset drift of magnetometer with irradiation

For gain drift measurement, coil with excitation sine wave (3 Hz) was used, driven from an auxiliary NI card (± 10V drive, with a 2 kΩ stable resistor in series with coil, which then behaves more like current source). When this signal is extracted from magnetometer's reading (bandpass), its envelope change enables the calculation of gain deviation; the processed data are shown in Fig. 9.

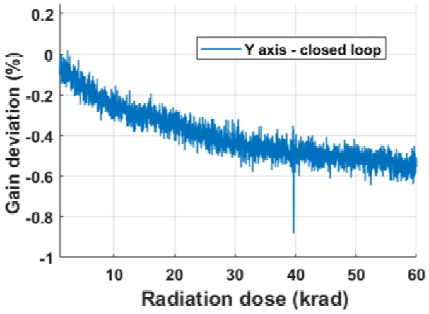

Fig. 9. Gain drift of magnetometer with irradiation

IV. PARAMETERS OF FINAL PROTOTYPE

The prototype's magnetic noise (Fig. 10) was measured in a six-layer permalloy shielding, allowing sub-pT/rtHz noise density to be measured.

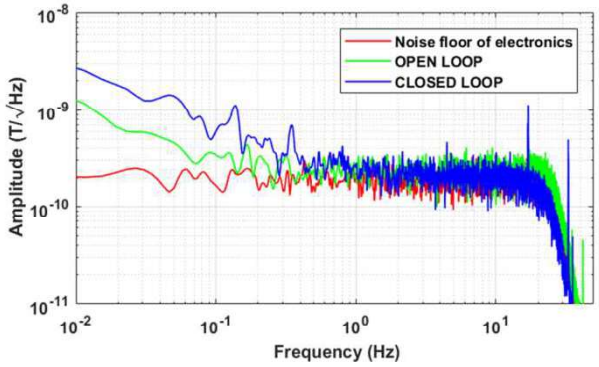

Fig. 10. Noise density spectra comparison

Sensitivity and orthogonality temperature coefficients (TCs) were obtained using the fast thin-shell calibration method [16] while the temperature of the magnetometer was varied within the range of -10 °C to 20 °C (Fig. 11, 12).

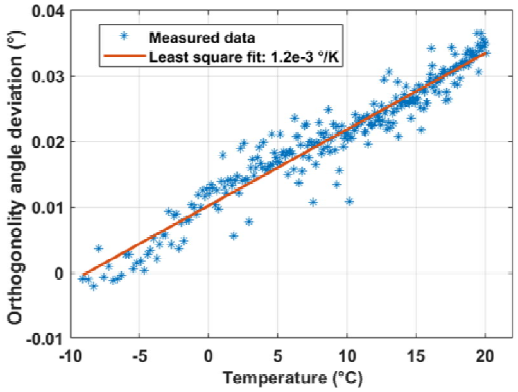

Fig. 11. Temperature drift of orthogonoality angle (X to Y axis)

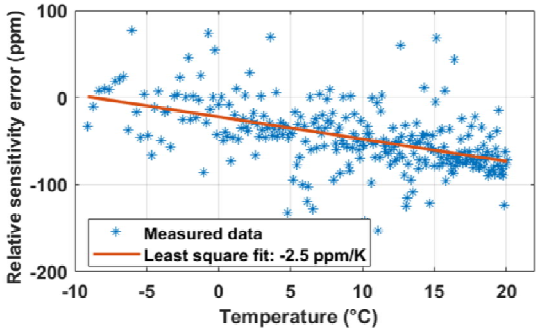

Fig. 12. Temperature drift of gain/sensitivity of magnetometer

The offset drift thermal coefficient was measured in a six-layer permalloy magnetic shielding with an embedded cryostat/thermostat, with temperature ranging from -15 °C to 22 °C without any noticeable hysteresis (Fig. 13) - only small dynamic error in part of fast cooling.

Authorized licensed use limited to: CZECH TECHNICAL UNIVERSITY. Downloaded on April 23,2024 at 13:57:12 UTC from IEEE Xplore. Restrictions apply.

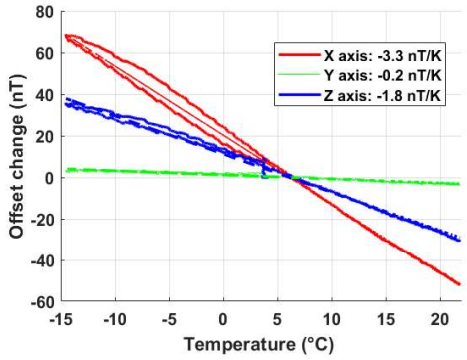

Fig. 13. Temperature offset drift of magnetometer

For nonlinearity and cross-field measurement, a magnetic field sweep with magnitude of ± 100 µT with 400 steps was applied, and the magnetometer's response was logged. Excited axis nonlinearity (obtained by subtraction of a least-square ideal line) was considered to be the nonlinearity itself, while the response of the perpendicular axis gave information about cross-field sensitivity (the radiation testing is described in detail in section III). All measured parameters are summarized and compared to commercial magnetometer [17] in Table 1 and photos of the prototype are shown in Fig 14.

TABLE I. PARAMETERS OF THE DEVELOPED PROTOTYPE
[a]At component level

Parameter	Value	Commercial magnetometer
Range	± 100 µT	± 60 µT
Nonlinearity	± 50 ppm	NA
Offset TC	< 3.5 nT/K	NA
Sensitivity TC	< 10 ppm/K	NA
Orthogonality TC	< 0.01 °/K	NA
Crossfield sensitivity	± 50 ppm	NA
Noise density @ 1 Hz	250 $pT_{RMS}/\sqrt{Hz}$	<8000 $pT_{RMS}/\sqrt{Hz}$
Integral noise 0.1-10Hz	780 pT_{RMS}	NA
Bandwidth (-3 dB)	30 Hz	< 9 Hz
Sample rate	126 Sa/s	< 18 Sa/s
Maximum TID[a]	50 krad	10 krad
Irradiation gain drift	<200 ppm/krad	NA
Irradiation offset drift	<1 nT/krad	NA
Power consumption[b]	650 mW @ 5V	550 mW @ 5V
Interface	TTL UART	RS485
Dimensions	35 x 90 x 7 mm	45 x 69 x 20 mm

[b]Remains constant over irradiation up to 50 krad

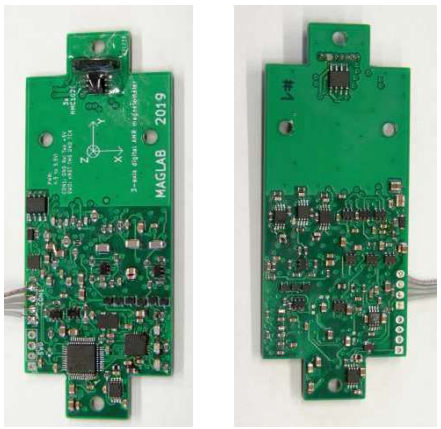

Fig. 14. Photo of magnetometer prototype (left - top side, right - bottom side)

V. CONCLUSION

The radiation testing made it clear that the voltage regulator TPS71733 is the most problematic part of our design. After replacement of this LDO by TPS7A4901, which seemed to work well even with a TID of 100 krad and the substitution of voltage reference REF3430, we expect to achieve radiation tolerance even better than 50 krad. We also plan to test our redesign on a ^{60}Co source in the near future. If we have the opportunity to carry out tests with other types of radiation, we will of course do so and report the results.

Despite the limitations noted in the preceding paragraph, the prototype presented here behaves well under irradiation and temperature change, with its parameters comparable to commercial solutions such as NewSpace Systems NMRM-001-485 [17]. So this novel COTS concept of a digital feedback AMR magnetometer is a promising avenue for future research (e.g., digital feedback for fluxgate).

ACKNOWLEDGMENT

This work was supported by a Student Grant Competition (SGS) at CTU in Prague (No. SGS19/177/OHK3/3T/13). We also wish to express our thanks to Drs. Plaček and Cabalka from ÚJV Řež, a. s. for permitting us a chance to perform radiation testing and their helpfulness.

REFERENCES

[1] D. M. Miles, I.R. Mann, M. Ciurzynski, D. Barona, "A miniature, low-power scientific fluxgate magnetometer: A stepping-stone to cube-satellite constellation missions," Journal of Geophysical Research: Space Physics 121(12), December 2016, DOI: 10.1002/2016JA023147

[2] P. Brown et al., "Space magnetometer based on an anisotropic magnetoresistive hybrid sensor," Review of Scientific Instruments 85, 125117, 2014, https://doi.org/10.1063/1.4904702

[3] P. Brown, "Magnetoresistive magnetometer for space science applications," Meas. Sci. Technol. 23 (2012) 025902 (11pp), http://dx.doi.org/10.1088/0957-0233/23/2/025902

[4] D. Novotný, V. Petrucha, M. Janošek, "A Digitally Compensated AMR Magnetometer," IEEE Transactions on Magnetics, pp(99):1-5, October 2018, DOI: 10.1109/TMAG.2018.2873235

[5] S. Sordo-Ibáñez et al., "A Front-End ASIC for a 3-D Magnetometer for Space Applications by Using Anisotropic Magnetoresistors," IEEE Transactions on Magnetics, Volume: 51 , Issue: 1 , Jan. 2015, DOI: 10.1109/TMAG.2014.2356976

[6] STM32F334 datasheet, ST Microelectronics, DS9994 Rev 9, 2018, Available online at https://www.st.com/resource/en/datasheet/stm32f334k4.pdf

[7] 1- and 2-Axis Magnetic Sensors HMC1001/1002/1021/1022, Honeywell Aerospace, N61-2056-000-000, 04/2019, available online at: aerospace.honeywell.com

[8] K. Mohamadabadi, C. Coillot, and M. Hillionew, "New Compensation Method for Cross-Axis Effect for Three-Axis AMR Sensors," IEEE Sensors Journal, VOL. 13, NO. 4, April 2013, DOI: 10.1109/JSEN.2012.2236511

[9] ESCIES - European Space Components Information Exchange System, https://escies.org

Authorized licensed use limited to: CZECH TECHNICAL UNIVERSITY. Downloaded on April 23,2024 at 13:57:12 UTC from IEEE Xplore. Restrictions apply.

[10] R. Kingsbury et al., "TID Tolerance of Popular CubeSat Components," IEEE Radiation Effects Data Workshop (REDW), 2013, DOI: 10.1109/REDW.2013.6658220

[11] H. Quinn et al., "Single-Event Effects in Low-Cost, Low-Power Microprocessors," IEEE Radiation Effects Data Workshop (REDW) 2014, DOI: 10.1109/REDW.2014.7004596

[12] R. Netzer et al., "Total Ionizing Dose Effects on Commercial Electronics for Cube Sats in Low Earth Orbits," IEEE Radiation Effects Data Workshop (REDW) 2014, DOI: 10.1109/REDW.2014.7004607

[13] K. Avery, J. Finchel, J. Mee, W. Kemp, "Total Dose Test Results for CubeSat Electronics, IEEE Radiation Effects Data Workshop, January 2011, "DOI: 10.1109/REDW.2010.6062504

[14] F.J. Franco, Y. Zong, J.A. Agapito, A.H. Cachero, "Radiation effects on XFET voltage references," IEEE Radiation Effects Data Workshop, 2005, DOI: 10.1109/REDW.2005.1532680

[15] ESCIES - European Space Components Information Exchange System, "Radiation: Theory, Definitions - Gamma Radiation," Available online: https://escies.org

[16] Michal Janošek et al, "Magnetic Calibration System With Interference Compensation," IEEE Transactions on Magnetics, Vol. 55, No. 1, January 2019, DOI: 10.1109/TMAG.2018.2874169

[17] NMRM-001-485 magnetometer, NewSpace Systems, Available online at www.newspacesystems.com

Authorized licensed use limited to: CZECH TECHNICAL UNIVERSITY. Downloaded on April 23,2024 at 13:57:12 UTC from IEEE Xplore. Restrictions apply.

4.5. Radiation hardening and full characterisation of developed AMR magnetometer

This paper continues in the previous research, where radiation testing was performed. In this work, the same radiation source has been utilised, with the same TID and almost the same rate. This allowed to compare with previous result to get better confidence. TID in this case was also 100 krad, as this value is often used in space-grade electronic characterization. Significant improvements have been observed. Not only that improved prototypes survived such a dose but also offset, gain drift and power consumption was measured to be very stable.

Moreover, full conventional characterisation was done to obtain all parameters.

In reference to IEEE copyrighted material which is used with permission in this thesis, the IEEE does not endorse any of CTU's products or services. Internal or personal use of this material is permitted. If interested in reprinting/republishing IEEE copyrighted material for advertising or promotional purposes or for creating new collective works for resale or redistribution, please go to http://www.ieee.org/publications_standards/publications/rights/rights_link.html to learn how to obtain a License from RightsLink. If applicable, University Microfilms and/or ProQuest Library, or the Archives of Canada may supply single copies of the dissertation. DOI: 10.1109/TIM.2020.3043867

Characterization of a Digital AMR Magnetometer for Space Applications

David Novotny, *Graduate Student Member, IEEE*, Vojtech Petrucha, *Member, IEEE*, Michal Dressler, *Graduate Student Member, IEEE*, and Antonin Platil

***Abstract*— In this article, we present research, development, calibration, and characterization of a novel concept of a digitally compensated, low-noise magnetometer based on anisotropic magnetoresistance sensors that is suitable for space applications. The main idea of the design was to reduce the number of precise analog components while using the digital signal processing power available in a modern microcontroller. Our most recent effort targeted lowering power consumption, enhancement of radiation hardness, and overall improvement of the parameters. The principle of operation is presented in detail, along with a detailed description of the instrumentation used to characterize the real instrument, including its noise, linearity, and temperature stability in the range of −20 °C to +70 °C. The results of total ionizing dose (TID) testing at a gamma-ray irradiation facility are discussed at the complete magnetometer and part levels. This is an extended version of an article presented at I2MTC 2020 that contains the results of a second radiation test done with a slightly modified design. The instrument worked well throughout the entire irradiation session (TID of 1.05 kGy over 72 h), and the stability of main parameters was very good (50 pT/Gy offset and 1 ppm/Gy sensitivity stability).**

***Index Terms*— Anisotropic magnetoresistance (AMR), commercial off-the-shelf (COTS), digital compensation, microcontroller, radiation tolerance, SmallSat, space magnetometer.**

I. Introduction

MAGNETOMETERS are used in many different applications in space. Navigation and orientation stabilization of a satellite using different actuators (e.g., magnetotorquers and reaction wheels) is a typical example, as is space weather monitoring to protect sensitive instruments, e.g., ESA's SOSMAG project [1], but they also have purely scientific applications like studying the magnetosphere of Earth, other planets, and celestial bodies [2]. Precise magnetic sensors used here are usually based on the fluxgate principle [3], [4] or anisotropic magnetoresistance (AMR) [5], [6]. While fluxgates achieve lower noise and better stability, AMRs are cheaper, lighter, and more widely available commercially; they can also potentially achieve stability similar to fluxgates, as presented in [7]. These factors make AMRs attractive for low-cost, low-power applications.

Manuscript received July 31, 2020; revised October 31, 2020; accepted November 24, 2020. Date of publication December 10, 2020; date of current version January 8, 2021. This work was supported by the Grant Agency of the Czech Technical University in Prague, grant No. SGS19/177/OHK3/3T/13. The Associate Editor coordinating the review process was Dr. Chao Wang. *(Corresponding author: David Novotny.)*

The authors are with the Department of Measurement, Czech Technical University in Prague, 16627 Prague, Czech Republic (e-mail: novotd12@fel.cvut.cz; petruvoj@fel.cvut.cz; dressmic@fel.cvut.cz; platil@fel.cvut.cz).

Digital Object Identifier 10.1109/TIM.2020.3043867

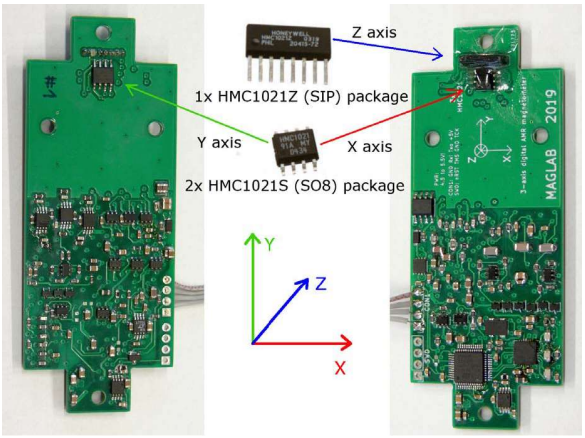

Fig. 1. Photograph of the AMR magnetometer (top and bottom side of the PCB; the AMR sensor triplet is visible on top of the picture)

Space-grade magnetometers use special parts—application-specific integrated circuits (ASICs) [6], [8] or radiation hardened field programmable gate arrays (FPGAs)—to achieve better radiation immunity and lower power consumption. But the use of ASICs or other special radiation-tolerant devices makes them costly and thus not easily obtainable for smaller projects with limited budgets.

In the magnetometer described in this article (see Fig. 1), we used only COTS parts, without any specification of those components' radiation tolerance. While lists of COTS-tested parts exist [9], they do not include many modern active components: microcontrollers, operational amplifiers, voltage stabilizers, references, analog-to-digital converters (ADCs), and so on. Some parts, including AMR magnetic sensors, have been tested in different published projects [10]–[13], but these devices have been submitted to only one test—a total ionizing dose (TID) using ^{60}Co gamma rays, neutrons, and heavy ions—and do not provide complete information concerning their behavior in space conditions.

In this article, we present significant improvements and a detailed characterization and testing of the second version of the magnetometer. The changes are based on the results of the first version's radiation testing and parameter evaluation presented in [14]. Our goal was to construct a device that can survive 1 kGy of gamma radiation without a significant

1557-9662 © 2020 IEEE. Personal use is permitted, but republication/redistribution requires IEEE permission.
See https://www.ieee.org/publications/rights/index.html for more information.

Authorized licensed use limited to: CZECH TECHNICAL UNIVERSITY. Downloaded on April 23,2024 at 13:57:52 UTC from IEEE Xplore. Restrictions apply.

change in the main parameters (satellites in low Earth orbit can experience 0.04–0.4 kGy/year of mission [13]) while keeping the price and power consumption low enough to be suitable for the small satellite segment.

Section II describes the entire concept and details its operating principle, with an emphasis on digital feedback and the improvements referred to above.

In Section III, we present the set-up and method used to characterize the overall instrument's performance (e.g., noise and linearity measurements) and the estimation of the temperature dependencies of the main calibration parameters (sensitivities, nonorthogonality angles, and offsets).

In Section IV, we present the results of a TID test done at a ^{60}Co gamma irradiation facility. We used identical setup as during the first measurement because it proved to be accurate and reliable. The access to the facility is extremely limited for us, so we designed the test setup to collect the maximum amount of information. A custom measurement system based on a PXIe frame, two data acquisition cards, and the LabView control software was employed to acquire a variety of analog and digital signals during a 72-h irradiation session that involved a TID of 1.05 kGy (105 krad) (same values as in the previous one [14]). Two identical magnetometers were tested simultaneously in order to assess the credibility of the results. We acquired 15 channels per one magnetometer to determine the degradation of different components, such as the effects of drifting voltage reference, any op-amp offset shift, or problems in the AMR sensor itself (which were not anticipated—with respect to our experience from the first testing as well as the available publications [15]).

Finally, all the main parameters of the magnetometer are summarized and compared with a commercial device.

II. Description of Magnetometer Prototype

The concept presented uses only commercial off-the-shelf (COTS) components. As an MCU (microcontroller unit), the STM32F334 [16] was chosen for its high-resolution pulsewidth modulation (PWM) capability for digital feedback compensation. All signal processing after analog-to-digital conversion is software-based. The magnetic field in each axis is sensed by HMC1021 [17], and the AMR sensor is operated as a closed-loop compensation system using the built-in offset coil. This sensor was chosen because its sensitivity is among the highest available on the market. Although the HMC1001 provides higher sensitivity, the HMC1021 has the advantage of an internal offset coil with a sufficiently high current to magnetic field ratio. Moreover, it is available at a much lower price. Both are also available in SO8 (S) and SIP (Z) packages for simpler implementation of vector field measurement.

With feedback compensation, the sensor is used only as a zero indicator, and measurement output is the level of compensation current that is fed to the offset coils. Because this indirect method of measurement has traditionally enabled higher performance in terms of linearity, stability, and hysteresis [18], it was chosen. It can be compared to open-loop parameters of a sensor from its datasheet (nonlinearity in CL: 40 ppm, in OL: 1000 ppm, gain stability; 5 ppm/K in CL, 600 ppm/K in OL with constant current supply; 3000 ppm/K in OL with constant voltage).

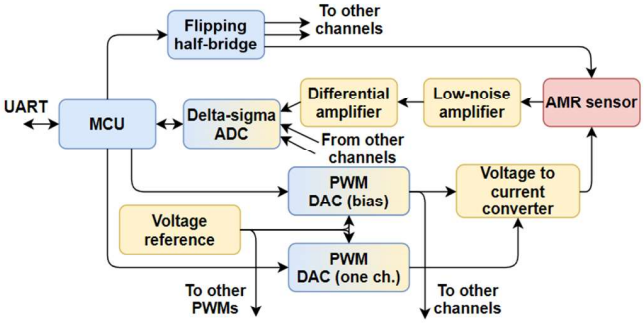

Fig. 2. Block diagram of the magnetometer (only one axis is shown).

As this is an enhanced version of our previous design, we were able to replace parts identified as problematic during the first radiation test campaign (the low-drop voltage regulator and voltage reference). The feedback current source was also modified to improve transfer function (TF) linearity.

This approach extended the durability of the magnetometer under irradiation from 500 to at least 1000 Gy. Component optimization in the PWM-digital-to-analog converter (DAC) design also improved linearity and offset temperature stability. Higher loading impedance (lower current) for the multiplexer ($U1$ and $U2$ in Fig. 3) that creates a precise-amplitude PWM signal led to better linearity of the concept. Bias compensation resistors used in front of inverting inputs of operating amps decreased offset drift with temperature by balancing the input current bias that caused excess drift.

Fig. 2 presents a simplified block diagram of the magnetometer's electronics; for the sake of clarity, only one axis is shown.

AMR sensors often implement flipping (set/reset) coils that can be used to change (or "flip") the polarity of sensor sensitivity. This process is usually carried out periodically with frequencies in the Hz to kHz range and offers advantages such as electrical offset elimination, which is why we chose it. During a flipping pulse (0.65 A for 10 μs in our case), the measurement reported by the AMR sensor is very noisy. Flips represent only a fraction (2%) of the total measurement time, but they can still cause excess noise. To solve this problem, the measurement during flipping and the measurement immediately after are not used flipping (because of settlings in the analog path); demodulation is stopped for these two samples per flip pulse. This means that for 3906 Sa/s and a 216-Hz flipping frequency (18 samples per flipping period), four samples (two during set and two during reset flip) are not used and thus 22% of measurements per flip period are discarded.

The static TF of the magnetometer in the SET/RESET state of the flipping mode is described in (1) and (2). Equation (3) represents the result of a synchronous demodulation applied to the measurement data modulated by the flipping process

$$V_{\text{set}} = K_A \cdot (O_{\text{AE}} + K_{\text{LNA}} \cdot (O_{\text{LE}} + O_{\text{SE}} + K_{\text{AMR}} \cdot (B_m + O_B))) \quad (1)$$

Authorized licensed use limited to: CZECH TECHNICAL UNIVERSITY. Downloaded on April 23,2024 at 13:57:52 UTC from IEEE Xplore. Restrictions apply.

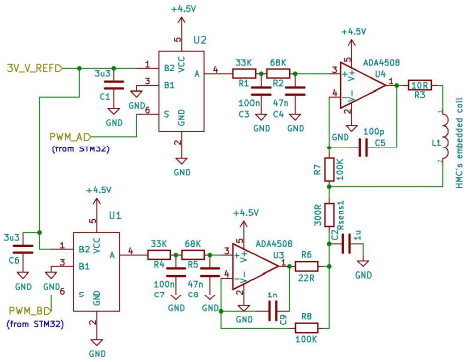

Fig. 3. Circuit diagram of a PWM-based differential compensation circuit.

$$V_{\text{res}} = K_A \cdot (O_{\text{AE}} + K_{\text{LNA}} \cdot (O_{\text{LE}} + O_{\text{SE}} - K_{\text{AMR}} \cdot (B_m + O_B))) \tag{2}$$

$$V_{\text{out}} = V_{\text{set}} - V_{\text{res}} = 2 \cdot K_A \cdot K_{\text{LNA}} \cdot K_{\text{AMR}} \cdot (B_m + O_B) \tag{3}$$

where $V_{\text{set}}, V_{\text{res}}$ is the voltage output of the bridge in the SET/RESET state (V), V_{out} is the output voltage after demodulation (V), K_A is the internal gain of ADC $(-)$, O_{AE} is the offset of ADC (V), K_{LNA} is the gain of low noise amplifier (LNA) $(-)$, O_{LE} is the offset of LNA (V), O_{SE} is the electrical offset of AMR bridge (V), K_{AMR} is the sensitivity of the AMR bridge (V/T), B_m is the measured magnetic field (T), and O_B is the magnetic offset of the sensor (T).

Equation (3) shows that, after demodulation carried out in the firmware, the offset of the magnetic measurement is given only by the magnetic offset of the sensor itself. There is no contribution of the signal conditioning chain, making it unnecessary to use dc-precise operational amplifiers or ADC converters. Another important advantage is implied; there are no low-frequency (LF) noise requirements on the signal chain. The flipping frequency is set to approximately 216 Hz as a compromise between the useful bandwidth of the magnetometer and the digital signal processing speed (3.91-kSa/s sample rate of ADC). This frequency was also selected to ensure minimal interference with the local 50-Hz line frequency disturbing signal and its harmonics. For sensor preamplifier design, only noise at this frequency and the bandwidth of the magnetometer are relevant. Most op-amps have $1/f$ corner on lower frequencies, so at 216 Hz only their white noise is significant (should be at least two times smaller than Johnson–Nyquist noise of AMR bridge, for HMC1021—1100 Ω and 25 °C it is 4.3 nV/$\sqrt{\text{Hz}}$, so white noise density of amplifier below 2 nV/$\sqrt{\text{Hz}}$ is suitable).

In the feedback topology, the gain stability is given only by the compensation circuit (Fig. 3). The dynamic performance is affected only by the gain change of the sensor itself and its conditioning circuit. This can be obtained from the frequency response at a zero frequency.

Equation (4) describes output voltage of AMR bridge, (5) relates to computed DAC value based on AMR bridge voltage in Laplace image domain, and (6) is obtained by combining (4) and (5) together. It describes transfer function of DAC in relation to measured magnetic field and we can use it to show that for a zero frequency (dc gain, $s = 0$), TF is given only by (7)

$$V_{\text{out}} = K_{\text{AMR}} \cdot \left(B_m - \text{DAC}_{\text{COMP}} \cdot K_{\text{coil}} \cdot \frac{V_{\text{DAC\_ref}}}{\text{R}_{\text{sens}}} \right) (\text{V}) \tag{4}$$

$$\text{DAC}_{\text{comp}} = \frac{K_i}{s} \cdot K_{\text{LNA}} \cdot \frac{\text{ADC}_{\text{range}}}{\text{V}_{\text{ADC\_ref}}} \cdot V_{\text{out}} (-) \tag{5}$$

$$H(s) = \frac{\text{DAC}_{\text{comp}}}{\text{B}_m} = \left(\frac{\text{V}_{\text{ADC}_{\text{ref}}}}{K_i \cdot K_{\text{LNA}} \cdot \text{ADC}_{\text{range}} \cdot K_{\text{AMR}} \cdot} \cdot s + K_{\text{coil}} \cdot \frac{V_{\text{DAC\_ref}}}{\text{R}_{\text{sens}}} \right)^{-1} (T^{-1}) \tag{6}$$

$$H(0) = \frac{R_{\text{sens}}}{K_{\text{coil}} \cdot V_{\text{DAC}_{\text{ref}}}} (T^{-1}) \tag{7}$$

where DAC_{comp} is the value set on compensation-DAC $(-)$, $V_{\text{ADC\_ref}}$ is the reference voltage of ADC (V), $\text{ADC}_{\text{range}}$ is the top value of ADC $(-)$, K_i is the integrator constant $(-)$, K_{coil} is the embedded coil constant (T/A), R_{sens} is the sense resistor of the voltage to current converter (Ω), and $V_{\text{DAC\_ref}}$ is the reference voltage of DAC (V).

This means that the only contribution to gain drift is given by the constant of the compensation coil, sensing resistor in the voltage to current converter, and the reference voltage source. The stability of the compensation system should be inherent (single pole TF), but this description is only approximate and does not consider delays of preamplifier or ADC's sampling that can cause oscillations. Stability must be ensured by the proper setting of the integrator constant K_i.

In a practical implementation, this means that there are only a very few requirements on the design of the electronics

1) stability and noise of the main voltage reference;
2) stability of the feedback current sensing resistor;
3) white noise (at 180–250 Hz) of the bridge amplifier;
4) stability and LF noise of op-amps in the voltage-to-current converter and in the voltage reference buffer.

A band-gap voltage reference was selected because it should be less susceptible to irradiation than Zener diode-based reference [19]. Our previous design used REF3430, while LTC6655 is used in the present design. As a low-noise preamp, OPA2210 was chosen for its low voltage and current noise at a flipping frequency and its low-voltage, rail-to-rail operation. For all other op-amps, where low LF noise was necessary, a low-voltage, rail-to-rail ADA4805 was used.

During radiation testing the current consumption of the magnetometer was precisely monitored. A sawtooth-like signal with an amplitude of several milliamps appeared superimposed on the steady current value of 122 mA (Fig. 4). This is caused by the function of an internal voltage regulator in the STM32 MCU. In another project that used the same microcontroller (STM32F334) and a high-resolution timer (HRTIM), we also observed that the duty cycle of the PWM signal from the HRTIM drifted with the sawtooth shape at a magnitude of several ppm. Fortunately, this problem was solved by using a differential DAC design. The distortion is the same for all channels; it behaves like a varying offset, and when the voltages generated by two channels are subtracted, the effect is suppressed.

Authorized licensed use limited to: CZECH TECHNICAL UNIVERSITY. Downloaded on April 23,2024 at 13:57:52 UTC from IEEE Xplore. Restrictions apply.

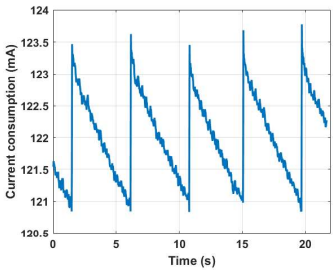

Fig. 4. Current consumption of the magnetometer; sawtooth distortion caused by STM32 internal voltage regulator.

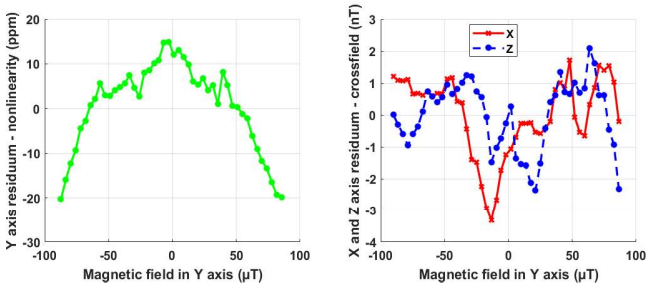

Fig. 5. Linearity (left) and cross-field (right) errors.

III. Conventional Measurements

A. Linearity and Cross-Field Measurement

The linearity of the magnetometer was measured using precise PC-controlled current source driving a Lee–Whiting coil system (single axis). The magnetometer itself was placed in the precise center of this coil. While LabView-based software controlled current to the coil system in a staircase-like linear sweep, it also recorded data from the magnetometer. This process contained 50 points of measurement in the ± 90-μT range and was repeated 10 times; the results were averaged to decrease noise. Those results are shown in Fig. 5. The linearity error (INL) is approx. ± 20 ppm of FS, while the cross-field error is within ± 3 nT and mostly due to environmental noise.

B. Noise Measurement

The magnetic noise of the prototype was measured in a six-layer permalloy shielding. The attenuation factor of the shielding is approximately 10^5 in the horizontal direction and 10^3 in the vertical, allowing sub-pT/$\sqrt{\text{Hz}}$ noise density to be measured (Fig. 6). The sensor was placed at the bottom of the shielding while it sent data over a serial link to the PC that recorded the data. From the data record, power spectral density was calculated using Welch's method (10 min length, 126 Sa/s, NFFT $= 32768$).

The results indicate that the sensor itself can perform even better because noise is dominated by acquisition and compensation electronics noise, which is due to a power consumption tradeoff: a prototype developed in our previous research [7] performed with approximately half the noise but consumed three times more power. This is an unfortunate consequence of the linear dependence of the sensor's sensitivity to the sensor supply voltage while its power consumption is quadratically dependent.

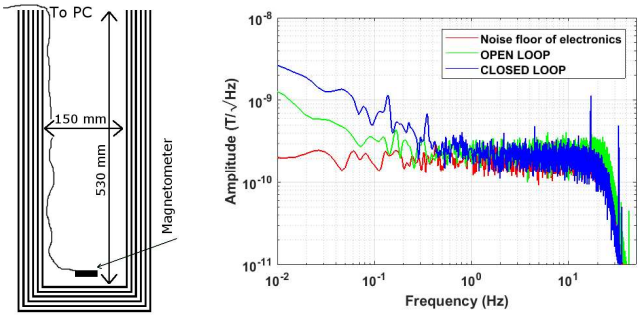

Fig. 6. Drawing of the measurement setup (left). Noise spectrum density comparison for one axis (magnetometer implements digital low-pass filter with 30-Hz cutoff frequency, so higher frequencies are not shown) (right).

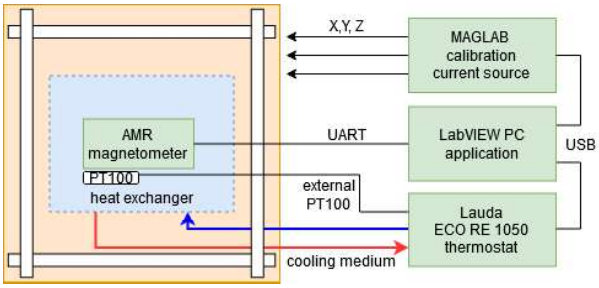

Fig. 7. Block diagram of calibration system. The PC LabView application communicates with the current source and thermostat via a USB virtual COM port. The AMR magnetometer temperature is measured by a PT100 platinum sensor connected to the Lauda thermostat's external input.

C. Temperature Drifts Measurement

Magnetometer calibration parameters and their temperature dependence were measured using a tri-axial coil system equipped with a custom temperature-controlled chamber (Fig. 7). The calibration system consists of a 60-cm Merritt (E–W) coil pair and two modified-Helmholtz (N–S, vertical) coil pairs driven by a custom-built three-channel current source and a LabView application. The temperature chamber is made of a hollow plastic cylinder (10 cm inner diameter, 25 cm length) wrapped with PTFE tubing as a heat exchanger used with a Lauda ECO-RE1050S heating and cooling thermostat that can control the temperature of a circulating media (Kryo-51, polydimethylphenylsiloxane, basically a silicon oil) in the range of -50 °C to 120 °C. However, due to insufficient chamber isolation and low heat conductivity between the heat exchanger and the AMR magnetometer, the lowest temperature in the calibration temperature sweep achievable in a tolerable time span is -20 °C.

The procedure for obtaining magnetometer calibration linear coefficients is based on a thin shell method [20], [21], which typically uses a coil system to create a set of known field vectors with constant magnitude that are distributed uniformly on the surface of a virtual sphere. The method was modified to enable easier realization in our laboratory with nonnegligible magnetic noise disturbances, where the magnetic noise values are about 100 nT_{pp} in horizontal components and up to 1 μT_{pp} in vertical (0–10-Hz band). To overcome magnetic field variations and human-made disturbances (appearing as a $1/f$ noise), each vector from the 55-point thin shell vector

Authorized licensed use limited to: CZECH TECHNICAL UNIVERSITY. Downloaded on April 23,2024 at 13:57:52 UTC from IEEE Xplore. Restrictions apply.

set was measured relatively in two steps. In the first step (8), the coil system field $\mathbf{b}_c$ was set to a manually adjusted value to create approximately zero field inside, and the magnetometer output $\mathbf{e}_m$ measuring field $\mathbf{b}_m$ (which also contains the immediate value of external disturbance $\mathbf{d}$) was recorded. This first step $\mathbf{b}_c$ value stays constant during the entire calibration because it compensates for Earth's field constant component. In the second step (9), the thin shell vector field is added to the coil system and the magnetometer output is recorded

$$\mathbf{b}_m(1) = \mathbf{b}_c(1) + \mathbf{d}(1) \tag{8}$$

$$\mathbf{b}_m(2) = \mathbf{b}_c(2) + \mathbf{d}(2) \tag{9}$$

$$\Delta\mathbf{b}_m = \boldsymbol{\Delta}\mathbf{b}_c + \boldsymbol{\Delta}\boldsymbol{d}. \tag{10}$$

By taking the difference of (8) and (9), the relative values can be established in (10). Assuming a fast magnetometer with short settling time, the steps can be applied rapidly enough for $\Delta\mathbf{d}$ to approach zero and the external field disturbance contribution to be suppressed.

The calibration parameters are obtained by solving a set of linear equations given by the following (11) magnetometer output model [20]:

$$\Delta\mathbf{b}_c = \begin{bmatrix} r_{11} & r_{12} & r_{13} \\ r_{21} & r_{22} & r_{23} \\ r_{31} & r_{32} & r_{33} \end{bmatrix} \begin{bmatrix} \mathrm{S}_1 & \mathrm{V}_{12} & \mathrm{V}_{13} \\ 0 & \mathrm{S}_2 & \mathrm{V}_{23} \\ 0 & 0 & \mathrm{S}_3 \end{bmatrix} \left(\Delta\mathbf{e}_m - \begin{bmatrix} O_1 \\ O_2 \\ O_3 \end{bmatrix} \right) \tag{11}$$

where r parameters are components of the rotation matrix between the magnetometer sensor triplet frame and the coil frame, S and O are sensitivities and offsets, and V parameters are related to sensor frame nonorthogonality; $\Delta\mathbf{e_m}$ is the magnetometer raw reading difference corresponding to $\Delta\mathbf{b_m}$ (10).

Since the procedure uses only relative magnetic field values, the information about the magnetometer sensor's offset absolute value is lost; only sensitivities, nonorthogonality angles, and the rotation matrix between sensor frame and coil frame can be retrieved.

This method is further described in [22], which also offers a description of active field variation compensation from a closely placed (2 m from coil center) magnetometer; however, that was not used for active compensation during sensitivity and nonorthogonality measurement in this case, only for offset drift estimation.

The calibration thin shell sequence radius magnitude was set to 70 μT, which is in the sensor's linear region (see Fig. 5). The chopping frequency was roughly 1 Hz; therefore, one full calibration took less than 2 min. The rms residues [21] of calibration fit are, on average, 5 nT for axes in the horizontal direction of Earth's magnetic field and 40 nT for the vertical (or 71 and 570 ppm relative error from the shell radius). The achievable calibration uncertainty of a fixed magnetometer (estimated from the standard deviation of multiple full calibration results) is about 100 ppm for sensitivity parameters and 10^{-3} degrees for angular parameters. The anticipated magnetometer parameters' drift values are lower, so the calibration sequence is repeated multiple times at each temperature. The total length of the calibration test was 10 h; the temperature profile is shown in Fig. 8.

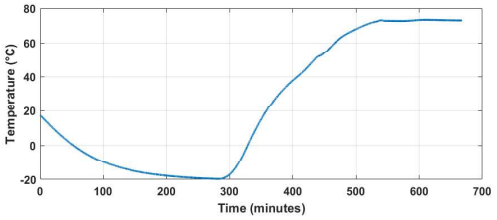

Fig. 8. Estimate of magnetometer temperature measured by an attached PT100. The temperature was controlled by setting the thermostat bath temperature to first minimum then maximum values (without closed-loop control from external sensor). Most of the thin shell calibrations (full 55 points) were done when the temperature was settled at the minimum or maximum values.

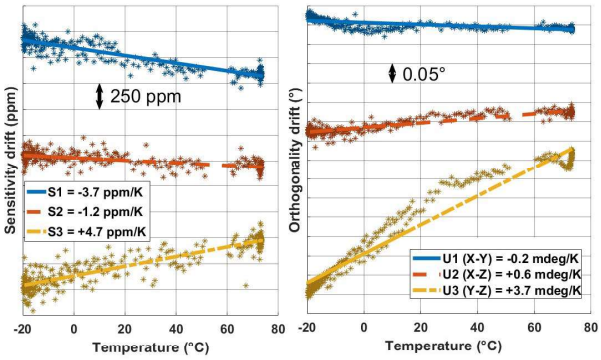

Fig. 9. Magnetometer sensitivity and nonorthogonality temperature dependence. The cross-axis angle notation is taken from [20]. The drift of parameter U3 (angle *YZ*, caused by the tilt of vertically mounted AMR IC) with the most significant drift is also clearly not linear, as it is probably caused by temperature expansion of the epoxy glue fixing the package.

1) Sensitivity and Nonorthogonality Calibration: The three sensitivity parameters and three angles describing the magnetometer's nonorthogonal frame were obtained from solution of a data set made from (11) by QR decomposition. The drift dependence of both parameter triplets is shown in Fig. 9. Its slope is clearly visible even during the heating process, where calibration counts were sparse and parameters thus more scattered. The most widely drifting channel is from the AMR sensor, which was in a vertically mounted SIP package on PCB, while the others were in a standard SO8 package.

2) Offset Drift Estimation: The offset drift can be only estimated from magnetometer data when no calibration vector is applied to the coil system. To distinguish drift from Earth's field variation, the magnetic field was simultaneously recorded by an external fluxgate magnetometer located approximately 0.5 m above the coil system. The external magnetometer coordinate frame did not have to be precisely aligned to the calibrated magnetometer frame because the method described in [22] was used to provide automatic alignment. The rotation transformation matrix was obtained from several minutes of recording magnetic field variations (assuming their zero-gradient, i.e., long-distance sources). Then, the offset drift can be plotted simply as the difference between the AMR magnetometer and the rotated-frame external magnetometer reading. The results (-0.9, 0.25, and -0.42 nT/K for *X*-, *Y*-, and *Z*-axis, respectively) are a bit worse than what we published in our previous research [7] and can be seen in Fig. 10. This is caused by

Authorized licensed use limited to: CZECH TECHNICAL UNIVERSITY. Downloaded on April 23,2024 at 13:57:52 UTC from IEEE Xplore. Restrictions apply.

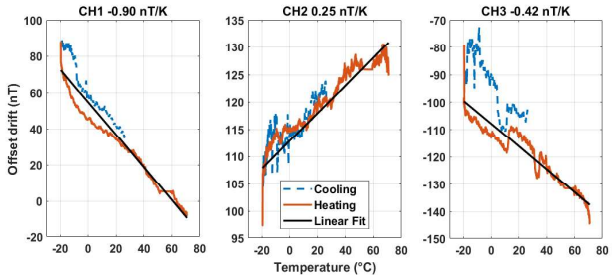

Fig. 10. Magnetometer offset temperature drift estimation for each magnetometer axis. The data are selected from simultaneously recording the AMR magnetometer and the external fluxgate during the calibration sequence. Only the data when no field is applied to the coil system are shown

integrating electronics and sensors much closer to each other (our magnetometer from [7] had separate sensor head and processing electronics). Electronics parts (especially ceramic capacitors) display remanent magnetization drifting with temperature.

IV. Radiation Testing

Because electronics operating in space must survive all types of radiation present in free space—gamma rays, neutron radiation, heavy ions, proton, and electron beam radiation—it would be optimal to test for all types. However, different radiation sources are not easily accessible even for academic and research purposes, so we have used ^{60}Co based gamma-ray irradiation that we could access through the ÚJV Řež facility near Prague. We consider this a first step in the instrument's qualification process. The test was planned in accordance with MIL-STD-883. The TID, based on the alanine-EPR dosimetry method, was 1.05 ± 0.03 kGy (105 ± 3 krad). This dose is related to the energy absorbed by water; for silicon (the main element in the tested electronics), it can be recalculated by (12) from [23]

$$D_{\mathrm{Si}} = D_{\mathrm{H_2O}} \cdot \frac{\mu_{\mathrm{Si}}/\rho_{\mathrm{Si}}}{\mu_{\mathrm{H_2O}}/\rho_{\mathrm{H_2O}}} = 0.898 \cdot D_{\mathrm{H_2O}}. \quad (12)$$

The corrected value for the TID absorbed by silicon is thus 943 ± 30 $\mathrm{Gy_{(Si)}}$(94.3 ± 3 $\mathrm{krad_{(Si)}}$). Irradiation by this dose was performed in 72 h. The results place the test in the low irradiation-rate category (0.36 rad/s). Second testing (actual prototype) was done in the same setup and TID as described for our first radiation testing.

A. Testing Setup (PXIe)

Monitoring of internal signals of the magnetometer and logging serial data and the generation of the testing signal to the external coil were implemented with a PXIe frame with an embedded controller, an NI-4302 data acquisition card, and an auxiliary NI-6251 card as a software watchdog for the magnetometer (performing reset in case the magnetometer would stop sending serial data) and the generation of the sinusoidal signal to the testing coil (Figs. 11 and 12). Measurement setup was controlled through LabView-based software with a remote access possibility.

Selected signals measured in the magnetometer are marked by letters A–M in Fig. 13. Voltage channels A–I were sampled

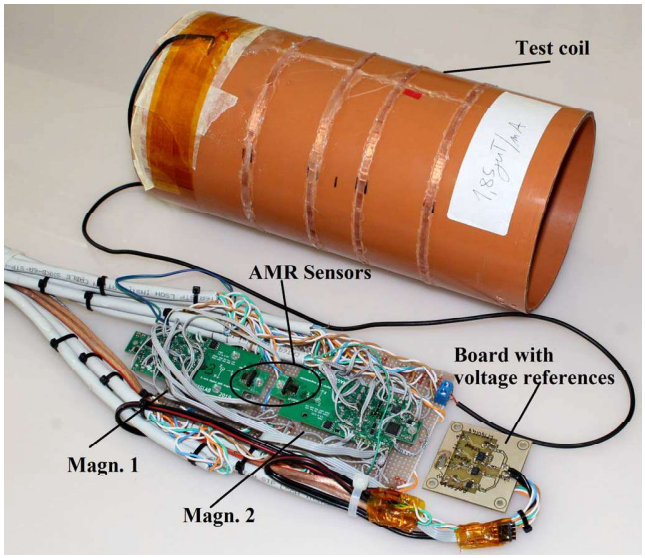

Fig. 11. Photograph of D.U.T. pulled out of testing coil.

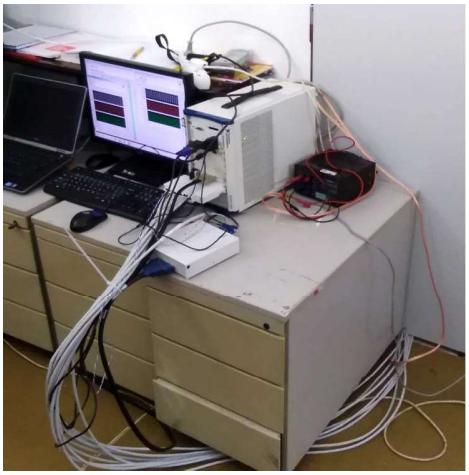

Fig. 12. Photograph of PXIe frame with PC in control room during irradiation.

at 60 Sa/s while J, K, L, and M signals were acquired at 5 kSa/s, fast enough to measure the square (flipped) signal at 216 Hz. Channel A was the current measurement through a 0.25-Ω shunt resistor. Signal G was measured on a 300-Ω sense resistor of a voltage-to-current converter. For one of the magnetometers, axes X and Z were operated in open loop mode, while the Y-axis was in a closed loop. The X-axis had completely disconnected feedback (see the strikethrough of the signal in the diagram), while the Z-axis had a constant value set on digital compensation to measure the drift of compensation current. Second magnetometer operated in closed-loop for all axes, without intervention to its normal operation by measurement.

B. Results of Irradiation

All data acquired using the PXIe measurement system were postprocessed (filtered, decimated, subtracted, or demodulated, depending on the signal) and are presented in Figs. 14–19. Some also contain data from the first radiation testing to show

Authorized licensed use limited to: CZECH TECHNICAL UNIVERSITY. Downloaded on April 23,2024 at 13:57:52 UTC from IEEE Xplore. Restrictions apply.

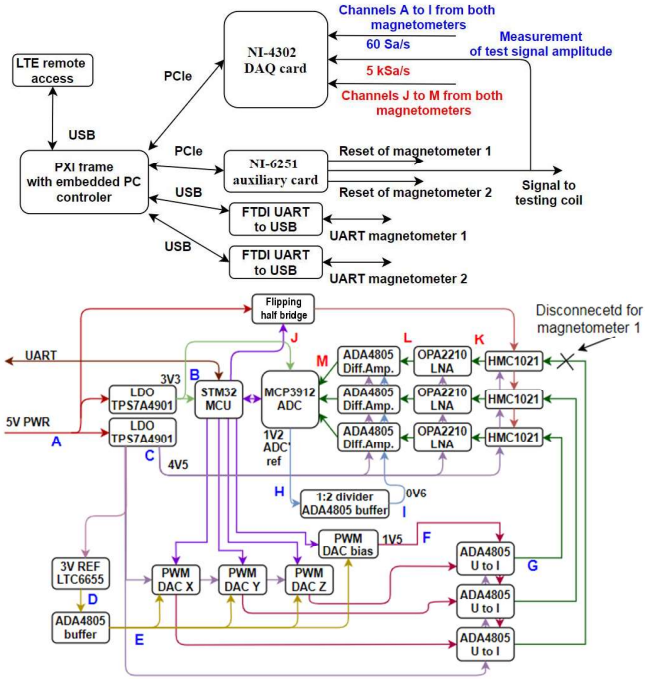

Fig. 13. Circuit diagram of PXIe acquisition system with highlighted test points on the magnetometer's circuit.

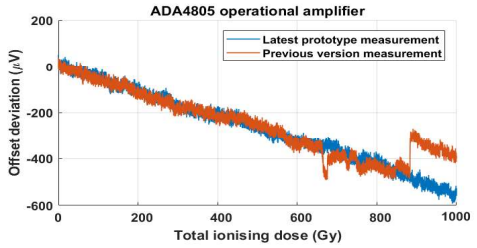

Fig. 14. Drift of ADA4805 op. amp. offset with increasing TID.

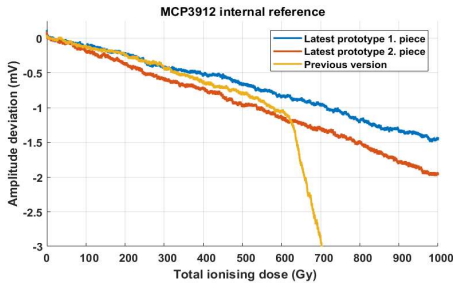

Fig. 15. Drift from initial value of AD converter's internal reference.

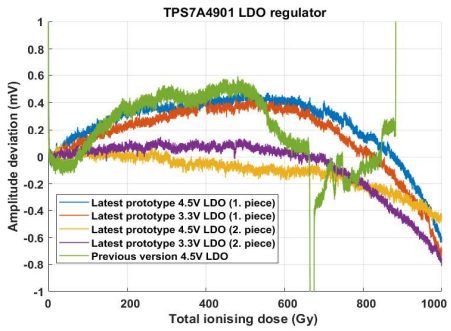

Fig. 16. Comparison of drifts from nominal voltage of five pieces of LDO voltage regulators.

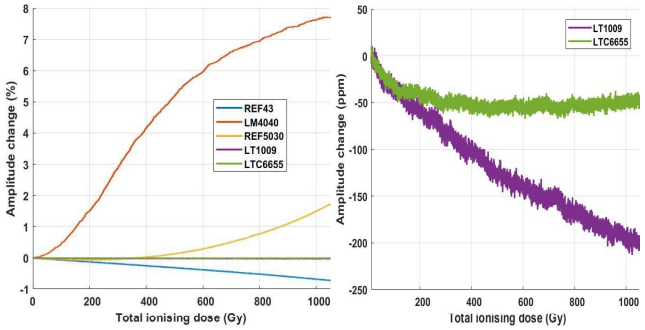

Fig. 17. Comparison of different voltage references to test their nominal voltage drift with irradiation (LTC6655 and LT1009 are very small in comparison with the others; they are overlaid in the graph on the left, so a detail of these two references is provided on the right).

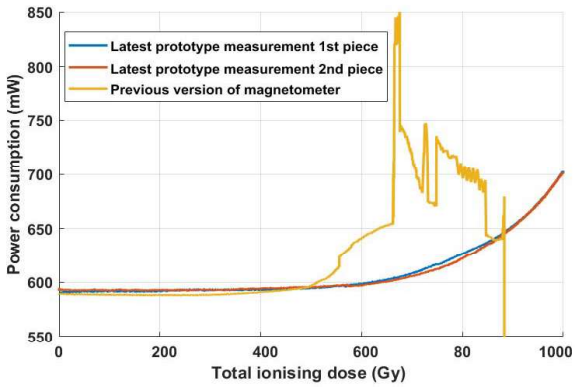

Fig. 18. Comparison of power consumption of two recent prototypes with increasing TID.

that the behaviors were similar (in case of parts that worked nominally). All graphs use TID (Gy) on the horizontal axis. Fig. 14 shows the offset drift for the ADA4805 operational amplifier (approximately -0.5 μV/Gy). The curve is very similar for both measurements; the jumps in the previous version trace were caused by a power supply failure that occurred at 550 Gy. The internal voltage reference of the AD converter showed -1.7 μV/Gy drift (Fig. 15); again, the low-dropout (LDO) regulator malfunction influenced the previous version. The TPS7A4901 voltage regulator worked very well in all cases, exhibiting almost negligible drift with respect to irradiation (Fig. 16). Main voltage reference is used to define the scale factors, so we took special care to select the part with the lowest drift. Fig. 17 shows the drift of five different parts; we observed that the LTC6655 was superior to all the others; it was thus chosen for the final design. Power consumption (Fig. 18) remained practically constant through approximately 500 Gy, at which point an exponential rise was observed; again, this was very consistent for both units tested during the second campaign.

Authorized licensed use limited to: CZECH TECHNICAL UNIVERSITY. Downloaded on April 23,2024 at 13:57:52 UTC from IEEE Xplore. Restrictions apply.

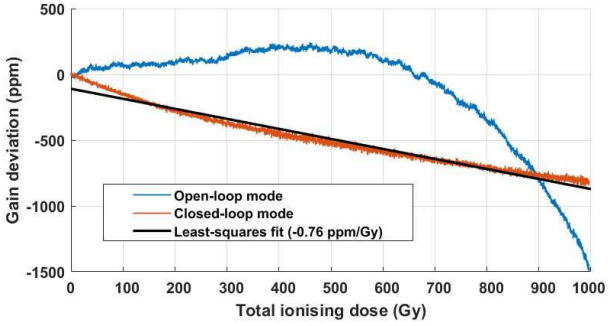

Fig. 19. Gain drift of magnetometer derived from analysis of recorded serial data from irradiated magnetometers.

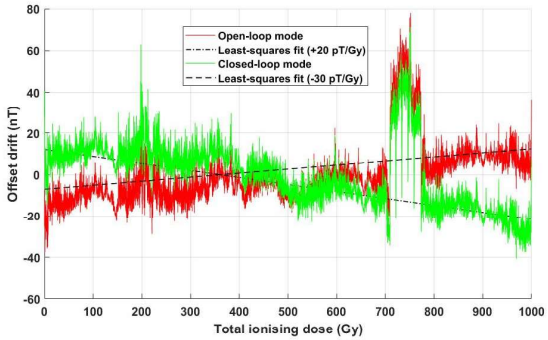

Fig. 20. Offset drift of magnetometer during irradiation.

TABLE I
COMPARISON OF PRESENTED WITH COMMERCIAL MAGNETOMETER

Parameter	Magn. described in this paper	Commercial magnetometer
Range	± 100 μT	± 60 μT
Nonlinearity	± 20 ppm	NA
Offset TC	< 1 nT/K	NA
Sensitivity TC	< 5 ppm/K	NA
Orthogonality TC	< 0.01 °/K	NA
Crossfield sensitivity	± 50 ppm	NA
Noise density @ 1 Hz	250 $pT_{RMS}/\sqrt{Hz}$	<8000 $pT_{RMS}/\sqrt{Hz}$
Integral noise 0.1-10Hz	780 pT_{RMS}	NA
Bandwidth (-3 dB)	30 Hz	< 9 Hz
Sample rate	126 Sa/s	< 18 Sa/s
Maximum TID	1000 Gy	100 Gy
Irradiation gain drift	<1 ppm/Gy	NA
Irradiation offset drift	<50 pT/Gy	NA
Power consumption	600 mW @ 5V	550 mW @ 5V
Interface	TTL UART	RS485
Dimensions	35 x 90 x 7 mm	45 x 69 x 20 mm

Data streamed from both magnetometers over a serial link (UART/USB converter) allowed us to obtain gain (sensitivity) and offset (bias) drifts with increasing TID. As one axis of both prototypes was excited by an external coil (3-Hz sinewave, 12 μT_{p-p} amplitude), we were able to obtain sensitivity drift by bandpass filtering data to extract 3-Hz excitation signal and calculate its envelope. The envelope magnitude drift from the initial value equals gain drift of −76 ppm/Gy (Fig. 19). Offset drift (Fig. 20) was calculated by low-pass filtering of the serial data to remove the excitation sine wave and environmental noise (but a very low frequency noise still cannot be fully suppressed by filtering—see the peak between 700 and 800 Gy caused by opening and closing neighbor irradiation chamber).

V. CONCLUSION

As expected, replacing parts identified as problematic during the first irradiation campaign significantly improved the magnetometer's resistance to gamma radiation. The level of >1000 Gy is more than sufficient for most short-duration missions in low Earth orbit. Two pieces were tested, and both provided practically identical results, which creates even more confidence in the results. Some of the STM32 microcontrollers were reported to be prone to single-event upsets (SEUs) or latch-ups (SELs) when bombarded with neutrons or heavy ions [11]. As SELs are reversible, power cycling by the power management unit would solve the problem. Still, much testing remains to be done (thermal vacuum, EMC, vibration testing, etc.).

Despite the limitations noted in the preceding paragraph, the updated prototype presented here behaves very well under gamma irradiation and temperature change. The parameters are either comparable to commercial solutions such as NewSpace Systems NMRM-001-485 [24] or perform significantly better, as in the case of noise density (Table I). So, this novel COTS concept of digital feedback AMR magnetometer is very promising and, it is hoped, can be deployed in space soon.

ACKNOWLEDGMENT

The authors wish to express our thanks to Dr. Plaček and Dr. Cabalka from ÚJV Řež, a. s. for giving us a chance to perform radiation testing and for their helpfulness.

REFERENCES

[1] S. Leitner *et al.*, "Design of the magnetoresistive magnetometer for ESA's SOSMAG project," *IEEE Trans. Magn.*, vol. 51, no. 1, pp. 1–4, Jan. 2015, doi: 10.1109/TMAG.2014.2358270.

[2] J. L. Burch, T. E. Moore, R. B. Torbert, and B. L. Giles, "Magnetospheric multiscale overview and science objectives," *Space Sci. Rev.*, vol. 199, nos. 1–4, pp. 5–21, Mar. 2016.

[3] M. Díaz-Michelena, "Small magnetic sensors for space applications," *Sensors*, vol. 9, no. 4, pp. 2271–2288, Mar. 2009, doi: 10.3390/s90402271.

[4] D. M. Miles *et al.*, "A miniature, low-power scientific fluxgate magnetometer: A stepping-stone to cube-satellite constellation missions," *J. Geophys. Res., Space Phys.*, vol. 121, no. 12, pp. 11839–11860, Dec. 2016, doi: 10.1002/2016JA023147.

[5] P. Brown *et al.*, "Space magnetometer based on an anisotropic magnetoresistive hybrid sensor," *Rev. Sci. Instrum.*, vol. 85, no. 12, Dec. 2014, Art. no. 125117, doi: 10.1063/1.4904702.

[6] P. Brown *et al.*, "Magnetoresistive magnetometer for space science applications," *Meas. Sci. Technol.*, vol. 23, no. 2, Feb. 2012, Art. no. 025902, doi: 10.1088/0957-0233/23/2/025902.

[7] D. Novotný, V. Petrucha, and M. Janošek, "A digitally compensated AMR magnetometer," *IEEE Trans. Magn.*, vol. 55, no. 1, pp. 1–5, Jan. 2019, doi: 10.1109/TMAG.2018.2873235.

[8] S. Sordo-Ibáñez *et al.*, "A front-end ASIC for a 3-D magnetometer for space applications by using anisotropic magnetoresistors," *IEEE Trans. Magn.*, vol. 51, no. 1, pp. 1–4, Jan. 2015, doi: 10.1109/TMAG.2014.2356976.

[9] *ESCIES—European Space Components Information Exchange System*. Accessed: Nov. 10, 2020. [Online]. Available: https://escies.org

[10] R. Kingsbury *et al.*, "TID tolerance of popular CubeSat components," in *Proc. IEEE Radiat. Effects Data Workshop (REDW)*, Jul. 2013, pp. 1–4, doi: 10.1109/REDW.2013.6658220.

[11] H. Quinn, T. Fairbanks, J. L. Tripp, G. Duran, and B. Lopez, "Single-event effects in low-cost, low-power microprocessors," in *Proc. IEEE Radiat. Effects Data Workshop (REDW)*, Jul. 2014, pp. 1–9, doi: 10.1109/REDW.2014.7004596.

Authorized licensed use limited to: CZECH TECHNICAL UNIVERSITY. Downloaded on April 23,2024 at 13:57:52 UTC from IEEE Xplore. Restrictions apply.

[12] R. Netzer, K. Avery, W. Kemp, A. Vera, B. Zufelt, and D. Alexander, "Total ionizing dose effects on commercial electronics for cube sats in low Earth orbits," in *Proc. IEEE Radiat. Effects Data Workshop (REDW)*, Jul. 2014, pp. 1–7, doi: 10.1109/REDW.2014.7004607.
[13] K. Avery *et al.*, "Total dose test results for CubeSat electronics," in *Proc. IEEE Radiat. Effects Data Workshop*, Jul. 2011, pp. 1–8, doi: 10.1109/REDW.2010.6062504.
[14] D. Novotný, V. Petrucha, M. Dressler, and A. Platil, "AMR magnetometer with digital feedback for space applications," in *Proc. IEEE Int. Instrum. Meas. Technol. Conf. (I2MTC)*, Dubrovnik, Croatia, May 2020, pp. 1–6, doi: 10.1109/I2MTC43012.2020.9129039.
[15] R. Sanz, A. B. Fernández, J. A. Dominguez, B. Martín, and M. D. Michelena, "Gamma irradiation of magnetoresistive sensors for planetary exploration," *Sensors*, vol. 12, no. 4, pp. 4447–4465, Apr. 2012.
[16] ST Microelectronics. (Sep. 2018). *STM32F334 Datasheet*. [Online]. Available: https://www.st.com/resource/en/datasheet/stm32f334k4.pdf
[17] Honeywell Aerospace. (Apr. 2019). *1- and 2-Axis Magnetic Sensors HMC1001/ 1002/ 1021/ 1022*. [Online]. Available: https://www.aerospace.honeywell.com
[18] K. Mohamadabadi, C. Coillot, and M. Hillion, "New compensation method for cross-axis effect for three-axis AMR sensors," *IEEE Sensors J.*, vol. 13, no. 4, pp. 1355–1362, Apr. 2013, doi: 10.1109/JSEN.2012.2236511.
[19] F. J. Franco, Y. Zong, J. A. Agapito, and A. H. Cachero, "Radiation effects on XFET voltage references," in *Proc. IEEE Radiat. Effects Data Workshop*, Jul. 2005, pp. 138–143, doi: 10.1109/REDW.2005.1532680.
[20] P. Brauer, J. M. G. Merayo, T. Risbo, and F. Primdahl, "Magnetic calibration of vector magnetometers: Linearity, thermal effects and stability," in *Proc. ESA Conf. SP-490*, 2001, pp. 1–7. [Online]. Available: http://citeseerx.ist.psu.edu/viewdoc/summary?doi=10.1.1.36.1718
[21] N. Olsen *et al.*, "Calibration of the Ørsted vector magnetometer," *Earth, Planets Space*, vol. 55, no. 1, pp. 11–18, Jan. 2003, doi: 10.1186/BF03352458.
[22] M. Janošek, M. Dressler, V. Petrucha, and A. Chirtsov, "Magnetic calibration system with interference compensation," *IEEE Trans. Magn.*, vol. 55, no. 1, pp. 1–4, Jan. 2019, doi: 10.1109/TMAG.2018.2874169.
[23] *ESCIES—European Space Components Information Exchange System, Radiation: Theory, Definitions—Gamma Radiation*. Accessed: Nov. 10, 2020. [Online]. Available: https://escies.org
[24] NewSpace Systems. *NMRM-001-485 Magnetometer*. Accessed: Nov. 10, 2020. [Online]. Available: https://www.newspacesystems.com

David Novotny (Graduate Student Member, IEEE) received the M.Sc. degree from Czech Technical University in Prague, Prague, Czech Republic, in 2018, with a focus on magnetic gradiometer for car detection and speed measurements, where he is currently pursuing the Ph.D. degree with the Department of Measurement, Faculty of Electrical Engineering.

His current research interests include radiation tolerant low-noise magnetic sensors, mainly anisotropic magnetoresistors (AMR) and digital signal processing methods and low-noise electronics.

Vojtech Petrucha (Member, IEEE) was born in Prerov, Czech Republic, in 1982. He received the M.Sc. degree in measurement and instrumentation and the Ph.D. degree in the same branch for work on the calibration of magnetometers from the Faculty of Electrical Engineering, Czech Technical University in Prague, Prague, Czech Republic, in 2007 and 2012, respectively.

He is currently a Research Assistant with the Department of Measurement, Faculty of Electrical Engineering, Czech Technical University in Prague. His research interests include the development, construction, calibration, testing and applications of sensor systems, especially the magnetic field sensors (AMR and fluxgate).

Michal Dressler (Graduate Student Member, IEEE) received the M.Sc. degree from Czech Technical University in Prague, Prague, Czech Republic, in 2019, with a focus on coil system for magnetometer calibrations with interference compensation, where he is currently pursuing the Ph.D. degree in gradiometer based on magnetic microwires with the Department of Measurement, Faculty of Electrical Engineering.

His current research interests include precise magnetometer calibrations and development of magnetometer electronics.

Antonin Platil received the M.Sc. degree from Faculty of Electrical Engineering, Czech Technical University in Prague, Prague, Czech Republic, in 1997, and the Ph.D. degree from the Department of Measurement, Faculty of Electrical Engineering, Czech Technical University in Prague.

Since 2010, he has been an Associate Professor with the Department of Measurement and mainly deals with various aspects of magnetic measurements, sensors, and systems.

Authorized licensed use limited to: CZECH TECHNICAL UNIVERSITY. Downloaded on April 23,2024 at 13:57:52 UTC from IEEE Xplore. Restrictions apply.

4.6. Measurement of magnetometer's noise using cross-spectral method

During any development and testing of high-performance magnetometer, measurement of its noise is important. Problem is that this noise of instrument can be many orders of magnitude lower than surrounding environmental noise of magnetic field. Especially in laboratory in a city like Prague, where public transportation (trams, metro) is powered with DC current. But even outside of city, magnetic field variations can be order of magnitude higher than the instrument's internal noise.

To cope with this problem, most magnetic laboratories use magnetic shielding. Usually, the shielding is made of multiple layers of highly soft magnetic material (like permalloy). Problem with shielding is that it is very costly, heavy and internal dimensions (defining the usable space) are usually quite limited.

One way to overcome this is using magnetic field compensation system – triaxial coils with current source that actively compensates magnetic variations measured by another low noise magnetometer connected to the system – either in closed loop like [36] or in open loop [37]. This is still costly solution, requires big space and it is not easily transportable.

For this reason, a novel method of noise estimation has been developed and is shown in the publication below. Using second magnetometer (possibly with even higher noise), measurement can be done even in an environment with big magnetic noise/variations. Because both magnetometers experience these common environmental variations + their own noise, calculating cross-spectrum-density can be used to subtract this common part of the measurement, leaving only magnetometers own noise that is to be found.

In reference to IEEE copyrighted material which is used with permission in this thesis, the IEEE does not endorse any of CTU's products or services. Internal or personal use of this material is permitted. If interested in reprinting/republishing IEEE copyrighted material for advertising or promotional purposes or for creating new collective works for resale or redistribution, please go to http://www.ieee.org/publications_standards/publications/rights/rights_link.html to learn how to obtain a License from RightsLink. If applicable, University Microfilms and/or ProQuest Library, or the Archives of Canada may supply single copies of the dissertation. DOI: 10.1109/SENSORS47087.2021.9639875

Low frequency noise investigation of pT-level magnetic sensors by cross-spectral method

Michal Janošek[1], David Novotný[1], Michal Dressler[1] and Elda Saunderson[2,3]
[1]Dept. of Measurement, Czech Technical University in Prague, Prague, Czech Republic
[2]Directorate Space Science, South African National Space Agency, Hermanus, South Africa
[3]Stellenbosch University, Stellenbosch, South Africa

2021 IEEE Sensors | 978-1-7281-9501-8/21/$31.00 ©2021 IEEE | DOI: 10.1109/SENSORS47087.2021.9639875

***Abstract*— We present a simple method to estimate the noise of magnetic sensors running in the Earth's field range by establishing the cross-power spectrum density during ambient field operation and performing spectral subtraction. This method has advantages to the usual subtraction of two sensors outputs, mainly in requirements for synchronization of the sample rate and gain calibration. With this method, verified in simulation and measurements with AMR magnetometers, we could use a fluxgate as a second sensor in order to estimate the low-frequency noise of an HTS SQUID in the ambient field.**

Keywords—magnetic sensor; noise; SQUID; fluxgate; AMR; correlation

I. INTRODUCTION

Estimating the ultralow frequency (ULF, 0.01-1 Hz) noise levels of magnetic sensors in a laboratory is not a straightforward task once the expected noise levels of the sensor are in the order of pT. The first option is to use a magnetic shielding cylinder ("zero-field cylinder") [1]. An even better option is a shielded room with large dimensions and "active shielding". The state-of-the-art "BMSR-2" with 8 layers states about 1×10^4 to 1×10^5 shielding factor between 0.01 and 1 Hz [2]; however, such an establishment is out of reach of a typical laboratory. We have estimated the shielding factor of a compact 6-layer magnetic shielding cylinder (length 0.75 m, inner diameter 17 cm) available at the CTU as approx. $1x10^4$ between 10 and 100 mHz and 2×10^4 at 20 Hz [3]. For a typical laboratory noise of 10 nT/√Hz @ 1 Hz, the transverse shield attenuation would yield about 1 pT/√Hz "residual" noise at 100 mHz.

The problem with finite shielding factors can be mitigated by doing the noise measurements with the shield in a low noise environment. However, for the HTS DC SQUID (High-temperature-superconductor Superconducting Quantum Interference Device) magnetometer, the noise obtained in a zero-field environment might be much smaller than when exposed to the Earth's magnetic field (~20 - 60 μT) during geomagnetic observations [4]. Although the SQUID sensor design can be optimized to reduce the effect of "flux trapping" and subsequent ULF noise due to exposure to large magnetic fields [5], the researchers and manufacturers almost exclusively claim the sensor noise "in zero field", and rarely show noise figures at frequencies below 1 Hz [6], [7] because of its dependence on the electronics, setup and location.

An alternative to magnetic shields for estimating the sensor noise is measuring its output in a quiet ambient (Earth's) field [8]. The method is cheap and benefits from the real-world operation of the sensor, i.e., it is not artificially exposed to zero magnetic field. If ambient noise is lower than the predicted sensor noise, direct measurements can be performed, however, the ambient field cancellation method with two sensors, as described below, is utilized mostly.

A. Out of the shield – difference measurement

The most common method to reject ambient magnetic field and its noise is subtracting the outputs of two identical magnetic sensors; although more advanced methods might yield better results [9]. If we assume that the two sensors exhibit sensor noise $n_1(t)$ and $n_2(t)$, then it follows for the two noisy observations $y_1(t)$ and $y_2(t)$ of the ambient field $a(t)$:

$$y_1(t) = n_1(t) + a(t) \quad \text{and} \quad y_2(t) = n_2(t) + a(t) \qquad (1)$$

If observations are subtracted, the common (correlated) noisy ambient field $a(t)$ is removed. The basic condition is that $a(t)$ is the same at the two sensors. This can be met where the noise gradient is negligible (i.e. sufficiently far away from anthropogenic noise). Natural ambient field fluctuations (diurnal changes of the Earth's magnetic field, magnetic storms / field oscillations induced by Sun activity, thunderstorm discharges etc. - [8]) can be regarded as homogeneous on a local scale and thus $a(t)$ for two aligned and calibrated sensors will be the same.

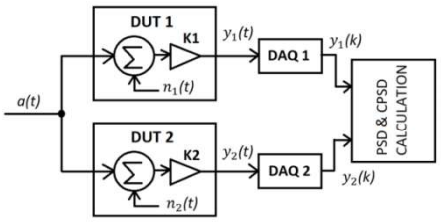

Fig. 1. Difference measurement method

If the condition that $n_1(t)$ and $n_2(t)$ are uncorrelated is met, and both signals are of the same magnitude and distribution, we can then write for Amplitude Spectral Density (ASD=√PSD, T/√Hz) of the individual sensor noise:

$$ASD\big(n_{1,2}(t)\big) = \frac{1}{\sqrt{2}} \cdot ASD\big(y_1(t) - y_2(t)\big) \qquad (2)$$

This method is convenient, however suffers from drawbacks. First, the two sensors have to be of similar noise performance, otherwise the estimation yields more towards the noise of the inferior sensor. Also, the noise floor is limited by coherent sampling, alignment and perfect calibration of the two sensors, i.e. $k_1a(t) \neq k_2a(t)$. Further, any gradient or de-correlation (i.e. due to the presence of ferrous objects) in the

978-1-7281-9501-8/21/$31.00 ©2021 IEEE
Authorized licensed use limited to: CZECH TECHNICAL UNIVERSITY. Downloaded on April 25,2024 at 13:48:28 UTC from IEEE Xplore. Restrictions apply.

ambient noise is not suppressed, requiring lowering the sensor-to-sensor distance [9] and/or using a low-gradient environment.

B. *Proposed method – cross-spectrum subtraction*

To overcome the first two limitations of the difference method, we propose to use a modified cross-spectrum method, as described i.e. in [10]-[12]. The cross-spectrum method was used to suppress the noise of the preamplifiers for magnetoresistive sensors [13] - here the uncorrelated noise was suppressed and noise of the magnetoresistors, far less than the noise floor of the preamplifiers, was revealed. In our case, we will however assume that the ambient magnetic noise is the only correlated component when logging the ambient field with two magnetic sensors. By calculating the cross-spectra and using the spectral subtraction method [14], however, we do not reconstruct the signal our case and stay in the frequency domain.

II. Cross-Spectral Noise Estimation in Ambient MAgnetic Field

With the "modified cross-spectrum method", we can calculate individual sensor noise while overcoming the drawbacks of the direct-subtraction method. Specifically, we can estimate the noise when using two sensors with different noise characteristics, which will be illustrated below even in the case of more than one order of magnitude difference (fluxgate vs SQUID sensors). Also, this method allows us to estimate the noise of a single SQUID sensor, as the ULF noise can differ significantly from sensor to sensor. In our setup [18] we have only one SQUID axis running; therefore the difference method cannot be used.

A. *Method description*

Firstly we have to obtain power spectrum densities (PSD) for measured signals and cross power spectrum densities (CPSD) for DUTs. As the PSD/CPSD is a Fourier transform of auto/cross correlation $R(k)$ of sampled signals [15], we can write for the first observation $y_1(k)$ - using the notation of equation (1) and skipping some mathematical operations after substituting $y_1(k) = n_1(k) + a(k)$:

$$R_{y_1}(k) = \frac{1}{N}\sum_{n=1}^{N} y_1(n)y_1(n-k) = \cdots = \\ = R_a(k) + R_{an_1}(k) + R_{n_{1a}}(k) + R_{n_1}(k) \quad (3)$$

Because $R_{an1} = R_{n1a}$, we can write:

$$R_{y_1}(k) = R_a(k) + 2R_{an_1}(k) + R_{n_1}(k) \quad (4)$$

The same applies for observation y_2(k):

$$R_{y_2}(k) = R_2(k) = R_a(k) + 2R_{an_2}(k) + R_{n_1}(k) \quad (5)$$

Cross-correlation between the two observations is then:

$$R_{y_1y_2}(k) = \frac{1}{N}\sum_{n=1}^{N} y_1(n)y_2(n-k) = \ldots = \\ = R_a(k) + 2R_{an_2}(k) + R_{n_1n_2}(k) \quad (6)$$

When subtracting the cross-correlation (4) from $R_{y1}(k)$:

$$R_{y_1}(k) - R_{y_1y_2}(k) = R_a(k) + 2R_{an_1}(k) + .. \\ .. + R_{n_1}(k) - \left(R_a(k) + 2R_{an_2}(k) + R_{n_1n_2}(k)\right) \quad (7)$$

If we can assume that $2R_{an_1}(k) = 0$ and $2R_{an_2}(k) = 0$ due to no correlation between DUT intrinsic noise and external noise, and that also $R_{n_1n_2}(k) = 0$ due to no correlation between the noise of both DUTs, it is left that:

$$R_{y_1}(k) - R_{y_1y_2}(k) = R_{n_1}(k) \quad (8)$$

which proves our method to be correct. Conversion between correlations $R(k)$ and power spectral density $S(f)$ can be expressed using Fourier transform F:

$$S(f) = F\{R(k)\} = \sum_{k=1}^{N} R(k)e^{-i2\pi fk} \quad (9)$$

The Welch's periodogram [15] estimates the averaged $S(f)$ with number of averages m, defined by window length and overlap. The number of averages influences the variance of the spectrum – $PSD = S(f)$ variance is approximately inversely proportional to m. During the estimation of $a(t)$ noise by calculating the CPSD, we need to suppress the non-correlated part of the y_1 and y_2 observations. The suppression further depends on the number of averages available, and is inversely proportional to $\sqrt{m}$ [10]. The minimum number of averages for Gaussian signals was shown to depend on the inverse coherence function γ^2 [16]: $m_{min} = 1/\gamma^2$.

B. *Verification with synthetic data*

For the initial testing of the proposed method, we generated synthetic data in MATLAB (white noise with additional pink noise). Using three arrays $n_1(k)$, $n_2(k)$, $a(k)$ of uncorrelated noise we obtained two "composite noise" observations $y_1(k)$, $y_2(k)$ - see equation (1). We simulated a frequent scenario with one "good" low-noise sensor and one "poor" sensor with higher noise. In this case the subtraction method cannot be used as it automatically leads to the noise of "poor" sensor. Results can be seen in Fig. 2.

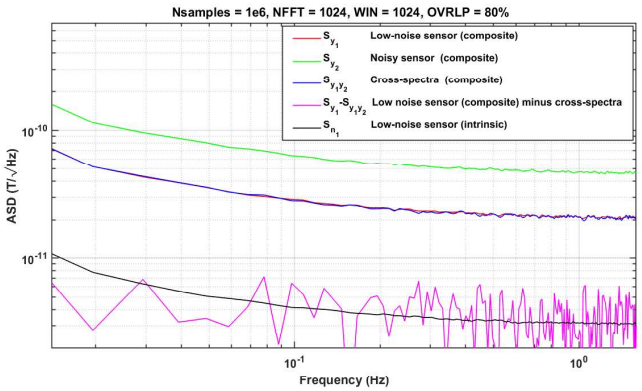

Fig. 2. Verification with simulated data – 1×10^6 samples, m ~4900

C. *Effects of imperfections – alignment, sample rate, gain*

For practical use of the method, multiple imperfect scenarios have been tested to verify its usability. Since we are doing computations in the frequency domain instead of the

Authorized licensed use limited to: CZECH TECHNICAL UNIVERSITY. Downloaded on April 25,2024 at 13:48:28 UTC from IEEE Xplore. Restrictions apply.

time domain, and the process can be assumed ergodic, it gives us inherent independence to time alignment (lead/lag has no effect on the CPSD subtraction method). Errors in sampling rate leads to worsening of results as shown in Fig.3 for real data. Error in gains (>10%) caused by imperfect calibration also lead to worse results, however, we have verified that even a 1% gain error is acceptable.

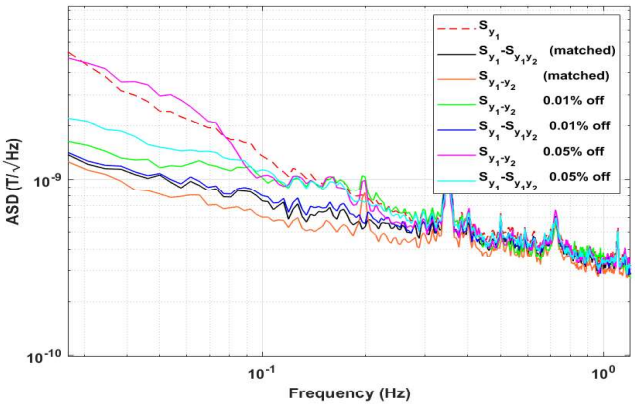

Fig. 3. Samplerate error simulation - effect on CPSD subtraction

D. AMR magnetometer noise estimation

The real-world measurement has been done using two identical AMR magnetometers [17] mounted on a wooden desk with 18 cm spacing, shown in Fig. 4. Both magnetometers streamed data over a serial link with the same sampling rate, and the data were recorded on a PC. Even at such a small distance, crosstalk between compensation windings of AMR sensors is negligible, as the compensation windings are on the AMR chip, and thus yield negligible magnetic moments. In Fig. 4 we see that the calculated noise of AMR#1 (black trace) matches the direct measurement of S_{n1} in a 6-layer shield (magenta) closely.

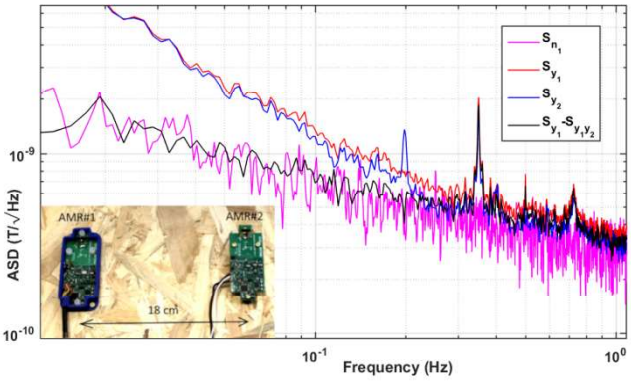

Fig. 4. AMR – noise measurement results and photo of the setup

III. Field Estimation of SQUID Noise

At SANSA Space Science, we are operating an unshielded HTS SQUID for geomagnetic observations [18]. A single Z-axis sensor type M2700 (StarCryo, USA), is connected to flux-feedback-loop electronics type SEL-1 (Magnicon, Germany) - see Fig. 5. The analog output is digitized with two 24-bit cards, NI-9252 and AD24-ETH. For this study we used the latter, as it offers lower noise at the expense of bandwidth. The ULF noise of the SQUID could not be estimated yet as it is masked by ambient noise and we are lacking a second sensor performing equally well.

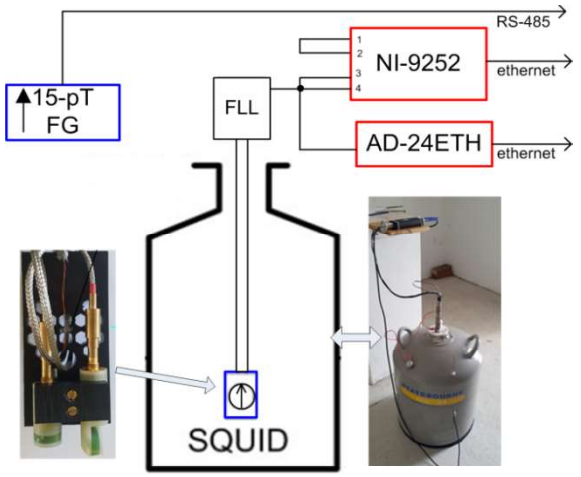

Fig. 5. HTS SQUID and fluxgate sensor setup

The AMR fluxgate and SQUID do not share a common ADC (the fluxgate output is digital). The only possible correlation would be from a noisy power supply, which is 12V DC buffered by lead-acid batteries. Fig. 6 shows a short record of sampled data and resulting spectra. Correlation between the fluxgate and SQUID data is evident from the time record; we also see that the "composite" fluxgate noise is also almost order of magnitude higher than of the SQUID.

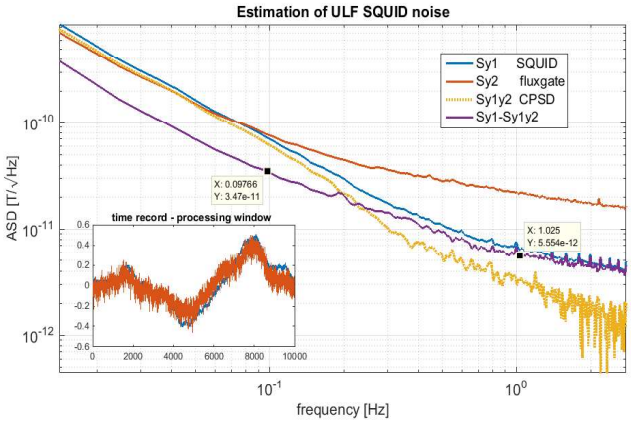

Fig. 6. SQUID and fluxgate data - time domain and noise estimation

The level of correlated ambient field noise of about 3 pT/√Hz at 1 Hz is reasonable since we observed similar values before with a 1-pT fluxgate magnetometer [19]. We can see that above approximately 200 mHz, the SQUID noise is dominating, with about 5 pT/√Hz at 1 Hz. Below 100 mHz the coherent ambient field noise dominates. The SQUID noise at 100 mHz (upper limit estimation) was established as about 30 pT/√Hz. A future measurement with the 1-pT fluxgate [19] as a third instrument will bring us more confidence in the potential of the presented method and reliability of the established SQUID noise.

Acknowledgment

M.J. and D.N. acknowledge the support of the Grant Agency of the Czech Republic, under grant No. 20-19686S. E.S. and M.D. acknowledge the support of the IEEE Magnetics Society through 2021 IEEE Educational Seed Funding. D.N. was also supported through the internal grant of the CTU Prague, No. SGS19/177/OHK3/3T/13.

Authorized licensed use limited to: CZECH TECHNICAL UNIVERSITY. Downloaded on April 25,2024 at 13:48:28 UTC from IEEE Xplore. Restrictions apply.

REFERENCES

[1] E. Baum and J. Bork, "Systematic design of magnetic shields", Journal of Magnetism and Magnetic Materials, 101(1-3), 1991, pp 69-74.

[2] J. Bork., H. D. Hahlbohm, R. Klein and A. Schnabel, "The 8-layered magnetically shielded room of the PTB: Design and construction", Biomag2000, Proc. 12th Int. Conf. on Biomagnetism. Espoo, Finland, 2001. pp. 970-73.

[3] M. Janosek, A. Zikmund and P. Ripka, "Tensor behaviour of magnetic shielding factor", 2011 INTERMAG Conference, April 25–29, 2011, Taipei, Taiwan, unpublished.

[4] C. P. Foley, et al., "Geophysical exploration using magnetic gradiometry based on HTS SQUIDs", IEEE Transactions on Applied Superconductivity, Vol 11, No 1, 2001, 1375-1378.

[5] R. Stolz, et al., "Superconducting sensors and methods in geophysical applications" Supercond. Sci. Technol., Vol. 34, 2021, 033001

[6] M. I. Faley, Y. V. Maslennikov, V. P. Koshelets, and R. E. Dunin-Borkowski, "Flip-Chip High-Tc DC SQUID Magnetometer with a Ferromagnetic Flux Antenna", IEEE Transactions on Applied Superconductivity, 28(4), 2018, pp. 1-5.

[7] S. Keenan, CSIRO Manufacturing, HTS SQUID magnetometers and gradiometers, available from www.csiro.au, accessed on 2/7/2021

[8] G. C. Constable and S. C. Constable, "Satellite magnetic field measurements: applications in studying the deep earth", The State of the Planet: Frontiers and Challenges in Geophysics, 2004, 150: pp. 147-159.

[9] P. J. M. Wőltgens, R. H. Koch, "Magnetic background noise cancellation in real-world environments", Review of Scientific Instruments, 2000, 71.3: pp. 1529-1533.

[10] E. Rubiola, F. Vernotte, "The cross-spectrum experimental method", arXiv preprint arXiv:1003.0113, 2010

[11] M. Sampietro, L. Fasoli, and G. Ferrari, "Spectrum analyzer with noise reduction by cross-correlation technique on two channels", Review of Scientific Instruments, 70.5, 1999 pp. 2520-2525.

[12] A. C. Cárdenas-Olaya, et al., "Noise characterization of analog to digital converters for amplitude and phase noise measurements", Review of Scientific Instruments, 2017, 88.6: 065108.

[13] N. A. Stutzke, S. E. Russek, D. P. Pappas, and M. Tondra, "Low-frequency noise measurements on commercial magnetoresistive magnetic field sensors", J. Appl. Phys., 97, 10Q107, 2005.

[14] S. V. Vaseghi, Advanced digital signal processing and noise reduction. John Wiley & Sons, 2008, pp. 333, ISBN: 0-471-62692-9.

[15] A. V. Oppenheim, R. W. Schafer and J. R. Buck, Discrete-Time Signal Processing, 2nd Ed., Prentice Hall, NJ, 1999, p.737-738.

[16] J. Biaire, L. K. J. Vandamme, "Uncertainty in Gaussian noise generalized for cross-correlation spectra", Journal of Applied Physics, 1998, 84.8: pp. 4370-4374.

[17] D. Novotny, V. Petrucha, M. Dressler and A. Platil, "Characterization of a Digital AMR Magnetometer for Space Applications", in IEEE Transactions on Instrumentation and Measurement, vol. 70, pp. 1-9, 2021, Art no. 9504309, doi: 10.1109/TIM.2020.3043867.

[18] T. Matladi, et al., "Correlation between fluxgate and SQUID magnetometer data sets for geomagnetic storms". In: E3S Web of Conferences. EDP Sciences, 2014, p. 02002.

[19] M. Janosek, et al., "1-pT noise fluxgate magnetometer for geomagnetic measurements and unshielded magnetocardiography", IEEE Transactions on Instrumentation and Measurement, vol. 69, No 5, 2019, pp. 2552-2560.

Authorized licensed use limited to: CZECH TECHNICAL UNIVERSITY. Downloaded on April 25,2024 at 13:48:28 UTC from IEEE Xplore. Restrictions apply.

4.7. Reducing power consumption by pulsed power supply

In the conference abstract presented below, the idea how to save power was to enable/disable power supply for AMR bridge only when ADC is sampling. This method allows to trade-off power consumption with measurement noise (resolution). During this research it was also found out that while theoretically noise should decrease proportionally to duty cycle due to aliasing, this relation is nonlinear and the best noise can be achieved even with smaller than 100 % duty cycle (where bridge is at all times powered on). On the other hand, power consumption of fast preamplifier and fast ADC needs to be considered.

Another interesting application is for powering AMR from higher voltage – as main power rails in space satellites can be higher – 12 or 24 V instead of 5 V. With considerably small duty cycle, power does not need to be regulated down to 5 V (as for continuous operation is necessary) which normally leads to additional losses.

Low-Power AMR Magnetometer Operated in Discontinuous Mode

David Novotný, Lukáš Mičan, Vojtěch Petrucha

In many applications including space missions, Anisotropic Magnetoresistors (AMR) based magnetometers raised their popularity [1,2] as they are solid-state off-the-shelf components with good radiation immunity [3]. One of the issues they suffer is low sensitivity and thus high noise induced by their bridge thermal noise as well as by preamplifier stage noise [4]. To overcome this problem, higher supply voltage of an AMR bridge can be used to raise the sensitivity. This seems to be straightforward but power dissipated on the sensor raises quadratically with bridge voltage and thus it can't be operated in „classical" continuous mode (due to overheating and excessive power consumption).

In our research we propose novel method of powering bridge by pulses allowing to obtain better sensitivity and less noise with AMR sensors. During these short pulses (100 us width and 4.5 ms period) we also perform flipping pulses (both S/R) while measuring bridge response with an analog-to-digital converter. Acquired data are then signal-processed on the fly by a microcontroller. In traditional method, 10 V in continuous mode with HMC1021 AMR sensor will dissipate 91 mW of power, while cycling power with a duty cycle of 1:45 means only 2 mW (considering zero overhead power). In mostly used triaxial version it is 273 mW vs 6 mW preserving other main parameters of the magnetometer unchanged.

To verify this idea we have developed single axis magnetometer (Fig. 1) with adjustable both bridge voltage as well as flipping current, with possibility of precise timing of all events. In the first trial/test, we have tried to obtain similar noise with pulsed 10 V bridge as we were able to get in our previous research with continuous supply of 10V [4], (see Fig 2.) After achieving this milestone (solving a lot of technical troubles) we tried 20 V bridge supply to verify expected noise reduction (as sensitivity doubles), but for now without result – at this voltage, AMR's electrical offset saturates the preamplifier. In the near future we aim to tackle this issue and to test the noise drift with temperature in different flipping current configurations.

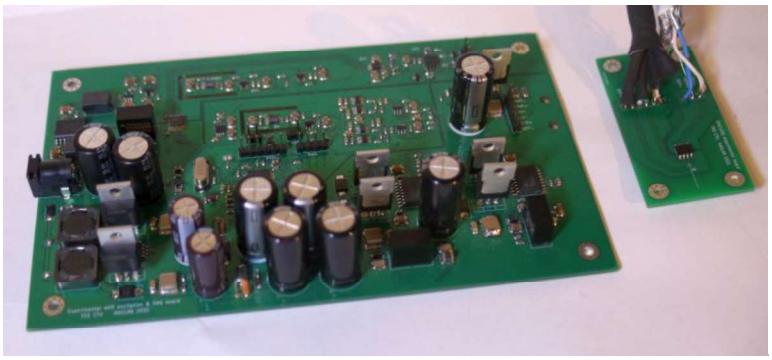

Fig.1 - Photo of the experimental prototype

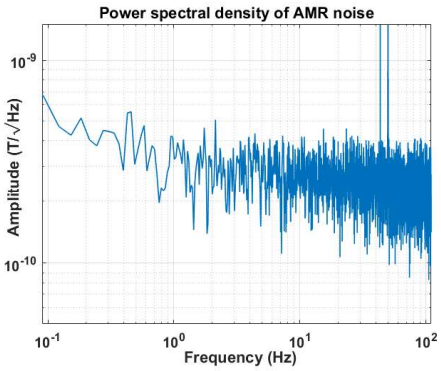

Fig.2 - PSD of noise with pulsed 10 V bridge voltage

[1] Leitner, Stefan, et al., IEEE Transactions on Magnetics, Vol. 51, No. 1 (2015)
[2] P. Brown et al., Review of Scientific Instruments, Vol. 85, No. 125117 (2014)
[3] Sanz, Ruy, et al., Sensors, Vol. 12, No. 4 (2012)
[4] D. Novotný, V. Petrucha, M. Janošek, IEEE Transactions on Magnetics, Vol. 55, No. 1 (2018)

4.8. Power saving algorithm utilizing open/closed loop switching

In paper below, which is currently (9/2024) in peer-review process (abstract/poster presented on EMSA 2024 conference) a novel algorithm is proposed. Idea is to reduce power consumption by disabling feedback compensation loop whenever its operation is not necessary. This can help significantly as feedback operation always require non negligible power. In the presented AMR magnetometer approx. 20 % of power consumption can be saved in this way.

The closed loop operation helps to greatly reduce temperature drift of magnetometer's sensitivity, to increase linearity and to remove hysteresis. In the proposed algorithm, closed loop is disabled by default and only turn on for a while when temperature of magnetometer or magnetic field measured changes over certain limit. When this happens, closed loop operation is turned on, a "calibration" measurement is taken as fast as possible, and closed loop is then disabled again. Then, after settling of open-loop, reading first valid open-loop measurement is stored. All following measurement is relative to the last "calibration" measurement.

Novel Power Saving Algorithm for AMR Magnetometer with Fast Settling Feedback Loop

David Novotný, Michal Janošek, Vojtěch Petrucha, Antonín Platil

Department of Measurement, Faculty of Electrical Engineering, Czech Technical University in Prague, Prague, Czech Republic

Power consumption plays a pivotal role in a variety of applications that use magnetometers (e.g. space applications, wearables, drones…). In this paper, a novel approach to reduce power consumption in magnetometers is proposed. We primarily focus on the AMR magnetometer, which was subjected to a series of tests. Nevertheless, this algorithm is broadly applicable to any magnetometer that employs a fast-enough feedback compensation. In precise magnetometers, feedback compensation is almost always utilized to obtain stability and linearity. Traditionally, this feedback compensation remains active for the entire duration the magnetometer is powered on. We propose an algorithm that disables this feedback for the majority of the time and enables it briefly only when necessary. This approach leads to a significant reduction in power consumption while maintaining full accuracy and low noise.

***Index Terms*—AMR, compensation, feedback loop, low power, magnetometer, precise**

I. Introduction

AMR magnetometers are used in various applications where the precise measurement of a small magnetic field is desired (e.g. Earth's magnetic field for navigation), while maintaining low power consumption and compact dimensions. They are also lightweight, solid-state instruments and are readily available off-the-shelf. These factors make them especially attractive for the space and avionics industries (e.g. cubesats, smallsats, or drones). AMR magnetometers have been utilized in many space applications, e.g. [1]-[3] for mapping magnetic fields, navigation in space, or actuating magneto torquers. They are also widely used to maintain heading in most drones (e.g. [4]). Since gyroscope measurements drift over time and tilt/roll measurements are corrected using an accelerometer, yaw can only be corrected with the help of a magnetometer (or, perhaps, in case of sophisticated systems, by camera or other external reference).

Given the high demand for low-power, precise AMR magnetometers, we propose a novel method for reducing power consumption while maintaining the instruments high precision and low noise levels.

For optimal precision and stability, AMR magnetometers almost always utilize feedback compensation. This closed-loop magnetic field compensation keeps the sensor itself within a zero magnetic field, significantly improving the magnetometer's linearity and temperature stability of sensitivity. A major advantage of AMRs is that they often come with embedded compensation windings, unlike fluxgate magnetometers, which require external coils wound on non-magnetic supports. This not only reduces cost and complexity while avoiding potential mechanical damage, but also it has been shown in [5] that it leads to excellent temperature stability. This is likely due to the silicone substrate, which is highly dimensionally stable with temperature, on which the winding and AMR bridge itself are built.

However, in many applications, the measured magnetic field is steady, with slow variations or only occasional fast perturbations. The same also applies to the temperature of the magnetometer itself. To leverage this, we propose a method that switches from an open-loop operation to feedback (closed loop) only when necessary. For this algorithm to be practical, the feedback-loop settling time should be as short as possible (this, of course, leads to a trade-off between precision and low power consumption). For the tested magnetometer (see Fig. 1) with a HMC1021 sensor, closed-loop compensation requires approx. 100 mW to steadily compensate a 50 µT field, but only 10 mJ per correction measurement when performed in 100 ms.

This approach may also enable the use of embedded compensation windings in the lowest-noise AMR on the market (as of 07/2024): the HMC1001. However, this sensor suffers from a poor compensation constant (low coil turns), leading to significantly high-power consumption when compensating even for the Earth's field (approx. 50 µT, depending on location). Consequently, this sensor is often used without compensation (in an open loop), where temperature dependency and nonlinearity are high. Thus, temperature measurement is employed to partially mitigate these issues [3].

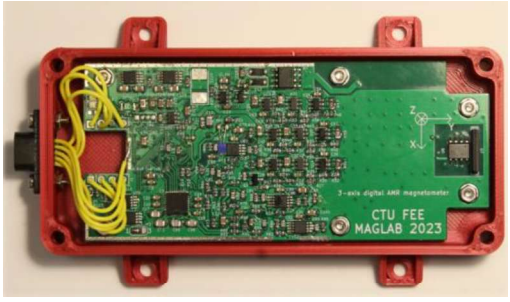

Fig. 1. Photo of testing prototype of the AMR magnetometer

Manuscript received April 1, 2015; revised May 15, 2015 and June 1, 2015; accepted July 1, 2015. Date of publication July 10, 2015; date of current version July 31, 2015. (Dates will be inserted by IEEE; "published" is the date the accepted preprint is posted on IEEE Xplore®; "current version" is the date the typeset version is posted on Xplore®). Corresponding author: F. A. Author (e-mail: f.author@nist.gov). If some authors contributed equally, write here, "F. A. Author and S. B. Author contributed equally." IEEE TRANSACTIONS ON MAGNETICS discourages courtesy authorship; please use the Acknowledgment section to thank your colleagues for routine contributions.

Color versions of one or more of the figures in this paper are available online at http://ieeexplore.ieee.org.

Digital Object Identifier (inserted by IEEE).

0018-9464 © 2015 IEEE. Personal use is permitted, but republication/redistribution requires IEEE permission.
See http://www.ieee.org/publications_standards/publications/rights/index.html for more information. (Inserted by IEEE.)

II. Magnetometer Operation Principle

A prototype of the presented digital AMR magnetometer consists of the blocks simplified in Fig. 2. The AMR sensor's output is pre-amplified, digitized by ADC, and then read out by an MCU. These data are digitally demodulated and used as input for a digital feedback regulator (a simple integrator). The output of the regulator sets the duty cycle of a PWM signal, which serves as a simple DAC to generate an analog voltage derived from a voltage reference. This voltage is then passed through an RC filter stage, fed into a voltage-to-current converter with an op-amp, and finally applied to the embedded feedback coil of the sensor.

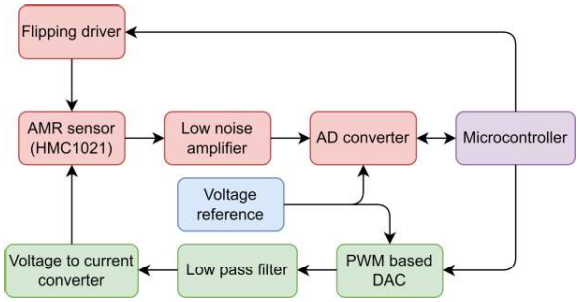

Fig. 2. Simplified block diagram of one axis of the AMR magnetometer

The magnetometer's output is then streamed through a serial link to the computer. In open-loop mode, the magnetometer outputs the demodulated and filtered signal measured by the ADC at the output of the amplified AMR bridge. In a closed-loop operation, the duty-cycle of the PWM signal is the output variable, as it is directly proportional to the compensation current and, thus, the compensation field, which – according to the principle of feedback operation – should equal the measured field.

III. Proposed Algorithm Description

The proposed algorithm uses three input variables to determine if a "calibration" measurement with a closed loop is necessary, namely: fluctuations in temperature, changes in the magnetic field, and the time elapsed since the last calibration. After a closed-loop "calibration" is performed, open-loop measurement is used as an additional ΔB to the last closed-loop absolute measurement.

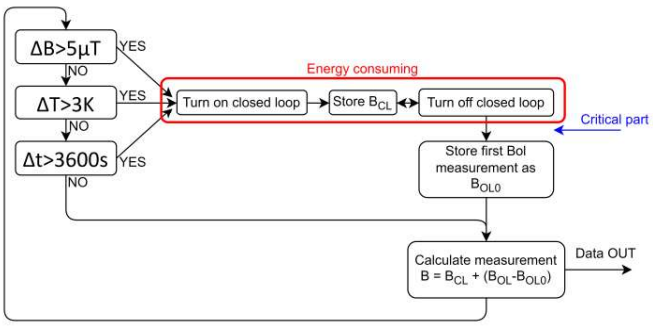

Fig. 3. Simplified flowchart of the proposed algorithm

IV. Algorithm Verifications

The first test of the algorithm examined how it reacts to a rising magnetic field that crosses the calibration threshold. Using an external coil (lee-whiting) and a waveform generator, a slowly rising magnetic field was generated, and the output of the magnetometer was recorded (see Fig. 4). The algorithm's action is visible as a correction (when ΔB > 1 μT). In this case, the open-loop mode was not measuring properly, thus, the closed-loop correction resulted in a jump in measurement equal to the inaccuracy of the open-loop measurement.

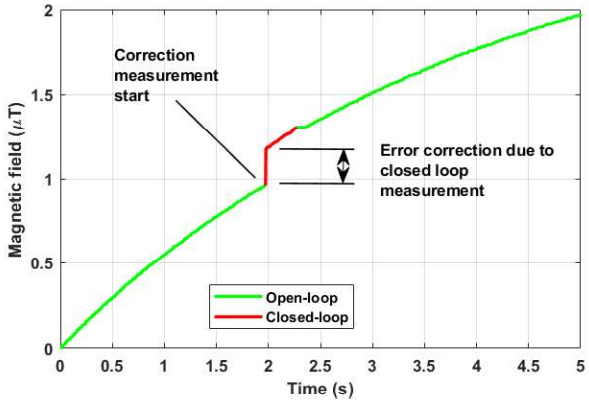

Fig. 4. Response of the proposed algorithm on externally generated rising magnetic field

Another important parameter of the magnetometer is its linearity. Since this method combines a linear closed loop with a non-linear open-loop mode, it was necessary to measure the resulting nonlinearity. The setup was similar to the above, this time with the magnetometer in the Lee-Whiting coil system driven by a controlled current source. A computer program performed a sweep of the magnetic field while controlling the current source and recording the output of the magnetometer.

Non-linearity in both open- and closed-loop modes has been measured, including with the proposed algorithm (where the criterion for calibration is set to ΔB > 5 μT). The measured data are compared to the Matlab simulation obtained from open- and closed-loop data separately (see Fig. 5).

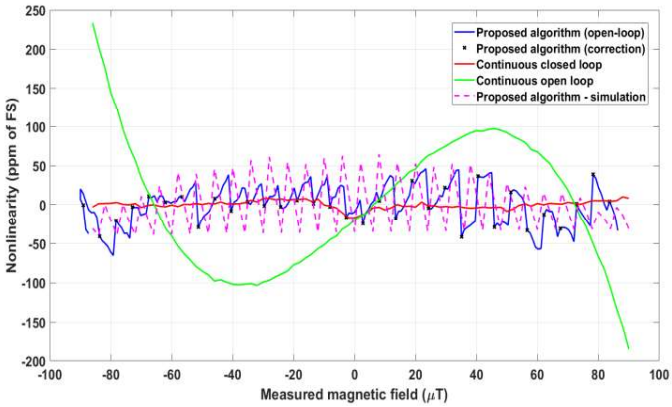

Fig. 5. Comparison of the magnetometer's nonlinearity in closed loop, open loop and with proposed algorithm

The AMR sensor itself (in an open loop) exhibits significant temperature dependence of the sensitivity, approx. 0.4 %/K (but this sensitivity can be suppressed to approx. 0.06 %/K by powering the sensor from a constant current source, though this comes with a cost of increased complexity and higher power consumption due to additional losses). To keep power consumption and complexity low, a voltage source is used (directly supplied from a low-noise, low-drop regulator).

All this means that in an open loop, the magnetometer will suffer from inaccuracy as the temperature changes from the last "calibration". One way to address this is to numerically compensate measurement for temperature variations. While this method is sometimes used [3], it requires characterization of every magnetometer in a temperature chamber due to variations in temperature coefficients. This approach is impractical, time-consuming, and potentially problematic due to the drift of this temperature coefficient over time.

The proposed algorithm instead takes a calibration measurement when the fluctuations in temperature from the last calibration measurement exceed a given threshold. The setting of this threshold depends on the acceptable level of inaccuracy; for example, to keep the maximum margin of error below 1%, a ΔT threshold of 3 K is used. This keeps the error within a ± 1% band, as shown in Fig. 6 below.

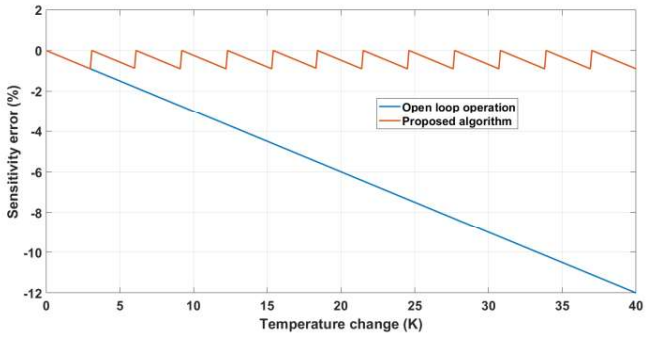

Fig. 6. Simulation of the proposed algorithm response to temperature change

To calculate the power savings achieved by the algorithm, current consumption has been monitored over time for both open loops, closed loops, and the proposed algorithm with calibration measurements. Since the magnetometer is fed a constant voltage, current consumption can be easily converted to power, as illustrated in Fig. 7 below.

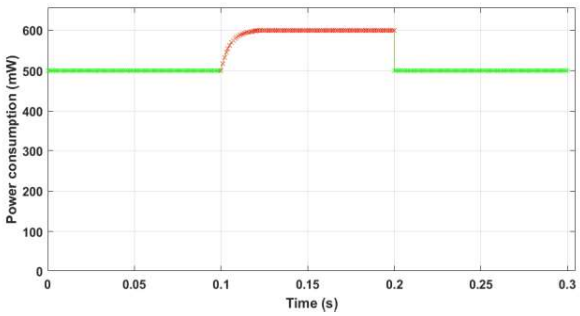

Fig. 7. Power consumption over time of the magnetometer in different modes (green – open loop, red – closed loop)

V. HARDWARE DESCRIPTION

To maintain a design that is low-cost, low-power, and low-noise—requirements that seem rather contradictory—a digital-to-analog converter (DAC) is implemented using a simple PWM + filter approach. Although DAC parameters greatly influence the final accuracy of the magnetometer, it has been demonstrated in [5] and [6] that this method is highly effective. The use of PWM as a DAC is also known from extremely precise metrology-grade calibrators, such as the Fluke 5700A [7], which indicates that when implemented correctly, its precision and accuracy are excellent. Generating the duty cycle itself is a very stable process, given by the crystal-based clock of the microcontroller and its timer peripheral. To obtain stable and precise voltage levels for the PWM signal, an analog multiplexer that switches between a stable voltage reference and ground is used.

When using PWM as a DAC, there are multiple contributing factors to the final performance that should be considered. Firstly, clock jitter at frequencies near the PWM's frequency can affect performance in terms of noise. This is also true for jitter or unstable voltage thresholds of the multiplexer, and instability of its Ron/Roff ratio can cause drift. However, from previous research [5], these effects seem negligible in the proposed schematic, which is derived from that research.

Due to the speed limitations of the multiplexer and also the trade-off between PWM frequency and resolution, the frequency cannot be too high. In our prototype, it is 16 kHz. To filter out its AC component, a simple 2-stage RC filter with a cut-off frequency of 160 Hz is used. To further speed-up this PWM DAC, a special AC-component removal circuit inspired by [8] is employed. The full schematic of the single-channel PWM DAC can be seen in Fig. 8 below.

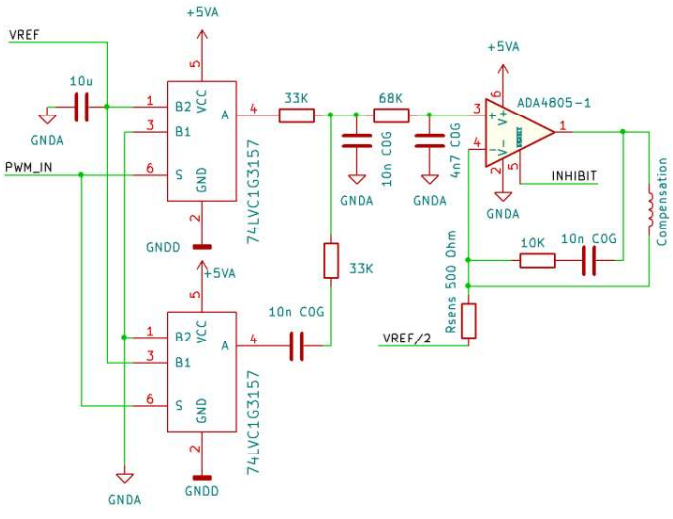

Fig. 8. Schematic of a single channel PWM based DAC

The trade-off between PWM frequency and its resolution is improved in two ways. Firstly, even though the microcontroller (STM32F334) has a 144-MHz clock, it has specialized delay-taps [9] that allow for sub-clock-tick

resolution by a factor of 32, equating to an equivalent frequency of 4.6 GHz, resulting in 18-bit resolution with a 16 kHz PWM. Secondly, an advanced technique—a hybrid PWM sigma-delta scheme inspired by [10] is used. The principle is that the least significant bit of the PWM duty cycle is manipulated in a 16 PWM clocks loop. Zero or one is added to the actual PWM duty cycle code word. When no 1 is added, it results in code N, when 8 ones are added, it results in N+0.5; and when only 1 is added, it results in N+1/16. This allows for an enhancement of the resolution by 4 bits, resulting in a total magnetometer resolution of 22 bits (47 pT at a 200 µT range, which is sufficient).

VI. SETTLING SPEED REQUIREMENTS

To take a calibration measurement using a closed-loop operation, the entire feedback chain must settle after turn-on to obtain a valid measurement. The settling time is primarily determined by the bandwidth of the DAC and the current source that converts its output voltage to current for the compensation winding. Additionally, the operational amplifier used in the current source must settle quickly after power-on (as it is inhibited in open-loop mode).

The feedback loop is controlled by a digital regulator implemented in the microcontroller (which is essentially a simple numeric integrator). To speed up the regulator and minimize its contribution to the settling time, its value is pre-calculated based on the last measurement before it starts to regulate.

For a two-stage RC filter with AC component removal, the analytical solution is quite cumbersome. However, for an evaluated prototype, a simulation of the step response can be seen in Fig. 9 below, where a sufficient 250-Hz bandwidth is used to achieve stable regulation of feedback in a closed-loop operation with a bandwidth of a few tens of Hz.

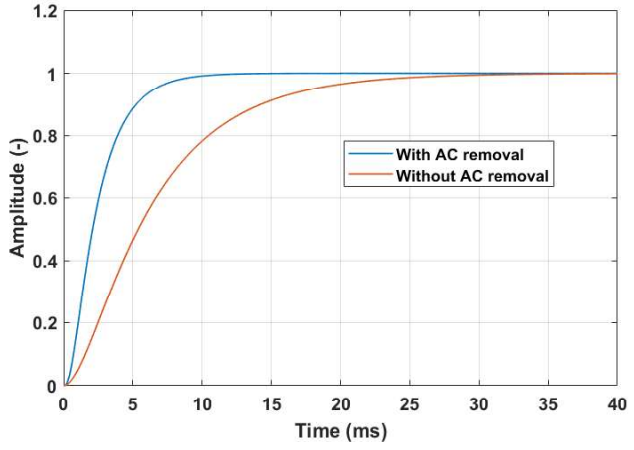

Fig. 9. Multisim simulation of a step response of a two-stage RC filter with and without AC-removal enhancement for comparison

From the simulation, settling below 1 LSB of the DAC takes approx. 15 ms, which is the minimum time required for a calibration measurement. In reality, the calibration time is longer (100 ms) for the settling of op amps, average multiple closed-loop samples and for overhead operations.

VII. CONCLUSION

With the presented method, a power reduction of approx. 100 mW is achieved. Given the magnetometer's total power consumption of 500 mW, this method can result in a 20 % reduction in power usage. This reduction is facilitated by the high field-to-current ratio of the embedded compensation winding in the HMC1021. An even more intriguing application of the proposed algorithm involves the use of the HMC1001 sensor. Although the HMC1001 offers lower noise, its compensation winding has a lower field-to-current ratio, making it impractical to use due to high power consumption. Appling this algorithm to the HMC1001 sensor will be the subject of ongoing research.

This method can be further improved using coarse/fine measurement switching. When high precision is not always required, a lower current can be supplied through the AMR bridge, resulting in lower power consumption (on the tested magnetometer, an additional 60 mW of energy can be conserved, albeit at the cost of increasing noise by a factor of three). Such a switching mechanism could be particularly useful in space missions where only coarse measurements might be necessary during navigation, whereas a precise scientific mode can be activated for mapping or capturing a magnetically interesting event.

ACKNOWLEDGMENT

This work was supported by the Grant Agency of the Czech Technical University in Prague, grant No. SGS22/170/OHK3/3T/13.

REFERENCES

[1] P. Brown et al., "Space magnetometer based on an anisotropic magnetoresistive hybrid sensor," Review of Scientific Instruments 85, 125117, 2014, https://doi.org/10.1063/1.4904702

[2] M. Díaz-Michelena, "Small Magnetic Sensors for Space Applications," Sensors, vol. 9, no. 4. MDPI AG, pp. 2271–2288, Mar. 30, 2009. doi: 10.3390/s90402271.

[3] Leitner et al., "Design of the Magnetoresistive Magnetometer for ESA's SOSMAG Project," IEEE Transactions on Magnetics, vol. 51, no. 1. Institute of Electrical and Electronics Engineers (IEEE), pp. 1–4, Jan. 2015. doi: 10.1109/tmag.2014.2358270.

[4] J.F Guerrero Castellanos, S. Lesecq, N. Marchand J. Delamare, *A Low-Cost Air Data Attitude Heading Reference System for the Tourism Airplane Applications, Sensors*, 2005 IEEE

[5] D. Novotny, V. Petrucha, M. Dressler and A. Platil, Characterization of a Digital AMR Magnetometer for Space Applications, in IEEE Transactions on Instrumentation and Measurement, vol. 70, pp. 1-9, 2021, Art no. 9504309, doi: 10.1109/TIM.2020.3043867.

[6] Novotný, D.; Petrucha, V.; Janošek, M. A Digitally Compensated AMR Magnetometer, IEEE Transactions on Magnetics. 2019, 55(1), ISSN 0018-9464.

[7] Fluke (2005), *5700A/5720A Series II Multi-Function Calibrator* (Service Manual). Accessed July 31, 2024. From Fluke website: https://assets.fluke.com/manuals/5720a___smeng0200.pdf

[8] S. Woodward, *Cancel PWM DAC Ripple with Analog Subtraction*, EDN. Accessed July 31, 2024. From EDN website: https://www.edn.com/cancel-pwm-dac-ripple-with-analog-subtraction/.

[9] STMicroelectronics (2020). *HRTIM cookbook* (Application Note No. AN4539). Accessed July 31, 2024. From STMicroelectronics website.

[10] STMicroelectronics (2017). *PWM resolution enhancement through a dithering technique for STM32 advanced-configuration, general-purpose and lite timers.* (Application Note No. AN4507). Accessed July 31, 2024. From STMicroelectronics website.

4.9. Preparing magnetometer for real space mission

During my PhD study I had an opportunity to participate in project LVICE[2] (Lunar Vicinity Complex Environmental Explorer) in order to make AMR magnetometer for this space mission as an auxiliary magnetometer to the main fluxgate.

Project had multiple stages that it must pass before it would be fully approved to launch and funded. After passing early stages (basically paperwork), first engineering prototypes of scientific instruments has been made (as well as the AMR designed for this mission).

The concept was to use low noise fluxgate magnetometer with low range (expected amplitude of magnetic field during mission has been few tens of nT) on expandable boom. Even though fluxgate would be distant from the probe, on boom (planned between 1 and 2 m length), it is still influenced by magnetic disturbances caused by the probe itself.

To avoid this problem, an auxiliary AMR magnetometer was planned inside of probe, near the other end of the boom. Both instruments were planned to measure magnetic field synchronously in order to mathematically subtract AMR data from fluxgate measurement in real time. This method is already well known [50, 51] and has been used in a space missions.

Unfortunately, LVICE2 project did not pass one of the last stages of approval. Nevertheless, lot of experiences has been gathered as well as know-how and there is still a chance to use them in future missions.

In reference to IEEE copyrighted material which is used with permission in this thesis, the IEEE does not endorse any of CTU's products or services. Internal or personal use of this material is permitted. If interested in reprinting/republishing IEEE copyrighted material for advertising or promotional purposes or for creating new collective works for resale or redistribution, please go to http://www.ieee.org/publications_standards/publications/rights/rights_link.html to learn how to obtain a License from RightsLink. If applicable, University Microfilms and/or ProQuest Library, or the Archives of Canada may supply single copies of the dissertation. DOI: 10.1109/SENSORS56945.2023.10325159

B. *Low noise sensor head*

As mentioned, the magnetic field to be measured in the cislunar space can be just units of nanotesla, so there was a request to decrease the noise even further. A similar design was used incorporating only three race-track sensors (40 × 17 × 3 mm^3 dimensions) with a 30 mm amorphous magnetic core length. With only three sensors, the internal structure is much simpler, fixed together more reliably by screws rather than by gluing (as in the 30 mm cube), but not symmetrical. We plan to build another unit with a six-sensor symmetrical design for comparison. Fig. 4 illustrates the sensor production; the final outer protective box is not shown. As the probe as well as the sensor head will be almost continually exposed to sunlight, no heater is currently planned in the design.

Fig. 4 Three 40 mm race-track-sensor–based triaxial fluxgate sensor head with a vector compensation of measured field (50 mm cube side).

C. *Fluxgate sensor electronics*

The mission budget does not allow for full deployment of radiation-tolerant parts or ASICs designed specifically for fluxgate signal conditioning in the space environment. A traditional, single-range, analog signal–conditioning approach allowed us to reach a sufficient measurement resolution even with 16-bit ADC, as the full scale is limited to ±500 nT (while there are also 18- and 20-bit versions of the ADC). The whole unit is managed by an MSP430FR5969 16-bit low-power microcontroller, which has a direct replacement in the form of a radiation-hardened part (MSP430FR5969-SP). The MCU generates all necessary signals for fluxgate sensor excitation, synchronous demodulation, daisy-chained external ADC handling, housekeeping measurements (sensor and electronics temperature, power rail voltages using internal 12-bit ADC), step-down DCDC converter synchronization, and RS422 communication. See Fig. 5 for a block diagram of the concept. Active parts were selected based on our previous experience (^{60}Co radiation testing) or based on the availability of direct or similar radiation-tolerant replacements or published data [10]. The electronics were built on a four-layer PCB with PC104 format dimensions to be stackable in a cube-sat format (Fig. 6).

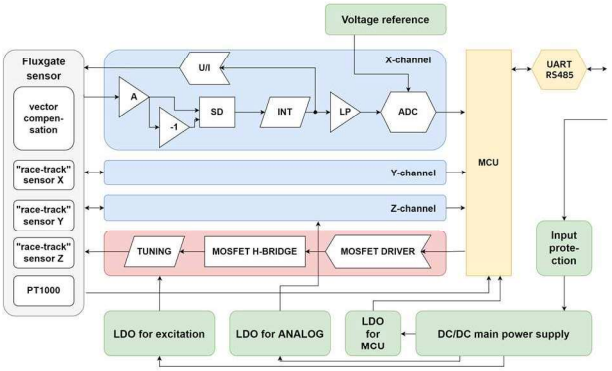

Fig. 5 Fluxgate magnetometer block diagram.

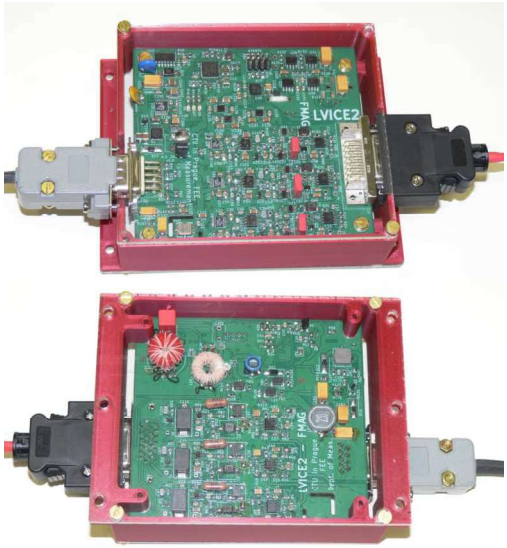

Fig. 6 Fluxgate magnetometer electronics prototype, PC104 format.

III. AMR Magnetometer Design

The anisotropic-magneto-resistance–based magnetometer is designed to sense perturbations coming from the probe itself (reaction-wheel operation, occasional switching of higher currents, etc.). It has a much higher full-scale range (currently ±100 μT), as it will be placed directly on the probe structure close to the boom release mechanism. The design is based on the construction described in [11]. HMC1021 sensors are used. We plan to test HMC1001, which has lower noise but also a compensation coil constant. That is problematic for Earth's like field full-scale range (compensation current 25 mA for 50 μT), but with a range limited, for example, to ±10 μT, it could provide significantly lower noise. The ratio between the fluxgate and AMR magnetometer noise defines the minimal length of the boom; the higher AMR sensor noise must be compensated by a 1/r^3 field decay rate. Fig. 7 presents a simplified block diagram of the device. The main microcontroller is an STM32F334, which has proved to be well resistant to radiation when tested for TID by ^{60}Co gamma source [11].

Authorized licensed use limited to: CZECH TECHNICAL UNIVERSITY. Downloaded on April 25,2024 at 13:49:15 UTC from IEEE Xplore. Restrictions apply.

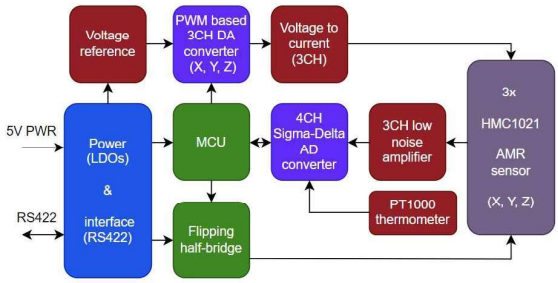

Fig. 7 Simplified block diagram of the AMR magnetometer.

Fig. 8 Triaxial AMR magnetometer prototype.

Recently, we also gathered some data from He nuclei irradiation of the whole magnetometer. The unit had to be restarted due to multiple SEL events, but as the power supply was cycled, there was no permanent damage. The magnetometer prototype is shown in Fig. 8. Components (only commercial off-the-shelf) are populated on both sides of the four-layer PCB.

IV. Results

A test campaign is in progress. Noise, linearity, and temperature dependencies were measured for the fluxgate magnetometer. Magnetic noise was measured in a six-layered MuMETAL magnetic shield; the results are shown in Fig. 9. The value of 5 $pT_{RMS}/\sqrt{Hz}$ at 1 Hz for the larger sensor is comparable to the best instruments used in space missions. It would be possible to go down to 2.3 $pT_{RMS}/\sqrt{Hz}$ at 1 Hz as indicated in the figure, but the power consumption and dimensions would be higher, which is not acceptable for the LVICE2 mission (mainly the increased power).

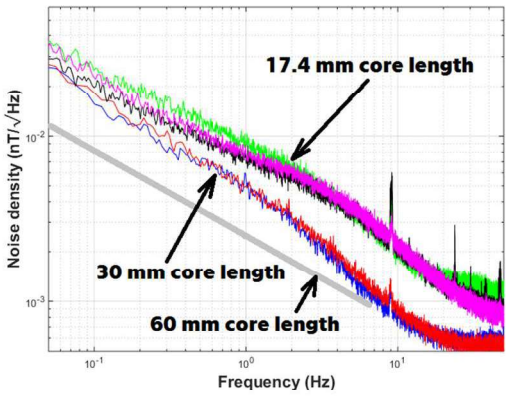

Fig. 9 Fluxgate sensor noise for digital output data, for two sensor heads of different sensor size—magnetic core length. The noise is 5 and 8 pT/√Hz at 1 Hz for 30 and 17.4 mm race-track cores, respectively. For comparison only, noise for a 60 mm long magnetic core is also drawn.

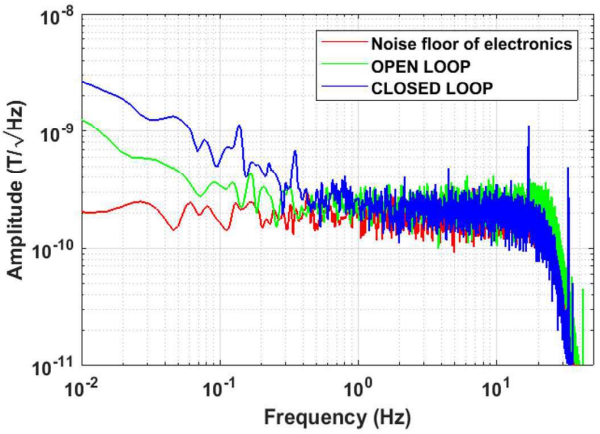

Fig. 10 AMR sensor noise (approx. 250 $pT_{RMS}/\sqrt{Hz}$ at 1 Hz for standard closed loop operation).

Fig. 10 presents the noise of the AMR magnetometer in open and closed loop modes, the second being the default. All other available parameters are summarized in Table 1.

TABLE I. AMR & FMAG Parameter Summary

Parameter	*AMR*	*Fluxgate*
Range	±100 µT	±500 nT
Noise	250 pT/√Hz at 1Hz	5 / 8* pT/√Hz at 1Hz
Linearity	±0.01% of full scale	±0.1% of full scale
Sampling	up to 3906 Sa/s	up to 250 Sa/s
Temp. coef.	<2 nT/K offset, <20 ppm/K sensitivity	<50 pT/K offset (sensor)
Orthogonality	<0.1°	<0.1° (after calibration)
Power	~0.6 W	~2 W
Dimensions	107 × 57 × 15 mm^3	electronics PC104 format, sensor (see text)
Mass	120 g with case (20 g bare PCB)	190/360* g sensor in box inc. cable, 350 g electronics in box

*see text; 30 mm or 50 mm cube side dimension sensor

In continuing work, we will concentrate on offset temperature stability improvement of the fluxgate sensor, as this will be critical for reliable magnetic field measurements, radiation testing of the fluxgate magnetometer prototype, and further testing of the AMR magnetometer (e.g., heavy ion irradiation, HMC1001 sensor application). Most important is the development and testing of the magnetic disturbance correction algorithms, as discussed e.g. in [5], including the algorithms for in-space calibration of mutual alignment of the AMR and fluxgate sensor and development of in-flight calibration algorithms [12, 13], as the possibility to calibrate the sensor offsets by motorized rotation of the whole spacecraft is not very feasible (potential navigation/motor firing risks and loss of fuel). The mission will also suffer from limited bandwidth for scientific data download, and we expect to explore ways to minimize the required bandwidth [14].

Acknowledgments

The presented work was funded through an ESA Contract in the Czech Third-Party Framework Project and by a grant (SGS22/170/OHK3/3T/13) by Czech Technical University in Prague.

Authorized licensed use limited to: CZECH TECHNICAL UNIVERSITY. Downloaded on April 25,2024 at 13:49:15 UTC from IEEE Xplore. Restrictions apply.

REFERENCES

[1] J. H. Piddington, "The cis-lunar magnetic field," *Planet. Space Sci.*, vol. 9, no. 6, pp. 305–18, 1962. doi:10.1016/0032-0633(62)90021-1

[2] M. de Soria-Santacruz et al., "An approach to magnetic cleanliness for the Psyche Mission," *2020 IEEE Aerosp. Conf., Big Sky, MT, USA, 2020*, pp. 1–15. doi:10.1109/AERO47225.2020.9172801

[3] O. D. Constantinescu, H. U. Auster, M. Delva, O. Hillenmaier, W. Magnes, and F. Plaschke, "Maximum-variance gradiometer technique for removal of spacecraft-generated disturbances from magnetic field data," *Geosci. Instrum.* vol. 9, pp. 451–69, 2020. doi:10.5194/gi-9-451-2020

[4] C. T. Russell et al., "The magnetospheric multiscale magnetometers," *Space Sci. Rev.*, vol. 199, pp. 189–256, 2016. doi:10.1007/s11214-014-0057-3

[5] W. Magnes et al., "Space weather magnetometer aboard GEO-KOMPSAT-2A", *Space Sci. Rev.*, vol. 216, Art. num. 119, 2020. doi:10.1007/s11214-020-00742-2

[6] H. U. Auster et al., "The THEMIS fluxgate magnetometer," *Space Sci. Rev.*, vol. 141, pp. 235–64, 2008. doi:10.1007/s11214-008-9365-9

[7] B. P. Weiss, "The Psyche magnetometry investigation," *Space Sci. Rev.*, vol. 219, p. 22, 2023. doi:10.1007/s11214-023-00965-z

[8] K. Greene, C. Hansen, B. B. Narod, R. Dvorsky, and D. M. Miles, "Tesseract – a high-stability, low-noise fluxgate sensor designed for constellation applications," *Geosci. Instrum. Method. Data Syst.*, vol. 11, pp. 307–21, 2022. doi:10.5194/gi-11-307-2022

[9] V. Petrucha and M. Butta, "Race-track fluxgate sensor scaling versus noise," *2021 IEEE Sensors, Sydney, Australia, 2021*, pp. 1–4. doi:10.1109/SENSORS47087.2021.9639560

[10] S. M. Guertin, M. Amrbar and S. Vartanian, "Radiation test results for common cubesat microcontrollers and microprocessors," *2015 IEEE Radiation Effects Data Workshop (REDW), Boston, MA, USA, 2015*, pp. 1–9. doi:10.1109/REDW.2015.7336730

[11] D. Novotny, V. Petrucha, M. Dressler and A. Platil, "Characterization of a digital AMR magnetometer for space applications," in *IEEE Trans. Instrum. Meas.*, vol. 70, pp. 1–9, 2021, Art no. 9504309, doi:10.1109/TIM.2020.3043867

[12] H. K. Leinweber, C. T. Russell, K. Torkar, T. L. Zhang and V. Angelopoulos, "An advanced approach to finding magnetometer zero levels in the interplanetary magnetic field," *Meas. Sci. Technol.*, vol. 19, p. 055104 (15 pp.), 2008. doi:10.1088/0957-0233/19/5/055104

[13] F. Plaschke, "How many solar wind data are sufficient for accurate fluxgate magnetometer offset determinations?" *Geosci. Instrum. Method. Data Syst.*, vol. 8, pp. 285–291, 2019 doi:10.5194/gi-8-285-2019

[14] D. Fischer, G. Berghofer, W. Magnes and T. L. Zhang, "A lossless compression method for data from a spaceborne magnetometer," *2008 6th Int. Symp. Comm. Syst., Networks Digital Signal Process., Graz, Austria, 2008*, pp. 326–30, doi:10.1109/CSNDSP.2008.4610829

Authorized licensed use limited to: CZECH TECHNICAL UNIVERSITY. Downloaded on April 25,2024 at 13:49:15 UTC from IEEE Xplore. Restrictions apply.

4.10. Radiation testing on HIMAC in Japan (unpublished)

During preparation of LVICE[2] mission, testing of magnetometer's engineering model has been performed. Results of conventional testing was almost the same as shown above in "Characterization of a Digital AMR Magnetometer for Space Applications" as main components of magnetometer remained the same, only interfaces changed. So, they are not shown here, but heavy-ions bombardment on HIMAC (Heavy Ion Medial Accelerator in Chiba) in Japan has shown interesting (at the moment unpublished) results that are presented below.

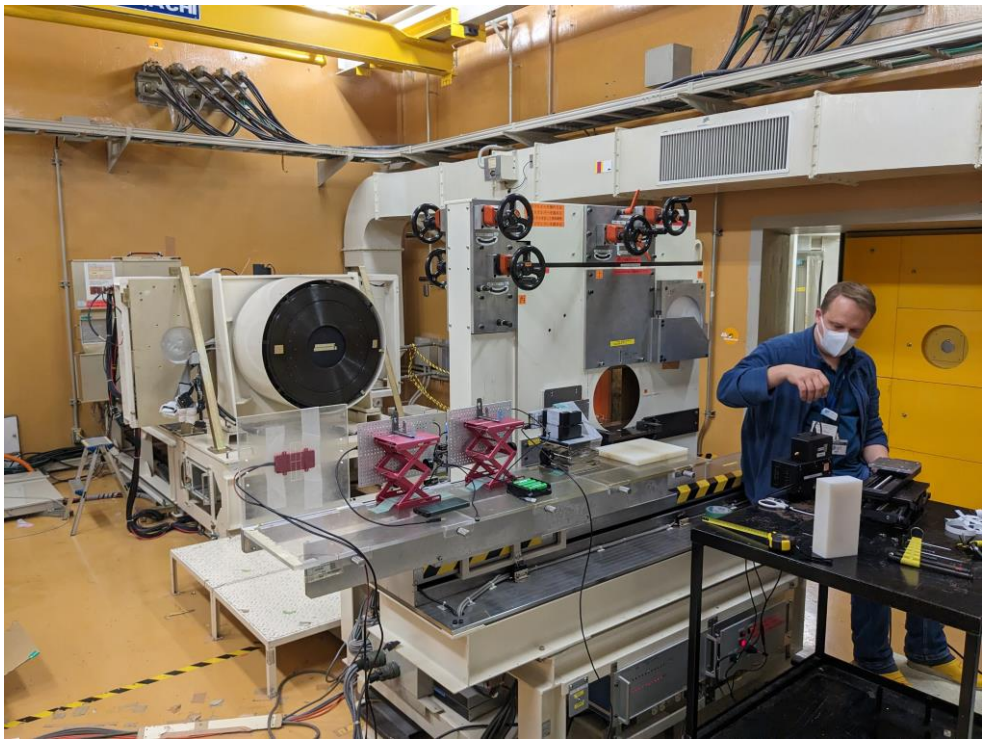

Fig. 6. Photo inside of HIMAC facility (beam output of accelerator)

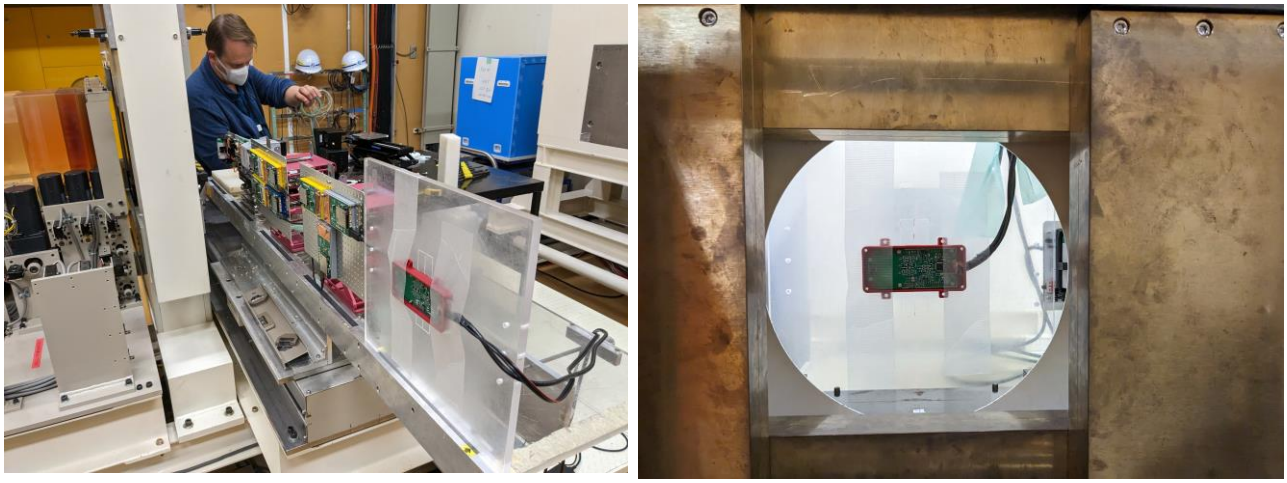

Fig. 7. Photo of developed AMR magnetometer prepared for irradiation by heavy-ion beam (right) and together with another instruments prepaed on moving table for irradiation during session (left)

After irradiation session, heavy-ions activated some of the elements in magnetometer, so it must stay stored in the facility until induced radiation drops below safe level (Fig. 10).

Fig. 8. Photo of induced radiation measurement using dosimeter probe

Due to the lack of time for preparation, only small amount of data has been collected (no sophisticated measurement setup with PXI frame in this session). Magnetometer streamed data over serial link and its power consumption has been monitored with DMM.

One of ADC's inputs has been shorted to see effect on its offset, another one connected to voltage reference to see gain drift. Third channel worked as normal, i.e. measuring AMR bridge output while MCU held this AMR in closed loop using DAC. Fourth (last) channel was used to measure temperature using Pt1000 sensor (assuming ADCs offset and gain drift caused by irradiation to be smaller than voltage change caused by temperature variations).

From data (see Fig 11-13 below) it is clear that the magnetometer has experienced multiple single event effects (SEE), because of temperature rise (Fig. 13), and also looking on DMM, current consumption spikes it was probably latch-up type (SEL). In the first few cases, magnetometer has been reset manually by power cycle, but it was found out that it recovers from that states by its own, so in most cases it was not power-cycled.

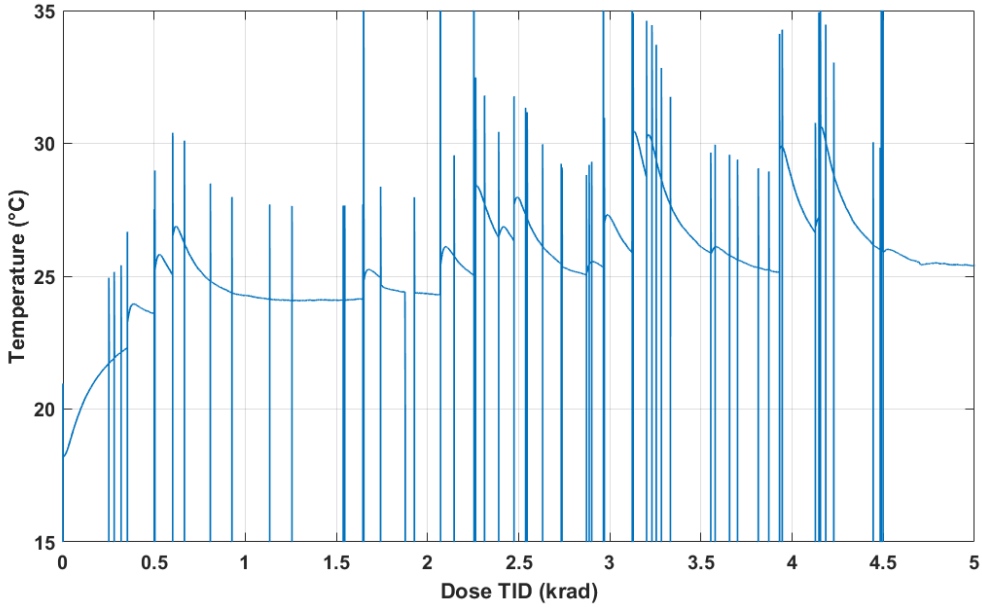

Fig. 9. Temperature measurement during irradiation
(fast spikes are caused by settling after mgm SEL induced reset, slow jumps due to real temp. swing – probably caused by SEL too)

In Fig. 12 below, offset and gain drift of used ADC can be seen, while offset remains almost unchanged, slight gain drift can be observed. Strong correlation between gain drift and temperature swing (Fig. 11.) can be seen, leading to conclusion that this gain drift is not caused by radiation but temperature swing instead. This can be supported by simple estimation: 100 ppm peak of gain drift at 0.5 krad TID from Fig. 12 corresponds with approx. 4 °C temperature change at 0.5 krad TID from Fig. 11. resulting in 25 ppm/K temperature dependence. Datasheet specifies gain temp. coef. to be typically 9 ppm/K, but there also play a role temp. dependence of the voltage divider (to obtain gain drift, one channel of ADC measured voltage reference, but divided to a half with resistors that also have approx. 100 ppm/K temp. coef.)

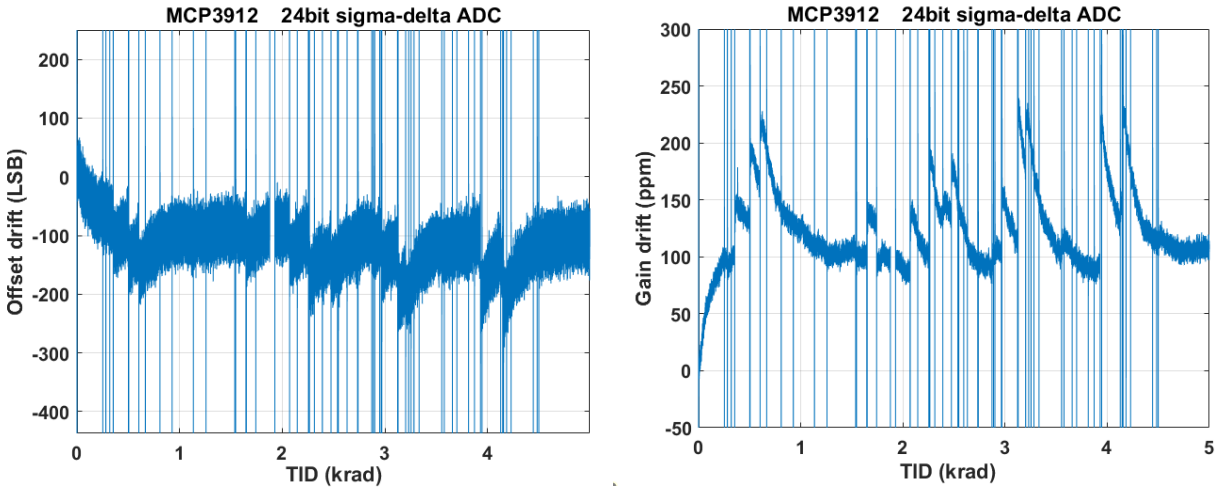

Fig. 10. Offset (left) and gain (right) drift of used ADC with increasing dose

In presented magnetometer, the advantage of its architecture is that slow change of the offset or gain of the ADC has almost zero effect on the resulting magnetic field measurement (Fig. 13). Offset and its drift is neglected using digital demodulation of AMR output (useful signal is AC modulated by AMR flipping, amplified and sampled by ADC and then demodulation into DC is done in software). Gain of ADC and its drift is neglected by feedback loop where sensitivity of the magnetometer is given by compensation coil constant and DAC's gain which seems to be stable.

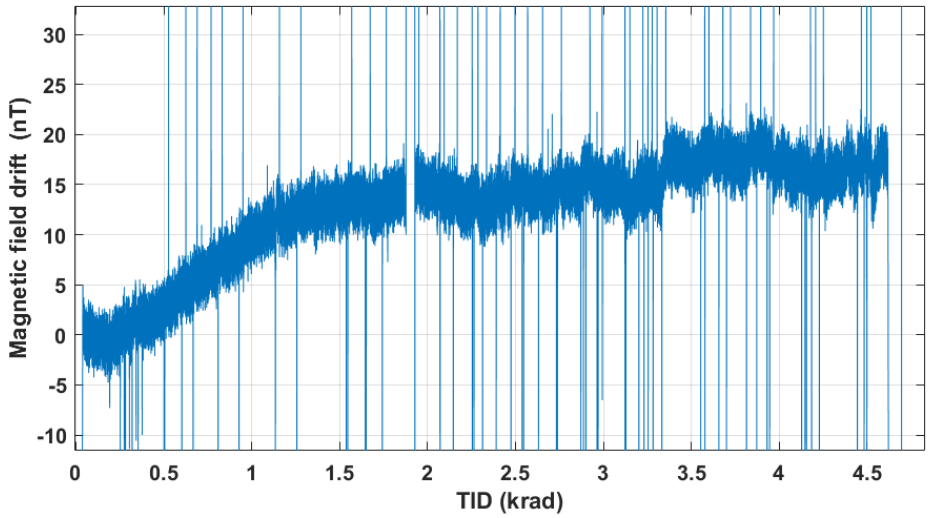

Fig. 11. Magnetic field measurement (in closed loop) during irradiation

4.11. Rocket flight of AMR magnetometer

During the preparation of a magnetometer for the LVICE[2] mission, an opportunity arose to test the instrument on a student sounding rocket from the University of KwaZulu-Natal in South Africa. This was possible thanks to a long-term collaboration between the South African National Space Agency (SANSA), the university, and my colleague Ing. Michal Janošek, Ph.D.The sounding rocket was planned to achieve an apogee of approximately 12-14 km and then land back with a parachute for payload recovery (three 1U cubesat-format payloads – 10x10x10 cm).

From our perspective, this flight of the magnetometer could count towards increasing its TRL, as it needed to survive the shock during launch, vibrations during flight, and steep temperature swings. I developed specialized hardware for storing data from this main magnetometer on two different memories for redundancy (an SD card and FLASH ICs). There were also two auxiliary magnetometers (MMC5983), an accelerometer and gyro (ICM-20608-G), an NTC thermometer, a 2G mechanical switch, and wireless (Xbee) communication with the logger.

As the payloads needed to be mounted inside the rocket hours before launch, most instruments and data logging had to be disabled, making reliable launch detection crucial. For this reason, a 2G mechanical switch, an accelerometer set to a 2G threshold, a temperature drop below 10°C, and finally an Xbee manual command were prepared to trigger detection.

Everything was prepared, sensors calibrated, and the payload mounted inside the rocket. Unfortunately, on the day of the flight, the weather conditions changed rapidly, and a fast decision had to be made. The apogee was decreased to 3 km, and the direction was changed to the sea with parachute ejection disabled. At that moment, no payload (and data) recovery was possible. Fast reprogramming of the firmware to at least send data wirelessly was done, but the wireless link was not designed for this purpose, so only a small amount of data from the first four seconds of flight was obtained.

Photos of the entire payload (logger + AMR magnetometer + battery + mechanical part) can be seen in Fig. 14. The launchpad and our ground station antenna can be seen in Fig. 15.

At the moment (7/2024), another launch is planned for 11/2024 with the same electronics but with a long-range, high-bandwidth wireless link and data compression to have the possibility to receive data from the whole flight.

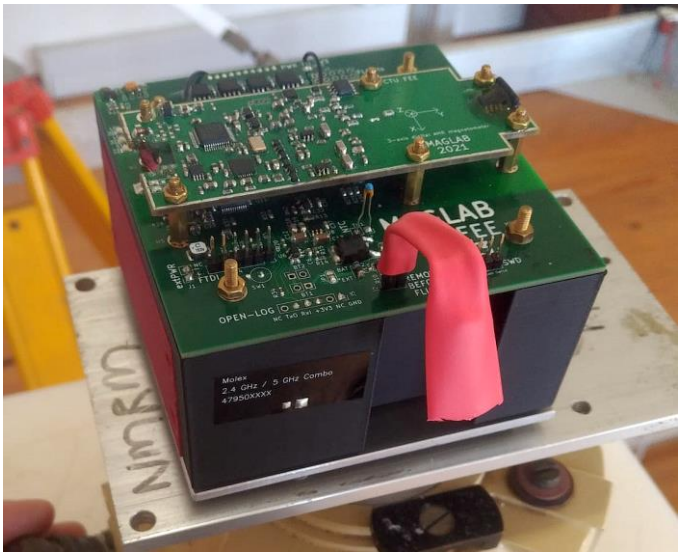

Fig. 12. Our flight logger with AMR mgm. nn top

Fig. 15. Ground station antenna pointed in flight direction

5. Conclusions

After summarizing the state-of-the-art and investigation of potential of different sensor technologies, designing of magnetometer for space applications has been focused from the beginning mainly on AMR sensors. The AMR sensors were chosen for their potential to partially replace or complement fluxgates. All four objectives from the chapter 3 were fulfilled:

I. Design AMR (and/or fluxgate) magnetometer with COTS components, that has the best possible parameters (at least comparable to state-of-the-art) and put emphasis to possible radiation tolerance.

This point is covered in chapters 4.1. to 4.3. and 4.6. AMR based magnetometer has been researched and developed prototype has even better parameters than commercial state-of-the-art AMR magnetometers. The latest prototype is using only COTS components that are well reachable by multiple distributors.

II. Perform set of tests and measurements on key parameters and radiation tolerance and try to enhance these parameters by finding and replacing susceptible parts

Radiation testing is discussed in chapters 4.4 and 4.5. and in 4.10. First radiation testing was performed with ^{60}Co gamma-rays and has identified problematic parts in design. During the second irradiation session, improved prototypes have been tested and confirmed good usability of the design. The level of >100 krad is more than sufficient for most missions on low Earth orbit. Two pieces were tested, both provided practically identical results giving more confidence to the results.

However, some of the STM32 microcontrollers were reported to be prone to single event upsets (SEU) or latch-ups (SEL) when bombarded with neutrons or heavy ions [33]. As the SEL was reversible, power cycling done by power management unit would solve the problem. In chapter 4.10 (HIMAC irradiation session), this susceptibility was confirmed. One way to manage this issue is migrating to different microcontroller with better radiation tolerance or using sufficient shielding of sensitive part of the electronics.

III. Reduce power consumption as much as possible to make that magnetometer most suitable for the space applications

In chapters 4.7 and 4.8 a novel methods of reducing power consumption are proposed. In 4.7 discontinuous power supply of AMR bridge is presented. And selective enabling of feedback loop only on demand, i.e. when necessary is presented in 4.8.

IV. If possible, prepare flight-ready magnetometer for real space mission

Preparing magnetometer for real space mission LVICE^2 (chapter 4.9) helped to summarize requirements for such instrument and even though there is still a lot of testing to be done before full commercial use in space (thermal vacuum, EMC, vibration testing etc.), most problematic part of development (radiation testing) is covered within this thesis.

As for many space projects TRL of instruments is important, an effort for at least flight on student rocket was taken. In chapter 4.11 rocket flight of AMR magnetometer prototype is covered.

6. List of own publications

6.1. Publications related to/used in the thesis

As publications are often the result of collaborative work, each publication listed below not only includes the percentage of co-authorship but authors contribution according to CRediT taxonomy.

[1] Novotný, D.; Petrucha, V.; Janošek, M. *A Digitally Compensated AMR Magnetometer,* IEEE Transactions on Magnetics. 2019, 55(1), ISSN 0018-9464.

*Co-authorship 50 %. **Novotný David:** Conceptualization, Methodology, Software, Investigation, Formal analysis, Visualization, Writing - Original Draft. **Petrucha Vojtěch:** Writing - Review & Editing, Supervision, Project administration, Funding acquisition. **Janošek Michal:** Supervision, Writing - Review & Editing.*

[2] D. Novotný and V. Petrucha, *High Dynamic Range Digital Fluxgate Magnetometer*, IEEE SENSORS, Rotterdam, Netherlands, 2020, pp. 1-4, doi: 10.1109/SENSORS47125.2020.9278852.

*Co-authorship 70 %. **Novotný David:** Conceptualization, Methodology, Software, Investigation, Formal analysis, Visualization, Writing - Original Draft. **Petrucha Vojtěch:** Supervision, Writing - Review & Editing, Resources*

[3] Novotný, D.; Petrucha, *V. High dynamic range fluxgate magnetometer*. In: Proceedings of IEEE Student Branch Conference Blansko 2018. Brno: Vysoké učení technické v Brně, 2018. p. 33-36. 1. ISBN 978-80-214-5661-7.

*Co-authorship 50 %. **Novotný David:** Conceptualization, Methodology, Software, Investigation, Formal analysis, Visualization, Writing - Original Draft. **Petrucha Vojtěch:** Writing - Review & Editing, Supervision, Project administration, Resources.*

[4] Novotný, D.; Petrucha, V.; Dressler, M.; Platil, A. *AMR Magnetometer With Digital Feedback for Space Applications*. In: 2020 IEEE International Instrumentation and Measurement Technology Conference (I2MTC 2020). Piscataway, NJ: IEEE, 2020. ISBN 978-1-7281-4460-3.

*Co-authorship 40 %. **Novotný David:** Conceptualization, Methodology, Software, Investigation, Formal analysis, Visualization, Writing - Original Draft. **Petrucha Vojtěch:** Writing - Review & Editing, Supervision, Resources. **Dressler Michal:** Software, Investigation, Formal analysis, Visualization, Writing - Review & Editing. **Platil Antotín:** Writing - Review & Editing, Supervision.*

[5] D. Novotny, V. Petrucha, M. Dressler and A. Platil, *Characterization of a Digital AMR Magnetometer for Space Applications*, in IEEE Transactions on Instrumentation and Measurement, vol. 70, pp. 1-9, 2021, Art no. 9504309, doi: 10.1109/TIM.2020.3043867.

*Co-authorship 50 %. **Novotný David:** Conceptualization, Methodology, Software, Investigation, Formal analysis, Visualization, Writing - Original Draft. **Petrucha Vojtěch:***

Writing - Review & Editing, Supervision, Resources. ***Dressler Michal:*** *Investigation, Formal analysis, Visualization, Writing - Review & Editing.* ***Platil Antotín:*** *Writing - Review & Editing.*

[6] M. Janošek, D. Novotný, M. Dressler and E. Saunderson, *Low frequency noise investigation of pT-level magnetic sensors by cross-spectral method*, 2021 IEEE Sensors, Sydney, Australia, 2021, pp. 1-4, doi: 10.1109/SENSORS47087.2021.9639875.

Co-authorship 40 %. ***Janošek Michal:*** *Conceptualization, Methodology, Investigation, Writing - Original Draft.* ***Novotný David:*** *Software, Formal analysis, Visualization, Writing - Review & Editing, Resources.* ***Dressler Michal:*** *Formal analysis, Visualization, Writing - Review & Editing.* **Saunderson Elda*:*** *Formal analysis, Writing - Review & Editing.*

[7] NOVOTNÝ, D., L. MIČAN, and V. PETRUCHA. *Low-Power AMR Magnetometer Operated in Discontinuous Mode*. In: MMM Intermag 2022 Abstract Book. 2022 Joint MMM-INTERMAG, New Orleans, LA, 2022-01-10/2022-01-14. Melville (NY): AIP Publishing LLC, 2022. p. 558-559. Conference abstract book.

Co-authorship 45 %. ***Novotný David:*** *Conceptualization, Methodology, Investigation, Formal analysis, Visualization, Writing - Original Draft.* ***Mičan Lukáš:*** *Software, Investigation, Writing - Review & Editing, Resources.* ***Petrucha Vojtěch:*** *Writing - Review & Editing, Supervision, Resources.*

[8] NOVOTNÝ, D., PLATIL, A., PETRUCHA, V., JANOSEK, M. *Novel Power Saving Algorithm for AMR Magnetometer with Fast Settling Feedback Loop. In: EMSA 2024* Abstract Book.. 2024, EMSA, Košice, Slovak Republic.

Co-authorship 50 %. ***Novotný David:*** *Conceptualization, Methodology, Software, Investigation, Formal analysis, Visualization, Writing - Original Draft.* ***Platil Antotín:*** *Writing - Review & Editing, Supervision.* ***Petrucha Vojtěch:*** *Writing - Review & Editing, Supervision.* ***Janošek Michal:*** *Writing - Review & Editing.*

[9] V. Petrucha, D. Novotný and K. Šobíšek, *Magnetometry Package for LVICE2 Mission: Triaxial Fluxgate and AMR Magnetometer for Scientific Data Production Near Moon*, 2023 IEEE SENSORS, Vienna, Austria, 2023, pp. 1-4, doi: 10.1109/SENSORS56945.2023.10325159.

Co-authorship 35 %. ***Petrucha Vojtěch:*** *Conceptualization, Methodology, Software, Investigation, Formal analysis, Visualization, Writing - Original Draft.* ***Novotný David:*** *Visualization, Writing - Review & Editing.* ***Šobíšek Kajetán:*** *Software, Writing - Review & Editing.*

6.2. Publications not related to the thesis

[10] Petrucha, V.; Novotný, D. *Testing and application of an integrated fluxgate sensor DRV425. Journal of Electrical Engineering.* 2018, 2018(69), 418-421. ISSN 1335-3632.

Co-authorship 50 %.

[11] Janošek, M.; Butta, M.; Dressler, M.; Saunderson, E.; Novotný, D.; Fourie, C. *1-pT noise fluxgate magnetometer for geomagnetic measurements and unshielded magnetocardiography.* IEEE Transactions on Instrumentation and Measurement. 2020, 69(5), 2552-2560. ISSN 0018-9456.

Co-authorship 5 %.

[12] Novotný, D.; Janošek, M.; Petrucha, V.; Pavelka, L.; Platil, A. *Vehicle's magnetic field modeling and mapping for its presence detection.* In: Magnetic Frontiers 2019: Magnetic Sensors - Abstract Book. Lisbon: Instituto Superior Técnico, Technical University of Lisbon, 2019.

Co-authorship 20 %.

[13] Janošek, M.; Butta, M.; Dressler, M.; Saunderson, E.; Novotný, D.; Fourie, C. *1 pT-noise fluxgate magnetometer design and its performance in geomagnetic measurements*. In: 2019 IEEE International Instrumentation and Measurement Technology Conference - proceedings. New York: IEEE, 2019. ISSN 2642-2077. ISBN 978-1-5386-3460-8.

Co-authorship 5 %.

[14] Hrakova, D.; Ripka, P.; Laposa, A.; Novotný, D.; Kroutil, J.; Povolný, V.; Kaman, O.; Veverka, P., *Inkjet-printed Mn-Zn ferrite nanoparticle core for fluxgate.* Journal of Magnetism and Magnetic Materials. 2022, 563 1-5. ISSN 0304-8853.

Co-authorship 10 %.

[15] Platil, A.; Novotný, D.; Ripka, P., *Improved Method for Linear Position Sensing through Conductive Wall*, In: The XIV. European Magnetic Sensors and Actuators Conference - Book of Abstracts. Košice: Univerzita Pavla Jozefa Šafárika, 2024. p. 179-180. ISBN 978-80-574-0340-1.

Co-authorship 30 %.

6.3. Responses to author’s publications (citations)

[1] A Digitally Compensated AMR Magnetometer

(C1) Manyosa, X.; Roma-Dollase, D.; Arqué, M.; Bonastre, B.; Jiménez, V.; Ramos-Castro, J.; Pons-Nin, J.; Martín, V. et al. MEMS miniaturized low-noise magnetic field sensor for the observation of sub-millihertz magnetic fluctuations in space exploration. Measurement: Journal of the International Measurement Confederation, vol. 230, 2024. ISSN 02632241. DOI: 10.1016/j.measurement.2024.114489

(C2) Liu, H.-F.; Luo, Z.-C.; Hu, Z.-K.; Yang, S.-Q.; Tu, L.-C.; Zhou, Z.-B.; Kraft, M. A review of high-performance MEMS sensors for resource exploration and geophysical applications. PETROLEUM SCIENCE, vol. 19, no. 6, pp. 2631 - 2648, 2022. ISSN 1672-5107. DOI: 10.1016/j.petsci.2022.06.005

(C3) N. Hadjigeorgiou, K. Asimakopoulos, K. Papafotis and P. P. Sotiriadis, "Vector Magnetic Field Sensors: Operating Principles, Calibration, and Applications," in *IEEE Sensors Journal*, vol. 21, no. 11, pp. 12531-12544, 1 June1, 2021, doi: 10.1109/JSEN.2020.3045660.

[2] High Dynamic Range Digital Fluxgate Magnetometer

(C4) Traore, P. S.; Asfour, A.; Konan, S.; Yonnet, J.-P. Stability Criteria of a High Sensitivity Digital GMI Magnetometer. IEEE TRANSACTIONS ON MAGNETICS, vol. 59, no. 2, 2023. ISSN 0018-9464. DOI: 10.1109/TMAG.2022.3198270

(C5) Shao, W.; Fan, J.; Tian, X.; Tang, S.; Yi, Z.; Liu, J.; Liu, B.; Huang, Y. et al. Design and Characterization of a Multi-Processed Differential Magnetic Field Probe by Using Asymmetric Calibration Method. IEEE SENSORS JOURNAL, vol. 22, no. 6, pp. 5723 - 5731, 2022. ISSN 1530-437X. DOI: 10.1109/JSEN.2022.3148002

[4] AMR Magnetometer With Digital Feedback for Space Applications

(C6) Baklezos, A.T.; Hadjigeorgiou, N.G. Magnetic sensors for space applications and magnetic cleanliness considerations Recent Trends on Electromagnetic Environmental Effects for Aeronautics and Space Applications, pp. 147 - 185, 2020. ISBN 9781799848790. DOI: 10.4018/978-1-7998-4879-0.ch006

[5] Characterization of a Digital AMR Magnetometer for Space Applications

(C7) Chen, K.-L.; Chen, J.-H. Contactless current measurement for suspended overhead lines using a magnetic field sensor array IET GENERATION TRANSMISSION & DISTRIBUTION, vol. 18, no. 7, pp. 1360 - 1371, 2024. ISSN 1751-8687. DOI: 10.1049/gtd2.13128

(C8) Zhang, Y.; Wu, C.; Liu, S.; Lv, Z.; Huang, X.; Wu, P. A Parking Detection Algorithm Based on Multitransitory Finite-State Machine Using Magnetic Wireless Sensor Network IEEE Internet of Things Journal, vol. 11, no. 5, pp. 8360 - 8372, 2024. DOI: 10.1109/JIOT.2023.3319340

(C9) Lee, C.; Kwon, I. Gain-Bandwidth Product Compensation Technique by 16-Unit Tail Current Control for a Radiation Tolerant Preamplifier With 0.9% Amplitude Drop up to 5 Mrad. IEEE TRANSACTIONS ON INSTRUMENTATION AND MEASUREMENT, vol. 73, 2024. ISSN 0018-9456. DOI: 10.1109/TIM.2024.3352700

(C10) Meng, T.; Huang, Z.; Mao, Y.; Liu, H.; Dong, H. Construction and Experimental Verification of a New Miniature Low-Noise Hall Sensor for Wide-Range Vector Magnetic Field Measurements. IEEE SENSORS JOURNAL, vol. 23, no. 18, pp. 21155 - 21162, 2023. ISSN 1530-437X. DOI: 10.1109/JSEN.2023.3302344

(C11) Wu, C.; Wu, P.; You, Y.; Yuan, Y. A Deep Learning Parking Detection Algorithm Using W-Shape Magnetic Wireless Sensor Networks. IEEE TRANSACTIONS ON INSTRUMENTATION AND MEASUREMENT, vol. 72, 2023. ISSN 0018-9456. DOI: 10.1109/TIM.2022.3229724

(C12) Strabel, B. P.; Regoli, L. H.; Moldwin, M. B.; Ojeda, L. V.; Shi, Y.; Thoma, J. D.; Narrett, I. S.; Bronner, B. et al. Quad-Mag board for CubeSat applications. GEOSCIENTIFIC INSTRUMENTATION METHODS AND DATA SYSTEMS, vol. 11, no. 2, pp. 375 - 388, 2022. ISSN 2193-0856. DOI: 10.5194/gi-11-375-2022

[9] Testing and application of an integrated fluxgate sensor DRV425.

(C13) Maia, H. T.; Xiao, C.; Li, D.; Grinspun, E.; Zheng, C. Can one hear the shape of a neural network?: Snooping the GPU via Magnetic Side Channel. PROCEEDINGS OF THE 31ST USENIX SECURITY SYMPOSIUM, pp. 4383 - 4400, 2022.

(C14) Saari, M. M.; Nadzri, N. A.; Zaini, M. A. H. P.; Ramlan, N. H.; Tsukada, K. A Low-Frequency Eddy Current Probe Based on Miniature Fluxgate Array for Defect Evaluation in Steel Components. IEEE TRANSACTIONS ON MAGNETICS, vol. 58, no. 2, 2022. ISSN 0018-9464. DOI: 10.1109/TMAG.2021.3076441

(C15) Saari, M. M.; Sakai, K.; Kiwa, T.; Tsukada, K. A sensitive magnetometer utilizing high-T-c SQUID for magnetic property characterization. MICROSYSTEM TECHNOLOGIES-MICRO-AND NANOSYSTEMS-INFORMATION STORAGE AND PROCESSING SYSTEMS, vol. 27, no. 9, pp. 3413 - 3420, 2021. ISSN 0946-7076. DOI: 10.1007/s00542-020-05198-6

7. References

[1] Leitner, Stefan, et al., "Design of the Magnetoresistive Magnetometer for ESA's SOSMAG Project." IEEE Transactions on Magnetics 51.1 (2015): 1-4. DOI: 10.1109/TMAG.2014.2358270

[2] Burch, J. L., et al. "Magnetospheric multiscale overview and science objectives." Space Science Reviews 199.1-4 (2016): 5-21.

[3] Díaz-Michelena, Marina. "Small magnetic sensors for space applications." Sensors 9.4 (2009): 2271-2288. DOI: 10.3390/s90402271

[4] D. M. Miles, I.R. Mann, M. Ciurzynski, D. Barona, "A miniature, low-power scientific fluxgate magnetometer: A stepping-stone to cube-satellite constellation missions," Journal of Geophysical Research: Space Physics 121(12), December 2016, DOI: 10.1002/2016JA023147

[5] P. Brown et al., "Space magnetometer based on an anisotropic magnetoresistive hybrid sensor," Review of Scientific Instruments 85, 125117, 2014, https://doi.org/10.1063/1.4904702

[6] P. Brown, "Magnetoresistive magnetometer for space science applications," Meas. Sci. Technol. 23 (2012) 025902 (11pp), http://dx.doi.org/10.1088/0957-0233/23/2/025902

[7] D. Novotný, V. Petrucha, M. Janošek, "A Digitally Compensated AMR Magnetometer," IEEE Transactions on Magnetics, pp(99):1-5, October 2018, DOI: 10.1109/TMAG.2018.2873235

[8] S. Sordo-Ibáñez et al., "A Front-End ASIC for a 3-D Magnetometer for Space Applications by Using Anisotropic Magnetoresistors," IEEE Transactions on Magnetics, Volume: 51 , Issue: 1 , Jan. 2015, DOI: 10.1109/TMAG.2014.2356976

[9] S. Sordo-Ibáñez et al., "A Front-End ASIC for a 3-D Magnetometer for Space Applications by Using Anisotropic Magnetoresistors," IEEE Transactions on Magnetics, Volume: 51 , Issue: 1 , Jan. 2015, DOI: 10.1109/TMAG.2014.2356976

[10] ESCIES - European Space Components Information Exchange System, https://escies.org

[11] Tumanski, S. Thin Film Magnetoresistive Sensors; Institute of Physics Publishing: Bristol,UK, 2001.

[12] Brown, P. & Beek, T. & Carr, Conor & O'Brien, Helen & Cupido, E. & Oddy, Timothy & Horbury, T.. (2012). Magnetoresistive magnetometer for space science applications. Measurement Science and Technology. 23. 025902. 10.1088/0957-0233/23/2/025902.

[13] 3-Axis Digital Compass IC HMC5883L, Honeywell Aerospace, Rev. F., available online at: https://aerospace.honeywell.com

[14] 1- and 2-Axis Magnetic Sensors HMC1001/1002/1021/1022, Honeywell Aerospace, N61-2056-000-000, 04/2019, available online at: https://aerospace.honeywell.com

[15] AFF755B MagnetoResistive Field Sensor, Sensitec, AFF755B.DSE.06, available at: https://www.sensitec.com

[16] NMRM-001-485 magnetometer, NewSpace Systems, Available online at www.newspacesystems.com

[17] Ripka, P. Magnetic sensors and magnetometers. Boston: Artech House, c2001. ISBN 15-805-3057-5.

[18] Korepanov, Valery & Marusenkov, Andriy. (2012). Flux-Gate Magnetometers Design Peculiarities. Surveys in Geophysics. 33. 10.1007/s10712-012-9197-8.

[19] Auer, M. & Scherzer, Maximilian & Valavanoglou, Aris & Leitner, Stefan & Magnes, Werner. (2018). Front-end ASIC for Spaceborne Fluxgate-Magnetometers.

[20] Miles, David & Bennest, J. & Mann, Ian & Millling, D.. (2013). A radiation hardened digital fluxgate magnetometer for space applications. Geoscientific Instrumentation, Methods and Data Systems. 2. 10.5194/gi-2-213-2013.

[21] Coillot, Christophe & Moutoussamy, J. & Leroy, Paul & Chanteur, Gerard & Roux, Alain. (2007). Improvements on the Design of Search Coil Magnetometer for Space Experiments. Sensor Letters. 5. 167-170. 10.1166/sl.2007.050.

[22] MAG612 miniature three-axis fluxgate, available at: https://www.bartington.com/mag612/

[23] Janošek, M.; Butta, M.; Dressler, M.; Saunderson, E.; Novotný, D.; Fourie, C. 1 pT-noise fluxgate magnetometer design and its performance in geomagnetic measurements. In: 2019 IEEE International Instrumentation and Measurement Technology Conference - proceedings. New York: IEEE, 2019. ISSN 2642-2077. ISBN 978-1-5386-3460-8.

[24] Olsen N, Tøffner-Clausen L, Sabaka T J, Brauer P, Merayo J M G, Jørgensen J L, Leger ´ J M, Nielsen O V, Primdahl F, Risbo T (2003), "Calibration of the Ørsted vector magnetometer," Earth, Planets Space, vol. 55, pp. 11–18, doi: 10.1186/BF03352458.

[25] Novotný, D.; Petrucha, V.; Janošek, M. A Digitally Compensated AMR Magnetometer. IEEE Transactions on Magnetics. 2019, 55(1), ISSN 0018-9464.

[26] D. Novotný, V. Petrucha, M. Dressler and A. Platil, "AMR Magnetometer With Digital Feedback for Space Applications," 2020 IEEE International Instrumentation and Measurement Technology Conference (I2MTC), Dubrovnik, Croatia, 2020, pp. 1-6, doi: 10.1109/I2MTC43012.2020.9129039.

[27] AD5791 datasheet, Analog devices, Rev. F, Available at https://www.analog.com/media/en/technical-documentation/data-sheets/ad5791.pdf

[28] STM32F334 datasheet, ST Microelectronics, DS9994 Rev 9, 2018, Available online at https://www.st.com/resource/en/datasheet/stm32f334k4.pdf

[29] F.J. Franco, Y. Zong, J.A. Agapito, A.H. Cachero, "Radiation effects on XFET voltage references," IEEE Radiation Effects Data Workshop, 2005, DOI: 10.1109/REDW.2005.1532680

[30] Brauer P, Merayo J M G, Risbo T, Primdahl F (2001), "Magnetic calibration of vector magnetometers: Linearity, thermal effects and stability," in Proc. ESA Conf. SP-490. [Online]. Available: http://citeseerx.ist.psu.edu/viewdoc/summary?doi=10.1.1.34.2694

[31] Michal Janošek et al, "Magnetic Calibration System With Interference Compensation," IEEE Transactions on Magnetics, Vol. 55, No. 1, January 2019, DOI: 10.1109/TMAG.2018.2874169

[32] ESCIES - European Space Components Information Exchange System, "Radiation: Theory, Definitions - Gamma Radiation," Available online: https://escies.org

[33] H. Quinn et al., "Single-Event Effects in Low-Cost, Low-Power Microprocessors," IEEE Radiation Effects Data Workshop (REDW) 2014, DOI: 10.1109/REDW.2014.7004596

[34] Miles, David & Narod, Barry & Milling, David & Mann, Ian & Barona, David & Hospodarsky, George. (2018). A hybrid fluxgate and search coil magnetometer concept using a racetrack core. Geoscientific Instrumentation, Methods and Data Systems. 7. 265-276. 10.5194/gi-7-265-2018.

[35] Isabelle Fratter, Jean-Michel Léger, François Bertrand, Thomas Jager, Gauthier Hulot, Laura Brocco, Pierre Vigneron, Swarm Absolute Scalar Magnetometers first in-orbit results, Acta Astronautica, Volume 121, 2016, Pages 76-87, ISSN 0094-5765, https://doi.org/10.1016/j.actaastro.2015.12.025.

[36] Billingsley Aerospace & Defense, Helmholtz Coils – Closed-Loop Calibration Systems [online]. 2024 [cit. 2024-07-17]. Available: https://magnetometer.com/products/helmholtz-calibration-systems

[37] M. Janosek, M. Dressler, V. Petrucha and A. Chirtsov, "Magnetic Calibration System With Interference Compensation," in IEEE Transactions on Magnetics, vol. 55, no. 1, pp. 1-4, Jan. 2019, Art no. 6000104, doi: 10.1109/TMAG.2018.2874169.

[38] Olsen, N., Tøffner-Clausen, L., Sabaka, T.J. et al. Calibration of the Ørsted vector magnetometer. Earth Planet Sp 55, 11–18 (2003). https://doi.org/10.1186/BF03352458

[39] ESCIES—European Space Components Information Exchange System. Accessed: Nov. 10, 2020. [Online]. Available at: https://escies.org

[40] R. Kingsbury et al., "TID tolerance of popular CubeSat components," in Proc. IEEE Radiat. Effects Data Workshop (REDW), Jul. 2013, pp. 1–4, doi: 10.1109/REDW.2013.6658220.

[41] H. Quinn, T. Fairbanks, J. L. Tripp, G. Duran, and B. Lopez, “Single event effects in low-cost, low-power microprocessors,” in Proc. IEEE Radiat. Effects Data Workshop (REDW), Jul. 2014, pp. 1–9, doi: 10.1109/REDW.2014.7004596.

[42] R. Netzer, K. Avery, W. Kemp, A. Vera, B. Zufelt, and D. Alexander, “Total ionizing dose effects on commercial electronics for cube sats in low Earth orbits,” in Proc. IEEE Radiat. Effects Data Workshop (REDW), Jul. 2014, pp. 1–7, doi: 10.1109/REDW.2014.7004607.

[43] K. Avery et al., “Total dose test results for CubeSat electronics,” in Proc. IEEE Radiat. Effects Data Workshop, Jul. 2011, pp. 1–8, doi: 10.1109/REDW.2010.6062504.

[44] Z. Jiao, L. Jiang, J. Sun, J. Huang, and Y. Zhu, “Outgassing Environment of Spacecraft: An Overview,” IOP Conference Series: Materials Science and Engineering, vol. 611, no. 1. IOP Publishing, p. 012071, Oct. 01, 2019. doi: 10.1088/1757-899x/611/1/012071.

[45] Samwel, Susan & Hady, A. A. & Mikhail, J.S. & Ibrahim, Makram & Hanna, Yousry. (2008). Studying the Total Ionizing Dose and Displacement Damage Dose effects for various orbital trajectories. Proceeding of the First Middle East-Africa, Regional IAU Meeting. 55-58.

[46] J. Wang, Z. Huo, and F. Wang, “TID evaluation based on variabilities of space radiation and device failure dose in typical navigation satellite orbits,” Microelectronics Reliability, vol. 137. Elsevier BV, p. 114747, Oct. 2022. doi: 10.1016/j.microrel.2022.114747.

[47] P. Jeannette, B. Lee, 2004. Environmental Conditions for Space Flight Hardware: A Survey [online]. Dynamic Range Corporation, 5-7 [cit. 2024-07-17]. Available at: https://ntrs.nasa.gov/citations/20060013394

[48] Z. Li and S. Dixon, "A Closed-Loop Operation to Improve GMR Sensor Accuracy," in IEEE Sensors Journal, vol. 16, no. 15, pp. 6003-6007, Aug.1, 2016, doi: 10.1109/JSEN.2016.2580742.

[49] J. Gao, J. Wang, Y. Shen, Z. Jiang, Y. Huang and Q. Yu, "Equivalent Magnetic Noise Analysis for a Tunneling Magnetoresistive Magnetometer," in IEEE Electron Device Letters, vol. 41, no. 9, pp. 1400-1403, Sept. 2020, doi: 10.1109/LED.2020.3007950.

[50] A. Sheinker and M. B. Moldwin, "Adaptive interference cancelation using a pair of magnetometers," in IEEE Transactions on Aerospace and Electronic Systems, vol. 52, no. 1, pp. 307-318, February 2016, doi: 10.1109/TAES.2015.150192

[51] Lee, J.; Jin, H.; Kim, K.-H.; Park, H.; Jo, W.; Jang, Y.; Kang, H.; Kim, E.; Choi, Y.-J. Correction of Spacecraft Magnetic Field Noise: Initial Korean Pathfinder Lunar Orbiter MAGnetometer Observation in Solar Wind. Sensors 2023, 23, 9428. https://doi.org/10.3390/s23239428

[52] Hospodarsky, G. B. (2016), Spaced-based search coil magnetometers, J. Geophys. Res. Space Physics, 121, 12,068–12,079, doi:10.1002/2016JA022565.

[53] François Bertrand, Thomas Jager, Axel Boness, William Fourcault, Gwenael Le Gal, et al., *A 4He vector zero-field optically pumped magnetometer operated in the Earth-field*. Review of Scientific Instruments, 2021, Volume 92, Issue 10, October 2021, pp.105005. doi: 10.1063/5.0062791.

[54] D. Novotný, “FPGA Controlled Magnetometer with Digital Output”, Bachelor thesis, Prague, 2016.

8. List of Abbreviations

AMR	...	Anisotropic Magnetoresistance
GMR	...	Giant Magnetoresistance
TMR	...	Tunnel Magnetoresistance
MGM	...	Magnetometer
FG	...	Fluxgate
COTS	...	Commercially-off-the-shelf
DMM	...	Digital Multi Meter
DVM	...	Digital Voltmeter
EMSA	...	European Magnetic Sensors and Actuators (conference)
ASIC	...	Application Specific Integrated Circuit
FPGA	...	Field Programmable Gate Array
MCU	...	Microcontroller Control Unit
PSU	...	Power Supply Unit
PWM	...	Pulse Width Modulation
LDO	...	Low Drop-Out
TC	...	Temperature Coefficient
TRL	...	Technology Readiness Levels
TID	...	Total Ionizing Dose
SEE	...	Single Event Effects
SEU	...	Single Event Upset
SEL	...	Single Event Latch-up
ADC	...	Analog to Digital Converter
ESA	...	European Space Agency
SOSMAG	...	Service Oriented Spacecraft Magnetometer
DAC	...	Digital to Analog Converter
HP	...	High pass (filter)
LP	...	Low pass (filter)
$LVICE^2$	...	Lunar Vicinity Complex Environmental Explorer
DAQ	...	Data Acquisition